ABSTRACT

OGHENEOVO IDOLOR. Leveraging Polymer-Water Interactions for Damage Detection in Polymer Composites. (Under the direction of Dr. Landon Grace).

Polymer composite materials are increasingly being adopted across civil infrastructure, oil & gas, marine, automotive, and aerospace industries. Achieving ubiquitous adoption would require new advances in development of non-destructive examination techniques which are cost effective, simple to utilize, and sensitive enough to ascertain the structural integrity of composite parts, especially in the absence of visible damage. A common characteristic of these materials is their tendency to absorb measurable moisture in nearly all operating environments. This absorbed moisture either becomes bound to the polymer network via secondary bonding interactions or exists as free water with negligible interactions. Damage creates fractures and new internal free volume where water molecules can exist in the latter state. Thus, this dissertation proposes a novel basis for nondestructive examination in polymer composites which leverages this locally-higher concentration of free water in damaged areas. Polymer-water interactions—determining the free or bound state of water—are characterized by near-infrared spectroscopy and microwave-range dielectric properties. Effects of humidity or precipitation-driven fluctuations in moisture content on water state distributions is also investigated. An effective algorithm for detection of localized damage via analysis of polymer-water interactions is developed based on a logistic regression machine learning approach. Results show a direct correlation between the extent of local damage and higher relative levels of free water at damage sites. Studies on the effects of paint and coatings indicate some loss in damage sensitivity, which can be improved by exposure to higher level of moisture contamination. They also indicate variation in moisture content has a significant effect on the water state distributions in damaged polymer composites, leading to discovery of damage-dependent hysteresis as a highly sensitive and reliable basis for damage detection.

Leveraging Polymer-Water Interactions for Damage Detection in Polymer Composites

by
Ogheneovo Idolor

A dissertation submitted to the Graduate Faculty of
North Carolina State University
in partial fulfillment of the
requirements for the degree of
Doctor of Philosophy

Mechanical Engineering

Raleigh, North Carolina
2021

APPROVED BY:

_____	_____
Landon Grace Committee Chair	Kara Peters
_____	_____
Mark Pankow	Maury Balik

DEDICATION

To my family and friends who supported me through this journey.

BIOGRAPHY

Ogheneovo Idolor was born and raised in Nigeria. He earned a bachelor's degree in mechanical engineering in 2011 from the University of Benin, Nigeria. After graduation he started his career in oil and gas facilities design and construction, where he was a materials, mechanical, and piping engineer for over 5 years. In 2017 he proceeded to the United States to pursue graduate studies in materials and mechanical engineering at North Carolina State University, where he joined Dr. Landon Grace's fluid-solid interaction research group. His research during this time involved understanding the dynamic behavior of absorbed water and its interactions with a polymer. He further leveraged this knowledge in pioneering the field of water-interaction enabled nondestructive examination for polymer composites. Ogheneovo is passionate about applying fundamental concepts in material science to solve problems that enable new and exciting possibilities in mechanical engineering.

ACKNOWLEDGEMENTS

I sincerely appreciate my doctoral advisor, Dr. Landon Grace, for seeing the potential in me and providing the opportunity to contribute to the great work which he started. I am grateful for his guidance, mentorship, and financial support during my graduate program. I am also thankful for the independence he allowed, enabling me to explore my research ideas and solve problems in unconventional ways. I couldn't ask for more from an advisor.

I am particularly grateful to my doctoral committee members—Dr. Kara Peters, Dr. Mark Pankow, and Dr. Maury Balik for the insightful discussions and contributions they made to my work. I appreciate their responsiveness, and the time invested in listening to my presentations and reviewing my dissertation.

I also appreciate the efforts of my research group mates—Kathrine Berkowitz, Rishabh Guha, Omkar Kaskar, Logan Bilich and others who worked with me in designing experiments, building experimental setups, collecting data, and processing data in and outside the laboratory. I am also thankful to William Woodbridge and Romeo Jump of the College of Natural Resources at North Carolina State University for assisting with a near-infrared spectrometer.

Finally, I am thankful to my lovely wife, Dr. Osahon Idolor, who encouraged and endured with me through the rigors of research. I thank my parents and siblings who supported my decision to pursue a doctoral degree and always remained there for me. I also appreciate my mentors and friends—Dr. Oluwaseun Awe, Tayo Olubode, Osaze Aghahowa, Ewomazino Ojogbo, Bassey Enebong Bassey, Samuel Enwenede, Dr. Felix Ewere, Dr. Victor Jayeola, AbdulWaheed Bishi, Noel Jagaba, and Aigbe Awenlimobor amongst many others who contributed to my success in graduate school. I also particularly appreciate my brother in-law, Dr. Courage Emokpae, who played a huge part in ensuring my success during the doctoral program.

TABLE OF CONTENTS

LIST OF TABLES

LIST OF FIGURES

CHAPTER 1: INTRODUCTION

1.1 Motivation

Across many industries, polymer composites are being adopted as replacements for traditional materials such as metals and plastics due to their high strength-to-weight ratios, ability to tailor their mechanical properties in different directions, corrosion resistance, and desirable electrical properties. The capabilities of these multi-functional next-generation materials are continuously being expanded and are beginning to be utilized as safety-critical components. Therefore, the ability to ascertain their structural integrity in a nondestructive manner has become a crucial factor in the selection of these materials.

Internal flaws may develop in these materials in many ways, these include: impact resulting from hail or a dropped tool, freeze-thaw cycling, fatigue loading, excessive strain, and defects introduced during the manufacturing process. Unlike metals, some of these effects may induce damage and weaken the structure, without any visible signs on the polymer composite surface. This is especially true when coating and paint has been applied on the surface (see Figure 1). Such a situation creates a potentially dangerous scenario, particularly for safety-critical components [1]. Hence, reliable, cost effective, and simple methods to nondestructively examine these materials would be essential to their continued adoption and application as safety-critical components.

Current nondestructive test methods for polymer matrix composites have various limitations. Firstly, they comprise very complicated systems—requiring an operator with specialized knowledge—which hinders widespread adoption. In addition, heavy capital investments are required for majority of the systems, putting it beyond the reach of many users. Also, each system has various limitations which include undetectable flaw orientations, characterization depth limitations, and material conductivity limitations. Another key limitation is

the challenge of characterizing sub-micron scale flaws, resulting in a high level of uncertainty in predicting the mechanical behavior of the structural components. This is primarily due to the inability to detect damage at its initiation phase, which is important in predicting yield point, remaining useful life, and future failure events in these materials [2].

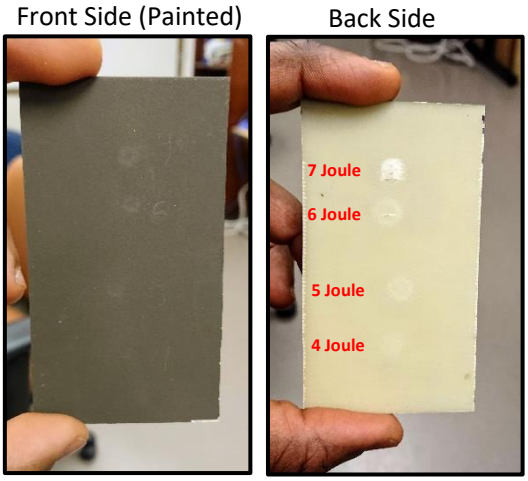

Figure 1: Coated composite impact-damaged at various levels showing front and back sides.

The highlighted limitations have led to various industries implementing mitigating measures to achieve similar levels of reliability as metals in safety-critical applications. These include compensating for the uncertainty during design and applying multiple inspection techniques, which both increase production costs. Compensation during design involves implementing a design approach which incorporates a higher level of uncertainty when working with polymer composites, leading to the counterproductive solution of adopting higher safety factors for safety-critical components [3].

Hence, new, improved, simpler, and effective methods for detection of damage in polymer matrix composites are still required. Therefore, this dissertation aims to provide a novel basis for nondestructive examination which is simple, reliable, and capable of detecting sub-micron scale

damage. This is achieved by using moisture—naturally absorbed by these materials—as an 'imaging' agent, by analyzing the nature of its interaction with the polymer matrix. Thus providing an effective tool for nondestructive examination in polymer composites.

1.2 Research Objectives

The objective of this dissertation is to investigate the potential for leveraging polymer-water interactions as a viable means for damage detection in polymer composites. The research develops novel techniques for damage detection based on this interaction. It also investigates the effects of typical conditions experienced by in-service polymer composites on the sensitivity to damage of this technique. The main objective consists of four parts including:

i) Characterize polymer-water interactions and investigate its sensitivity to damage using various spectroscopic techniques.

ii) Investigate the effect moisture absorption and desorption history has on sensitivity of polymer-water interactions to damage.

iii) Develop a localized damage detection algorithm for polymer matrix composites based on polymer-water interactions.

iv) Investigate the effect of painting and coatings on sensitivity of polymer-water interaction to damage.

The theories and experimental data presented will serve as a basis for future development and optimization of a water interaction enabled nondestructive examination technique.

1.3 Dissertation Outline

The dissertation comprises the following parts:

Chapter 2 is a literature review covering polymer composites, effect of moisture on polymer composites, and the current state of nondestructive examination techniques for polymer

composites. This chapter also provides some detail on polymer-water interactions and the states of moisture absorbed in polymer composites. Chapter 3 identifies characterization methods for polymer-water interactions and shows how water state distributions are affected by damage. Chapter 4 investigates the effect of absorption and desorption history on the sensitivity to damage of polymer-water interactions, and explores damage-dependent hysteresis as a reliable means for damage detection. In Chapter 5, a method to quantitatively identify damage in polymer composites based on polymer-water interactions and damage-dependent hysteresis is presented; a machine learning based approach is applied in understanding the relationship between moisture content, extent of damage and relative permittivity. Chapter 6 investigates the effects of paint and coatings applied to polymer composites on the ability to detect damage using polymer-water interactions. Chapter 7 provides a general conclusion of the dissertation and proposes future research directions.

CHAPTER 2: LITERATURE REVIEW

2.1 Composite Materials

Modern advances in technology requires multi-functional materials with properties traditional metals, polymers, and ceramics do not possess. Hence, composite materials which combine desirable features of these materials are required. Composite materials are made up of a combination of two or more materials with different properties. The properties of these materials are often complimentary, resulting in a material having a combination of desired features. These features include strength, stiffness, insulating properties, electrical properties, thermal stability, affordability, and even bulk to occupy empty space. Composites can be found even in nature, with typical examples including wood and bone. Composites can be classified in various ways as shown in Figure 2 [4]:

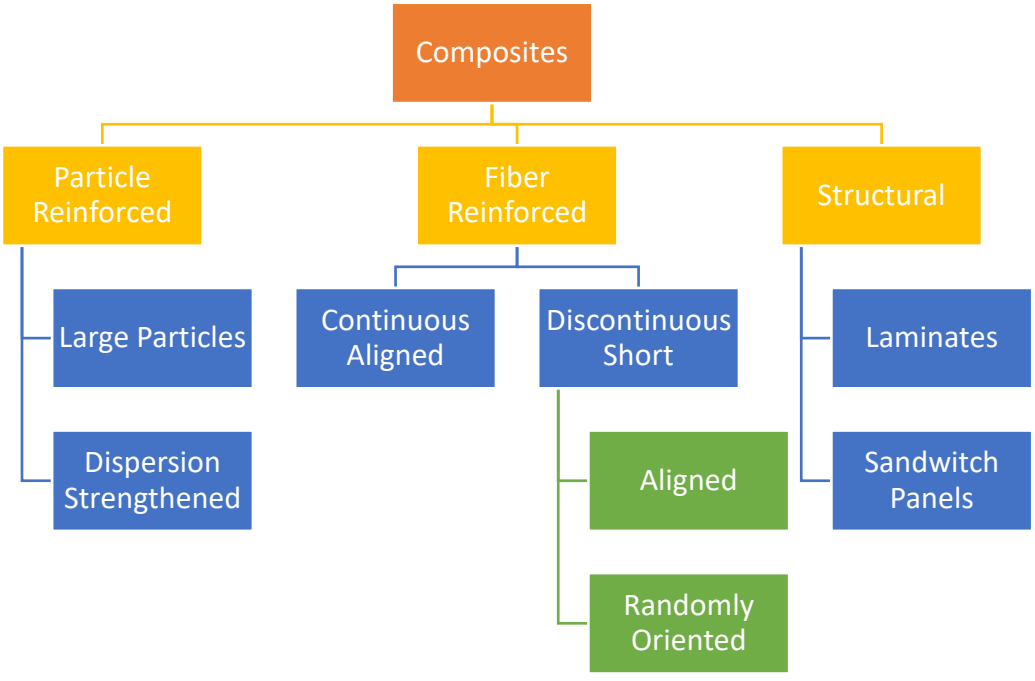

Figure 2: Classification of composites [4]

The focus of this work will be on structural laminates made from fiber reinforced continuous aligned composites. These composites are usually made up of a matrix material and reinforcement material. The matrix and reinforcement could be a metal, polymer, or ceramic material. The function of the matrix is to bind reinforcements together, transfer stresses to reinforcements, and protect reinforcements from mechanical damage. While the reinforcements are usually much stronger than the matrix, providing mechanical strength and stiffness to the composite.

2.1.1 Polymer Matrix Composites

Polymer matrix composites have a polymer based matrix which may be a thermoplastic or thermosetting polymer. The polymer matrix transfers load to fibers and prevents fiber buckling. Due to their good properties at room temperature, low production cost, and ease of production, polymer matrix composites have remained very attractive materials for a wide variety of applications including electrical, aerospace, marine, oil & gas, and civil infrastructure [5]. Meanwhile, complicated design techniques due their anisotropic nature, catastrophic failure, challenges in damage detection, and temperature limitations currently inhibit their widespread adoption.

Reinforcements

A wide range of reinforcements exist for polymer matrix composites. These are suitable for various applications and include glass, quartz, aramid, and carbon [6–8].

Glass: Glass fibers are widely used as reinforcements and are particularly attractive due to their relatively lower costs, electrical insulation, and non-attenuative properties for electromagnetic waves. Common types include: E-glass, S-glass, and quartz (crystalline form of glass), generally having a relatively higher density of ~ 2.5g/cc [9].

Carbon: Carbon reinforcements are very attractive in the aerospace industry due to their high strength, low density (~1.6 – 2.1g/cc), very low coefficient of thermal expansion (CTE), and corrosion resistance when paired with an appropriate resin [8]. While, their relatively higher cost, electrical conductivity, and strongly absorbing nature may pose challenges in certain applications.

Aramid: These are aromatic poly amide fibers, popularly known as Kevlar or Twaron. They could be low, intermediate, or high modulus fibers. They are the lowest density fibers (~1.5g/cc), and moderately priced between glass and carbon fibers. Unlike glass and carbon fibers, they have poor compressive strength but good tensile strength [7].

Matrix Resins

Thermosetting resins are widely used as matrices for polymer composites, with thermoplastic resins gradually increasing in popularity. While thermoplastics can be melted and reshaped, which is ideal for recycling, thermoset polymers cannot be reformed but have better mechanical and physical properties than thermoplastics. Thermosets are also easier to work with in processing into composites than thermoplastics. Commonly used thermoset resins include: epoxy, bismaleimide (BMI), polyimides, phenolic, and cyanate ester.

Epoxy: This resin is the most widely used in the aerospace industry, having a very good balance of properties such as high strength and stiffness, corrosion resistance, low density, and temperature stability. Epoxy resins are thermosetting polymers in which crosslinking occurs primarily through the reaction of an epoxide group. The basic chemical structure of the epoxy group is shown in Figure 3 (a) [10]. The type and properties of the epoxy could vary widely depending on the R and R' groups attached (see Figure 3 (a)). One of the most common commercially used epoxy resin is diglycidyl ether of bisphenol-A (DGEBA) shown in Figure 3 (b) [10]. Epoxy resins are cross-linked by reaction with hardeners. Amines and anhydrides are the most commonly used hardeners.

The most commonly used primary amine is diethylene triamine (DETA), see chemical structure in Figure 4. Epoxy is also hydrophilic in nature, with polar functional groups which interact with water molecules [11].

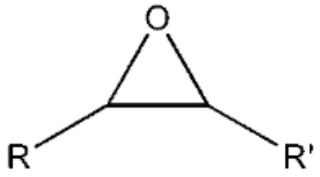

(a)

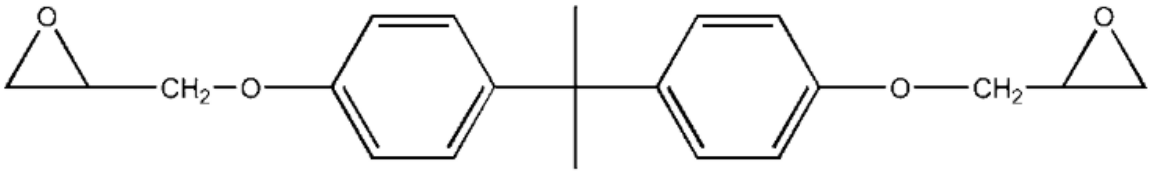

(b)

Figure 3: Epoxy — (a) Basic chemical structure (b) Diglycidyl ether of bisphenol-A (DGEBA) chemical structure *[10]*

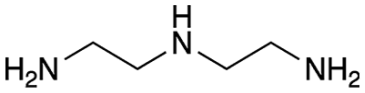

Figure 4: Hardener — Diethylene triamine (DETA) chemical structure

Bismaleimide (BMI): These are a class of thermosetting polyimide advanced resin, which have become popular for aerospace applications over recent years. This is due to their epoxy-like processing, stability at higher temperatures (up to 290 °C), and constant electrical properties for a wide temperature range [12]. Unlike epoxy, BMI is hydrophobic in nature. The general structure of BMI resin is shown in Figure 5.

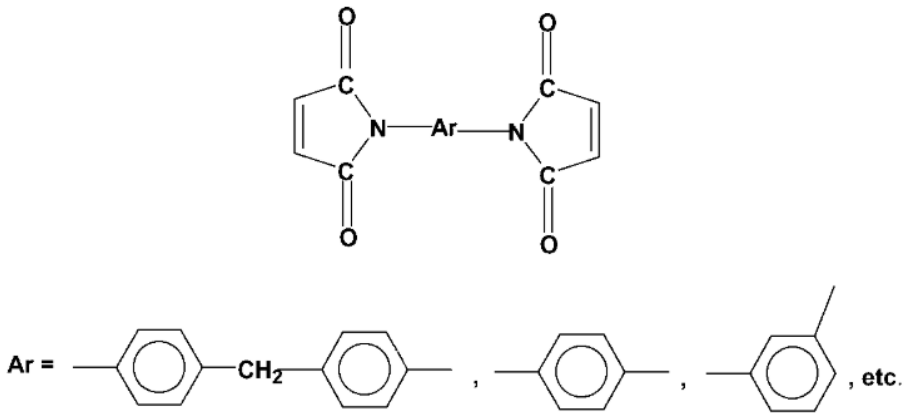

Figure 5: Bismaleimide (BMI) resin — general structure

2.1.2 Polymer Matrix Composite Fabrication

Fabrication techniques for polymer matrix composites include wet layups, vacuum layups, resin transfer molding, and use of prepreg. They generally involve various ways of combining the resin with the reinforcement before curing to make a part. High uniformity and low porosity are desired for polymer composite parts. Currently, best results are achieved by using prepreg and curing in an autoclave. Prepreg is a fabric which is supplied pre-impregnated with a resin in the uncured state; while, an autoclave is a pressurized oven. For flat laminates, the stacked prepreg can also be cured in a hot press as a substitute for an autoclave. To-date the hand lay-up of prepreg is still the most economical approach to produce the best quality parts of various sizes [13].

The various polymer composite fabrication techniques discussed have significant effects on the properties of the final laminate. Studies have shown that achieving a high fiber volume fraction and lower void fraction, not only produces a mechanically stronger laminate, but also results in a lower rate of moisture absorption and equilibrium moisture content [14]. This is due to the polymer matrix being the major source of affinity for moisture, unlike ceramic reinforcements [15]. Hence, fabrication technique could also be a major influence on moisture activity properties of a polymer matrix composite structure.

2.2 Moisture and Polymer Matrix Composites

2.2.1 Moisture Diffusion in Polymer Composites

Moisture is absorbed by polymer matrix composites in nearly all operating environments, due to the relatively small size of water molecules compared to polymer chains. Studies have reported as high as 6-7 wt. % moisture absorption in epoxy matrices [11,16], and over 2% moisture absorbed in polymer matrix composites [17]. This absorption is typically driven by traditional diffusion kinetics [18], polymer polarity [19,20], temperature [18], environmental humidity [16], and damage state of the material [21–24]. Ceramic reinforcements such as glass or carbon fiber do not absorb moisture [15], however, the fiber-matrix interface provides a preferential diffusion pathway for moisture ingress [25].

Numerous studies have been performed to understand the mechanisms of moisture diffusion in polymer matrix composite systems in an effort to map moisture content to material properties and performance. While most models simplify the interaction between penetrant (water) and host (polymer), several have accounted for more complex and realistic interactions. Among these are a dual-mode sorption model accounting for the presence of immobilization sites [15,26], a new hindered diffusion model extending the classical Langmuir-type and Fickian theories to consider the effects of both chemical and physical structure of polymeric composites [27,28], and modifications to the Fickian model to account for hygro-elastic relaxations and polymer–water interactions [29]. In general, the studies demonstrate the need for other considerations in predicting moisture absorption behavior in polymer matrix composites beyond the classical Fickian diffusion process due to the complexity of the polymer composite structure.

2.2.2 Adverse Effects of Moisture

Various adverse effects of moisture absorption on polymer composites have been reported in the literature. These include:

Plasticization: This involves structural changes to the polymer network that affects its glass transition temperature (T_g). The T_g of a polymer is particularly important because it determines the temperature above which the polymer changes from rigid and glassy to flexible and rubbery. This is used in determining the safe operating temperature of a polymer [30]. Moisture has been shown to reduce the T_g of polymers [16], making them unstable at lower temperatures.

Fiber-matrix debonding: Absorbed moisture has been known to attack the interfacial bond between the fiber reinforcement and the polymer matrix [15,25]. This leads to mechanical degradation of the adhesive and debonding of the fiber and matrix [15,31]. Since the matrix is responsible for transfer of load between fibers, this could cause localized stresses and degradation of global mechanical properties.

Hydrolysis: This is molecular degradation by breaking of polymer chains (chain scission) [32,33]. This is observed at higher levels of moisture uptake and leads to loss in mass of the polymer [24,34].

Other reported effects of absorbed water include micro-cracking and crazing, swelling, and internal stresses induced due to swelling [11,32].

Effects of Damage on Moisture Absorption

Damage in polymer matrix composites could be induced by localized impact, slowly growing cracks due to cyclic loads, generalized freeze-thaw, and degradation due to ultraviolet or elevated temperatures. These lead to physical damage in composite laminates which typically involves matrix cracks, debonding, and delamination that create relatively large voids within the

polymer matrix ranging from sub-micron scale to macroscale sizes [35]. These forms of damage have been shown to increases the diffusivity and equilibrium moisture level in polymer matrix composites [25]. This is primarily due to fractures creating alternative diffusion pathways within the polymer matrix and the formation of internal voids, providing sites for additional moisture retention [24,36,37].

2.3 Free and Bound States of Absorbed Water

Studies have shown that water absorbed in polymer composites may exist in one of two states. The first is the 'free' state, where the water molecule exists without any physical constraints or interaction with the polymer matrix. The other is 'bound' state, where it experiences physical constraints or secondary bonding interactions with the polymer matrix (see Figure 6) [11,38–40]. These secondary bonding interactions may vary in strength and include highly restrictive hydrogen bonding between water molecules and polar functional groups within the polymer network, dipole-dipole attractions, and weak van der Waals attractions [41]. The fact that water exists in the free or bound states in a polymer network is well-known and widely recognized in a number of industries where moisture absorption tends to be critical or problematic, e.g. food [42,43], pharmaceuticals [44], building & construction [45–47], cosmetics [48–50], aerospace radome [51,52], and biomedical industries [53,54].

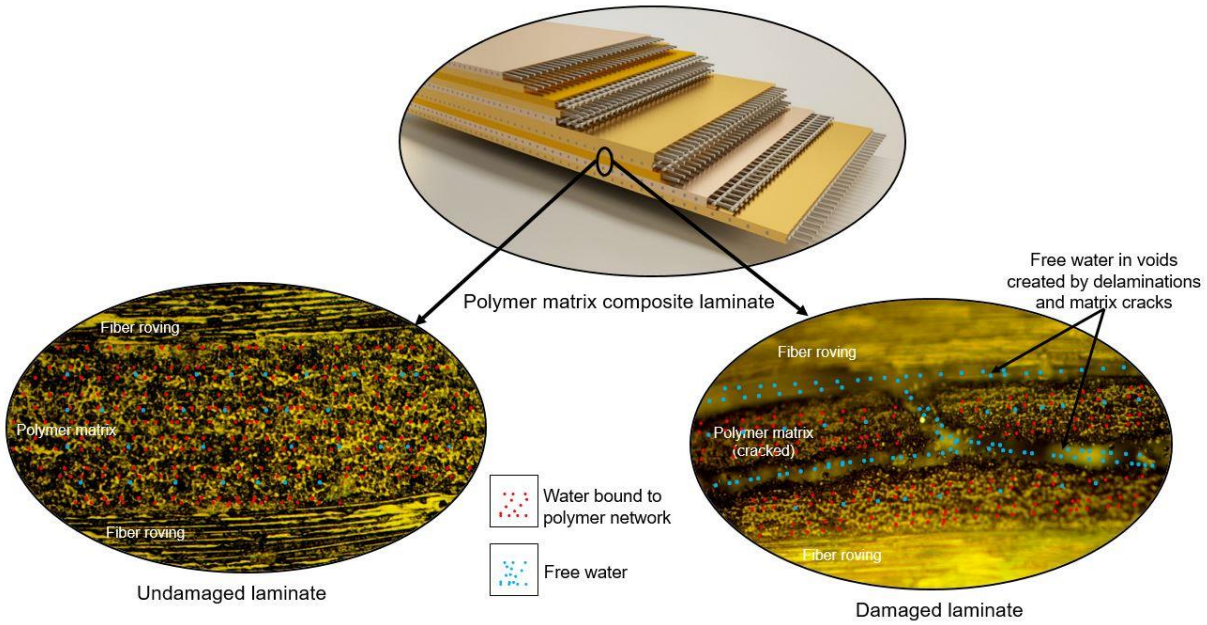

Figure 6: Difference in undamaged and damaged polymer matrix composites when moisture-contaminated.

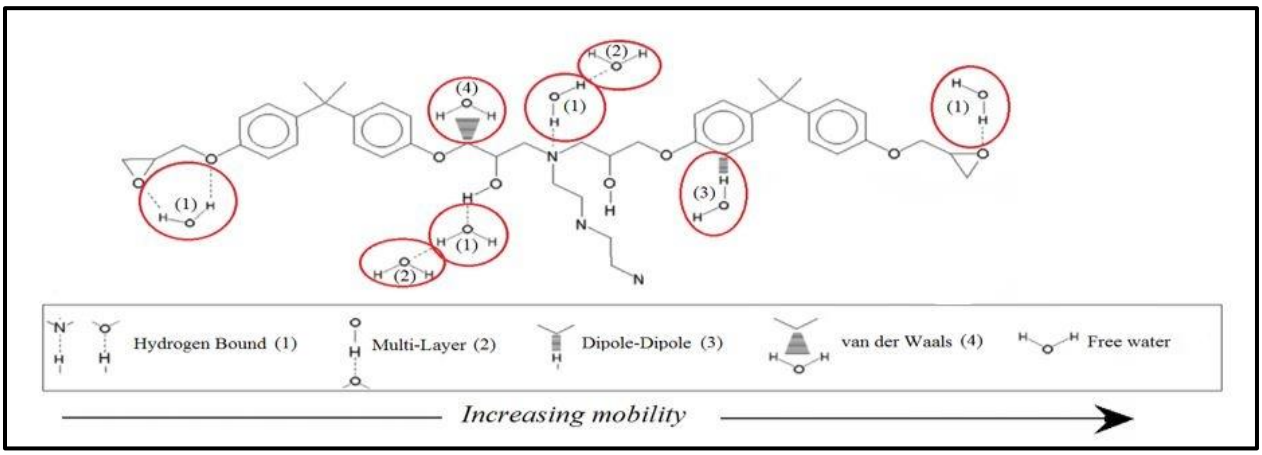

Figure 7: Types of polymer-water interactions (adapted from fig. 1 of ref. [41])

2.3.1 Characterizing the State of Absorbed Water

A review of published literature shows that free and bound water has been characterized via several spectroscopic techniques and analysis methods. These techniques include gravimetric moisture uptake [55,56], nuclear magnetic resonance [46,50,56], infrared spectroscopy [11,57],

dielectric spectroscopy [58], differential scanning calorimetry [41,53], heat of fusion of ice method [59], and molecular dynamics simulations [20,60,61] (see Figure 8). In previous studies, infrared spectroscopy has been applied in monitoring the effect of moisture uptake on an epoxy system [11,57,62]. These studies primarily investigated the effect of moisture contamination on mechanical properties and glass transition temperature (T_g), concluding that bound water is responsible for degradation of mechanical properties and plasticization in epoxies—leading to reduction in T_g [11,57,62]. The effect of moisture content on the distribution of free and bound water has also been studied using infrared spectroscopy, providing evidence of free water occupying micro-porosities and bound water interacting with the polymer matrix [11,39,40]. In studies by Musto et. al, methods were developed to perform quantitative analysis between the 6000 and 8000 cm^{-1} region of the infrared spectra—within which O-H activity is prominent. These were applied successfully in estimating the relative concentration of free and bound water absorbed into an epoxy specimen [11].

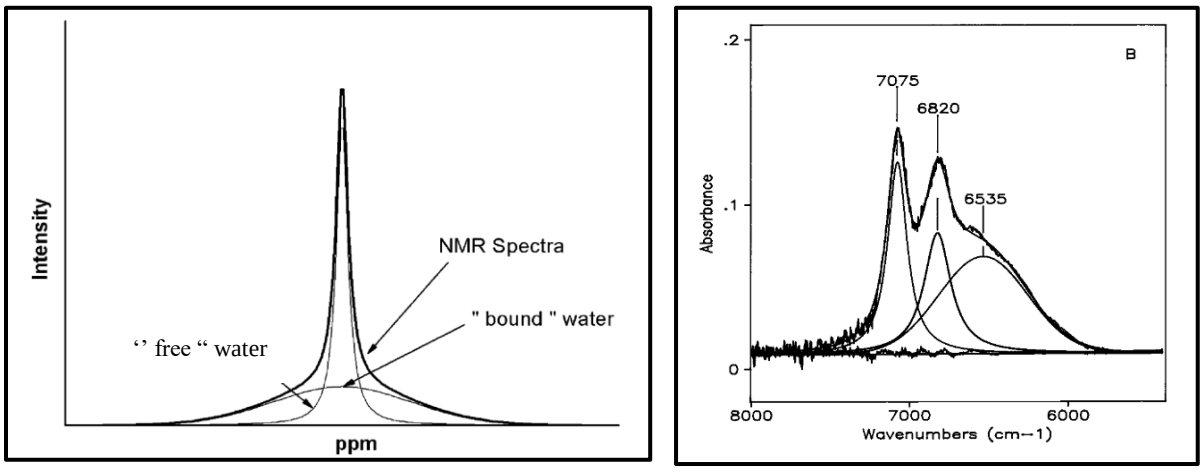

(a) (b)

Figure 8: Free and bound water characterized using (a) Nuclear Magnetic Resonance spectroscopy (adapted from fig. 1 of ref. [56]) (b) Near-infrared spectroscopy (adapted from fig. 8 of ref. [11])

Infrared Spectroscopy

Infrared spectroscopy is a well-developed and widely used technique; it provides the ability to qualitatively and quantitatively characterize water in both of its possible states. Infrared spectroscopy involves the use of light between 780 and 50000 nm (12800 – 200 cm^{-1}) in the electromagnetic spectrum [63]. At specific frequencies within this range, inter-atomic bond vibrations absorb energy from incident light at their resonant frequencies. In spectroscopic applications, the infrared spectra is divided into 'near' and 'mid' (NIR and MIR) frequency/wavelength ranges. A number of bond pairs and functional groups have their fundamental vibrational frequencies in the (MIR) region (<4000 cm^{-1}). Peaks at frequencies in the near-infrared region (>4000 cm^{-1}) are usually overtones and combinations of fundamental frequencies in the mid-infrared range [11,64]. Although the existence of many overtones and combination bands of fundamental vibrations make identifying peaks more complicated, great progress has been made in understanding the NIR region and its application in qualitative and quantitative analysis. Further general details on infrared spectral analysis is outside the scope of this work but is covered extensively in a number of published literature [65–67].

In the mid-infrared region, the influence of vibrations of O-H bonds resulting from symmetrical stretching, asymmetrical stretching, and bending, cover a wide band between 3800 and 2800 cm^{-1} [11,68]. The wide frequency range results from the influence of secondary bonding interactions—primarily hydrogen bonding in water-water and water-polymer pairs. These interactions cause a downward shift in resonance frequency of the water molecule's O-H bonds [11,68]. The magnitude of this shift is proportional to the strength of interaction, governed by the degree of electronegativity difference between atoms making up the polar functional groups involved in the hydrogen bond [68]. These groups could be polar functional groups within the

polymer network which have significant hydrogen bonding effects, or other water molecules with less severe effects. In the near-infrared region between 8000 and 6000 cm^{-1} peaks can be identified which are overtones or combinations of fundamental O-H vibrations in the mid-infrared region (see Figure 9) [69]. However, in this region the peaks are more distinctly separated and easier to analyze, making NIR the preferred region for analysis of water state [11].

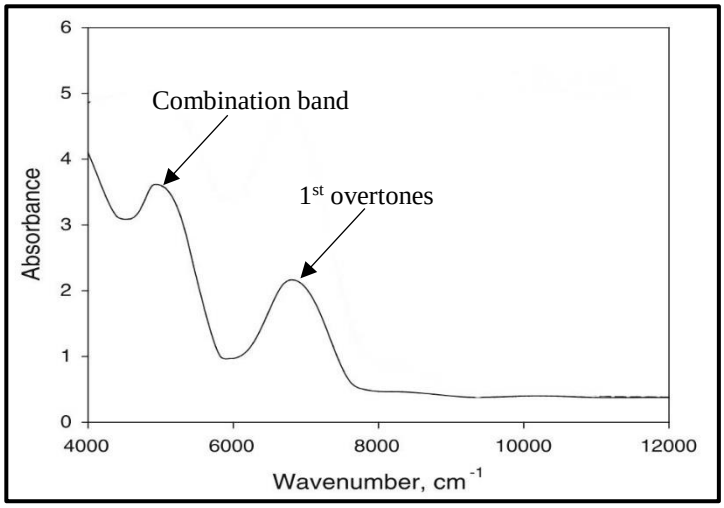

Figure 9: Near-infrared spectra for water (adapted from fig. 1 of ref. [69])

Dielectric Spectroscopy

Microwave frequency dielectric properties are very sensitive to moisture due to the dipolar nature of the water molecule. At these frequencies, the dipolar rotational polarization mechanism becomes active in an applied electromagnetic field; this dominates contribution to dielectric properties compared to other active atomic and electronic polarization mechanisms [70]. Depending on its state, absorbed moisture responds to an applied electromagnetic field in different ways. When in the free state, without any secondary bonding interaction with the polymer network, water molecules rotate with a changing electromagnetic field without any restriction. In the bound

state, water molecules are subject to interactions with the polymer network that impose various degrees of restriction to its dipolar rotation [41].

The ability of a water molecule to rotate in an applied electromagnetic field is closely related to its dipole moment, which is in turn closely related to the real part of dielectric constant—relative permittivity. Free water—without restriction to rotation—has a relatively high relative permittivity (~80) compared to firmly bound water (~3) [71–73]. Bound water has significantly lower relative permittivity that varies according to the nature of the imposed restriction to rotation [52]. These restrictions range from weakly interacting van der Waals forces and dipole-dipole attractions to highly-restrictive hydrogen bonding [41]. Therefore, the bulk relative permittivity of a polymer composite material consist of contributions from the polymer matrix, reinforcing fibers, bound water, and free water [52]. All of these possess relative permittivities which are relatively low except for free water having a significantly higher relative permittivity. Hence, very small quantities of absorbed moisture in the free state within the composite material would cause a measurable increase in relative permittivity.

Microwave frequency dielectric properties can be characterized in several ways which vary in accuracy, complexity, specimen material type, and applicable frequency range [74]. These include transmission line, free space, and resonance methods. The resonance method is the most accurate of these and involves the use of resonators and cavities, one of which involves the use of a split post dielectric resonant cavity shown in Figure 10 [52,74]. By monitoring the resonant frequency and its quality factor within this cavity, dielectric properties (relative permittivity and loss tangent) can be calculated [75]. The resonant frequency is highly sensitive to temperature, humidity, as well as the nature and volume of foreign bodies introduced into the resonant cavity [36].

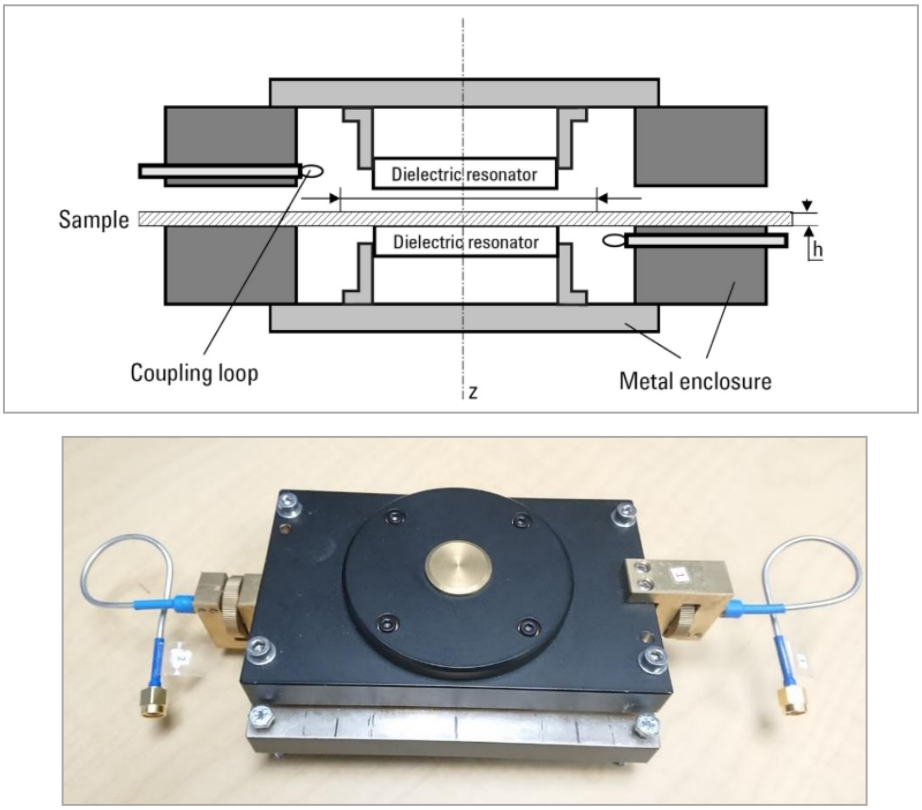

Figure 10: Cross-section and external image of a split post dielectric resonator. [52]

2.4 Nondestructive Examination of Polymer Matrix Composites

The primary objective of polymer matrix composite nondestructive examination techniques is to find and quantify voids and delaminations, determine porosity, and in a few cases identify debonding and micro cracks. These are generally referred to as hot spots. Typical lower limits of generally detectable defects range from 3 mm to 25 mm.

A brief description of some current NDE techniques for polymer composites is provided below:

Ultrasonic and Phased Array Ultrasonic (PAUT)

Involves using single or multiple ultrasound sensors (in the case of PAUT), which propagate signals (mechanical waves) usually within the 0.5 kHz and 10 MHz frequency range and measure transmission, reflections, or back scattering of mechanical waves in different

directions to create an image [76,77]. Time of flight is usually calculated and various modes such as A-scan, B-scan, C-scan, and D-scans can be applied to obtain various details. Usually a liquid such as water or oil is needed for acoustic coupling, but recent advances are enabling air coupling [78]. This is the most widely used inspection technique for polymer composites.

Strengths: Has no material limitations, and provides quantitative data.

Weaknesses: Can only characterize damage at and above the delamination phase, difficulty in detecting flaws aligned with the direction of wave propagation, and a coupling liquid may be required.

Radiography

These involve the use of x-rays, gamma rays and neutrons for internal imaging. In conventional x-ray radiography, an x-ray sensitive film is used to form a two dimensional projection image showing the relative attenuation, absorbance, or transmission of the signal by the various parts of the structure [76,77]. While x-ray computed tomography involves rotating the part and taking multiple images which can be stitched together to form a 3D image. Neutron imaging is a complimentary technique to x-ray imaging; it uses a neutron source in-place of an x-ray source. It is very sensitive to hydrogen containing compounds such as water. The neutrons penetrate deeper than x-rays and can be used for imaging behind heavy metals such as lead, which is not possible with x-rays [79].

Strengths: Has no material limitations, provides quantitative data, can characterize damage at sub-micron scale levels, and can provide 3D data.

Weaknesses: Safety issues surrounding radiation, and more suitable for laboratory based applications.

Shearography

This technique involves monitoring the behavior of a polymer composites surface using lasers, then exciting the surface by light, heat, or pressure. In- and out-of-plane displacement variations on the surface layer due to the excitation are then tracked. Strain fields are computed, and the location of sub-surface defects are determined from anomalies in strain responses [76,80].

Strengths: Has no material limitations, rapid wide area inspection capability, provides quantitative data, and no contact with material required.

Weaknesses: Limited to flaws close to the surface, and more suitable for laboratory based applications.

Infrared Thermography

In this technique, the surface of a polymer composite part is excited by optical radiation, electromagnetic stimulation, or ultrasonic mechanical waves to generate mild heating. The heat dissipation is then monitored using an infrared camera. Anomalies in the heat dissipation pattern is predictive of internal damage. It is used to detect flaws located near the surface [77]. The ability to detect damage effectively using this method is highly dependent on the thermal conductivity of the material [77].

Strengths: Has no material limitations, provides quantitative data, and no contact with material required.

Weaknesses: Limited to flaws close to the surface, only capable of detecting damage at and above the debonding phase.

Microwave

Involves the use of electromagnetic waves within the 1-50 GHz frequency range. It takes advantage of variations in relative permittivity within the structure in predicting damage. The

technique is limited to low-conductivity dielectric materials, due to reflection of microwaves by conductive materials. Variations of the technique are applied as ground penetrating radar and millimeter wave [77]. It is used widely in oil and gas applications such as pipelines due to the wide adoption of glass reinforced polymer composites due to their low cost and corrosion resistance.

Strengths: Ideal for thick composite structures, provides quantitative data, and no contact with material required.

Weaknesses: Limited to non-conductive materials only, capable of detecting damage at and above the delamination phase.

Acoustic Emission

This involves listening for ultrasonic transient elastic waves in a material, which are generated with damage progression. High energy mechanisms such as delamination and fiber breakage are captured, as well as low energy mechanisms such as matrix cracks [76].

Strengths: Capable of sub-micron scale damage detection, has no material limitations, and capable of real-time damage monitoring.

Weaknesses: limited ability to quantify localized damage, and mechanical loading is required.

The performance of these and other less widely used nondestructive examination techniques have been reviewed in a number of previous studies [76,81–84]. While some success has been demonstrated over the years at the macroscale, damage detection at sub-micron scales remains a challenge [35,76]. Other challenges include the inability to detect flaws of specific orientation, capture combined environmental-mechanical effects, detect damage beyond a certain depth, limitations to materials of specific types, and system complexity—requiring a highly skilled operator [77,81,82].

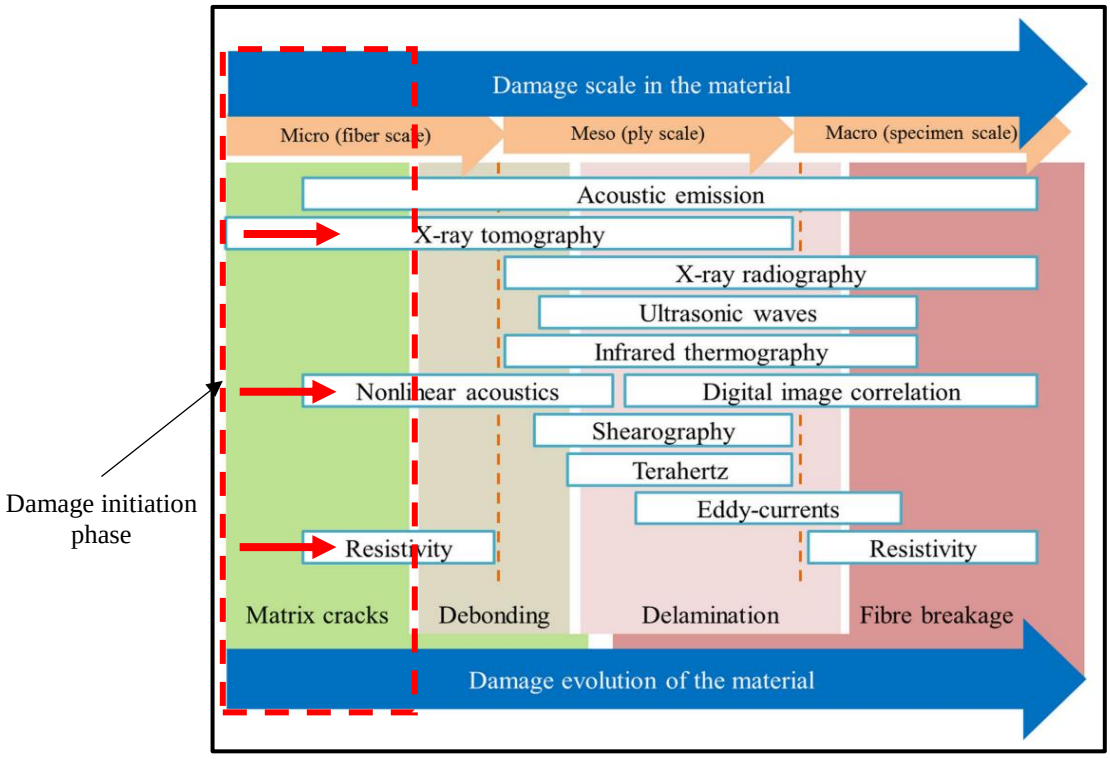

Figure 11: Nondestructive examination techniques for polymer matrix composites (adapted from fig. 4 of ref. [76])

CHAPTER 3: CHARACTERIZING POLYMER-WATER INTERACTIONS AND INVESTIGATING ITS SENSITIVITY TO DAMAGE

3.1 Rationale

Over the past two decades, there has been an increase in outdoor applications of polymers and their reinforced composites in electrical, aerospace, marine, oil & gas, and civil infrastructure applications. These applications exploit the high strength-to-weight ratio, corrosion resistance, insulating ability, and desirable dielectric properties that typically drive the adoption of polymer composites [85,86]. However, outdoor applications further complicate efforts to predict long-term performance and service life of polymer composites, an already difficult endeavor even in tightly controlled environmental conditions. Not only are these composites subject to continuous environmental loading such as thermal, moisture, and ultraviolet degradation, they are also prone to damage from hail, debris, and other potentially damaging low-velocity impacts which significantly reduce their residual strength [87]. The unpredictability of damage from these sources requires the use of inspection methods that can identify damage in safety-critical structures prior to catastrophic failure. Simple, reliable, and accurate detection of unexpected non-visible damage initiation and progression partially alleviates concerns associated with predicting performance and service life for polymer composite structures operating in complex environments. However, non-destructive detection of damage in polymer composites remains a challenge.

Damage characterization and non-destructive examination (NDE) methods for ascertaining the structural integrity of polymers and composite materials lag behind methods for their metal counterparts in accuracy, flexibility, cost, and simplicity. Methods that have been evaluated for use in polymers and polymer composites include visual inspection, ultrasound, infrared thermography, x-ray radiography, x-ray computed tomography, electromagnetic methods, acoustic

emission, acousto-ultrasonic, fiber-optic laser-ultrasound, and shearography, among others [35,76,81–83,88,89]. These methods have proven moderately successful in characterizing damage but have significant limitations. In general, they lack the ability to capture combined environmental-mechanical effects, characterize damage below the micron scale, or capture chemical changes that may act as precursors to physical damage during the early stages of damage initiation and progression. The ubiquity of moisture in outdoor environments, either through precipitation or humid air, is generally (and correctly) viewed as a contributing factor in performance degradation over time [17,51,90]. However, the presence of low-levels of moisture in composites that operate in outdoor environments may also enable non-destructive identification of small-scale physical or chemical damage due to the associated change in behavior of nearby water molecules.

Moisture within a polymer network exists in different states based on the nature of its secondary bonding interactions with the polymer network. These states have different effects on the host polymer. For example, plasticization is believed to occur as a result of absorbed moisture that interacts directly with the polymer network via secondary bonding mechanisms [11,30]. This type of water is generally referred to as moisture in the 'bound' state. Furthermore, in polymer composite radomes, water molecules residing in micro-voids that have no secondary bonding interactions with the polymer network are a significant contributor to radar performance degradation due to the associated signal attenuation. Such moisture is regarded as being in the 'free' state [51,52]. These two states of absorbed moisture have been documented extensively by various researchers using gravimetric moisture uptake behavior and numerous characterization tools [11,41,56,61,85,91,92]. Nuclear Magnetic Resonance (NMR) spectroscopy has been applied in studying moisture absorption behavior in polymers, leading to isolation of the effects of free

and bound components of absorbed moisture [56,93]. In other studies, molecular dynamics simulations, dielectric relaxation spectroscopy (DRS), differential scanning calorimetry (DSC), and vibrational (infrared) spectroscopy have successfully identified bound and free water as distinct absorbed water states [11,20,41,58,61]. Musto et al. performed vibrational spectroscopic analysis on epoxy specimens using mid and near infrared spectroscopy (MIR and NIR). In both cases, contributions from bound and free water were isolated and spectral ranges characteristic of specific types of hydrogen bonding interaction with the water molecule were identified. More importantly, a method to quantitatively estimate the fraction of free and bound water in a polymer specimen by means of NIR spectroscopy was developed [11].

Free and bound water also differ in their response to an applied electromagnetic field. Water, a dipolar molecule, polarizes by rotating in response to an applied electromagnetic field [73,92]. The polarizing tendencies of a material in an electromagnetic field can be described by its dielectric properties. These are usually defined in terms of the complex dielectric constant, comprising the relative permittivity (real part of dielectric constant) and loss tangent (ratio of imaginary to real part of dielectric constant). The ability of a material to polarize in an applied electromagnetic field is closely related to its relative permittivity [38,94], while its relative permittivity is partly dependent on the frequency of the applied electromagnetic field [38,70]. At different frequency ranges, certain mechanisms tend to dominate polarization and hence dielectric contribution as shown in Figure 12 [95].

Within 1 to 10 GHz (microwave frequency range), the dipolar rotational polarization mechanism dominates dielectric contribution [70,72]. Hence, dipolar molecules such as water are able to rotate with the changing electromagnetic field. The effects of other active polarization

mechanisms within the microwave range are minimal, while the larger ionic particles become inactive [70,72].

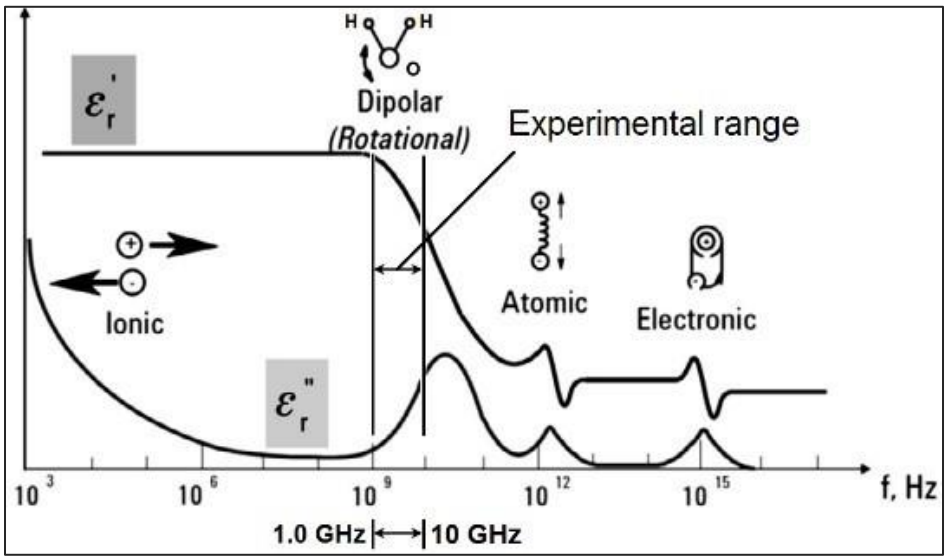

Figure 12: Changes of Real (ε'_r) and imaginary (ε''_r) parts of complex permittivity with frequency [95]

However, the degree of polarization achieved by a water molecule in a polymer network depends on the nature and extent of rotational restriction resulting from physical constraints and secondary bonding interactions with the polymer network [92]. Chemically, water interacts with the polymer network in various ways, including firmly-bound direct hydrogen bonds or less restrictive interactions such as multi-layer, dipole-dipole, or van der Waals forces [41,61]. Physically, restrictions also exist due to confinement of water molecules in small cavities such as nano-voids [96,97]. In such scenarios, water is considerably more restricted in its ability to rotate with an oscillating electromagnetic field. Water occupying micro or macro-voids and existing without interactions, however, is free to rotate. Therefore, the relative permittivity of free water within this frequency range is significantly higher (~80) [71], compared to that of firmly bound

water (~3) [72], while the relative permittivity of water in the intermediate states (e.g. van der Waals or multi-layer water) will fall somewhere between these two extremes [52,98]. Therefore, the bulk relative permittivity of a moisture contaminated polymer matrix composite is not only a function of the relative permittivity of the composite and amount of water present, but also the state of that water. The average state of a water molecule within the polymer network is dependent on the physical and chemical state of the polymer itself, which governs how the water interacts with the polymer. Therefore, changes in the absorbed water state may provide valuable insights regarding the polymer's physical and chemical state via analysis of the changes in the effective relative permittivity.

While near-infrared spectroscopy and microwave-frequency relative permittivity have been applied to polymer matrix composite damage detection in different ways [38,99,100], they have not been based on analysis of water interaction with the polymer. Also, near-infrared spectroscopy has been applied in detection of ultraviolet degradation and thermal damage in polymer matrix composites [99,100], but not in detection of physical damage.

The purpose of this study is to demonstrate the feasibility of a non-destructive evaluation method capable of identifying damage in polymer composites by analyzing the distribution and state of absorbed water molecules. The state and distribution of water is governed in part by the formation of multi-scale voids within the composite resulting from physical damage [101].

3.2 Materials and Methods

3.2.1 Test Materials

An epoxy/glass fiber laminate typical of the aerospace industry was used to fabricate test specimens. The matrix was an epoxy resin, trade name Hexcel F-161. The reinforcement was an 8-harness satin weave glass fabric, style 7781. A 304 x 355 mm laminate was formed from 16 plies

of prepreg, ensuring alignment of 0° and 90° directions for all plies. The laminate was cured in a hot press at 386 kPa; it was heated from room temperature at an average rate of 10 °C/minute to 180 °C. The laminate was held at 180 °C for 2 hours, pressure was then released, and the laminate was cooled at an average rate of 2 °C/minute to room temperature. This produced a laminate with an average thickness of 2.9 mm. Individual 54 mm diameter circular test specimens were cut from the larger panel using a diamond-tipped hole saw. This shape and size was necessary in order to meet both NIR spectroscopy and dielectric test specimen geometry requirements. In accordance with ASTM D3171 [102], laminate properties of 5 dried and undamaged specimens were obtained by means of resin burn-off. This was achieved in a high-temperature furnace maintained at 800 °C until elimination of all epoxy residue. Pre- and post-burn weight measurements allowed the estimation of resin, void, and fiber content. Laminate properties are provided in Table 1.

Table 1: Average epoxy/glass fiber laminate properties

Property	Mean (%)	Standard Deviation (%)
Fiber volume fraction	62.3	1.5
Resin volume fraction	32.3	1.1
Void volume fraction	5.4	0.7

3.2.2 Sample Preparation and Impact Setup

Circular specimens were dried in a vacuum oven at 65 °C until a stable weight was achieved according to ASTM D5229 [103]. After drying, low velocity out-of-plane impact was applied at the center of the test specimens, with the aim of inducing damage in the form of matrix cracking, fiber/matrix debonding, and delaminations in the laminate [104]. This was achieved using a drop tower equipped with a double-column impactor guide mechanism and a crosshead-mounted hemispherical striker tip of radius 9.4 mm, having a total drop-weight of 4.29 kg. The specimen was firmly secured within two steel fixture plates of thickness 3 mm, with circular 35 mm diameter

cut-outs. Impacted specimens were positioned concentrically around the cut-outs, ensuring impact at the center of the specimen. The setup was designed to simulate low velocity hail impact on an in-service laminate. Energy levels chosen were expected to generate damage that would not be visibly discernible when paint has been applied on the laminate. The amount of damage induced was varied by adjusting the crosshead height prior to drop, changing its potential energy. Four specimens each for three groups at 0 (undamaged), 3 Joule, and 5 Joule impact energies were created.

3.2.3 Moisture Contamination

Gravimetric, dielectric, and NIR data were recorded immediately prior to impact and immediately post-impact. Test specimens were then immersed in deionized water and maintained at 25 °C using a constant-temperature water bath. Specimen weights were measured using a high precision analytical balance. Specimen data was collected periodically over a 3-month period. At each measurement, gravimetric, dielectric (relative permittivity), and NIR absorbance data were recorded. Specimens were first carefully dried using a lint-free cloth and then maintained at ambient conditions for approximately 20 minutes. This eliminated the effects of surface moisture and resulted in a reduction of moisture loss rate from 0.23 mg/min within the first 5 minutes, to a fairly stable 0.03 mg/min after 20 minutes; this behavior was consistent and helped minimize uncertainties across measurements.

3.2.4 Optical Microscopy

Micrographs were obtained using a Nikon Eclipse LV150N optical microscope coupled with a vertically mounted CCD camera. Using a wet diamond-tipped saw, undamaged and 5 Joule damaged un-immersed specimens were cut along an axis through the impact location as shown in Figure 13. The cut surfaces were hand polished in several steps using silicon carbide sandpaper of

increasingly fine grit, from 400 to 3000. Images were taken at 10x and 20x magnification, while examining the damaged and undamaged specimens.

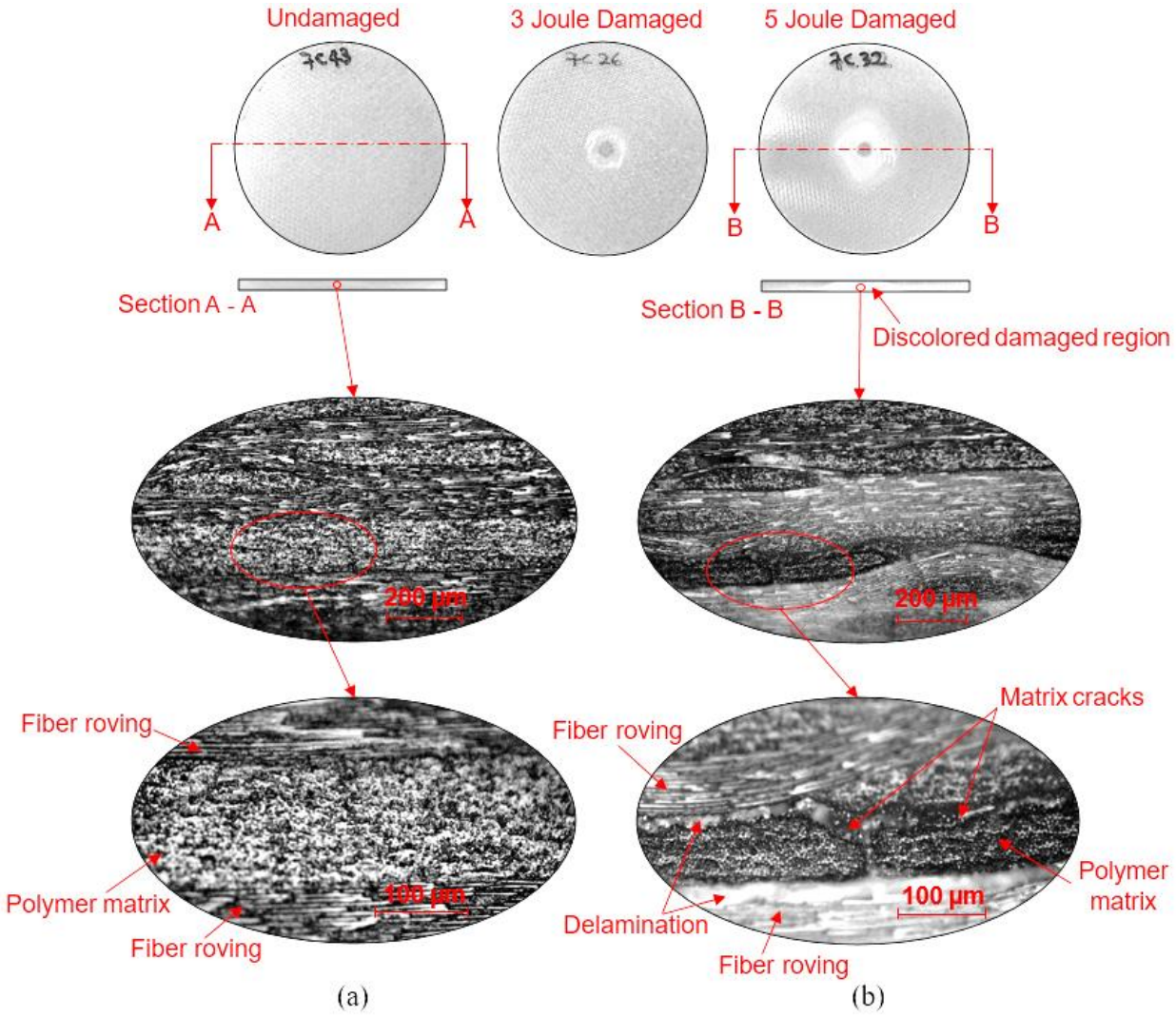

Figure 13: Sections for micrographs through specimens of (a) undamaged and (b) damaged laminates resulting from a 5 Joule impact

3.2.5 Near-Infrared Spectroscopy

The NIR spectra was obtained from a FOSS 6500 NIR unit equipped with a spinning sample cup module capturing diffuse reflectance from the specimen. The NIR unit produced scans

of the infrared spectra from wavelengths of 400 to 2500 nm (25000 to 4000 cm^{-1}) in steps of 2 nm. The wavenumber (cm^{-1}) unit is generally used in spectral analysis and will be adopted in this study. The unit sampled 32 random points at the center of the specimen within the aperture limits of the device, producing an average of these as the recorded spectrum for each scan. The specimen was scanned in this way three times, with an average of the three scans taken as the final spectra for each test.

To deconvolute the relevant spectral range into component peaks, a mixed Gaussian-Lorentzian function was adopted to model each peak [11]. Equation 1 gives this mixed function.

$$f(v) = (1 - L)\, H \exp[-\left(\frac{v - v_o}{w}\right)^2 (4\, In\, 2)] + L \frac{H}{4\,(\frac{v - v_o}{w})^2 \,+\, 1} \qquad (1)$$

Where

- v is wavenumber (independent variable)
- v_o is peak mean wavenumber
- H is peak height
- w is full width at half height (FWHH)
- L is fraction of Lorentzian character

A model spectra consisting of a combination of the appropriate number of peaks within that spectral range was fitted to the original spectra by applying an algorithm which minimizes the sum of squared error when the model is compared to the measured spectra. This was implemented by using a MATLAB® script to vary the four parameters (v_o, H, w, L) from Equation 1; these determine the shape and position of each peak. The peak combination that provided the closest model fit to the measured spectra was selected. Figure 14 shows a typical measured spectra within the range of interest, deconvoluted into its 3-peak model spectra.

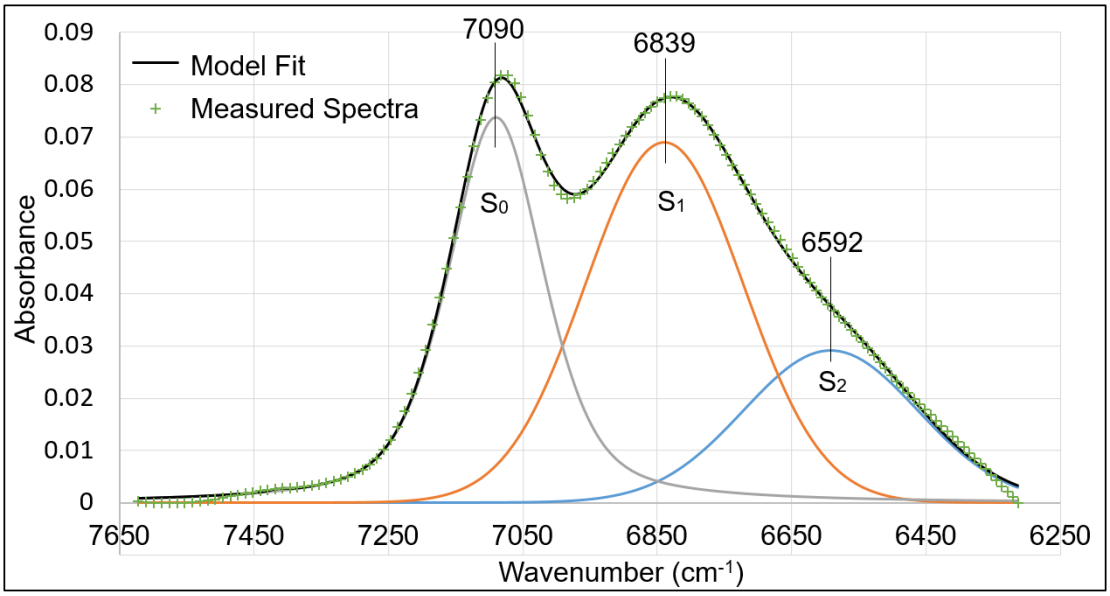

Figure 14: Typical curve fitting for water spectra of epoxy/glass fiber composite at 0.8 % moisture showing 3-peak model within spectral range 6250 to 7650 cm-1.

The area under each peak was then used to calculate the relative concentrations of the various water species according to Equation 2, similar to the methodology adopted in a previous study by Musto et. al. [11]. In previous studies, S_0, S_1, and S_2 were designated as different hydrogen bonding states of water, where the subscripts indicate the number of hydrogen atoms in the water molecule participating in external hydrogen bonding [11,41,105]. The approximate locations of the S_0, S_1, and S_2 peaks are shown in Figure 14.

$$\frac{C_x}{C_{total}} = \frac{A_x}{(A_0 + A_1) + \frac{a_x}{a_2} A_2} \tag{2}$$

Where

x Number of hydrogen atoms participating in hydrogen bonding (0, 1 or 2)

A_x Peak area for S_x species

C_x Concentration of S_x species

C_{total} Concentration of all species

a_x Integrated absorption coefficients for x species

Equation 2 holds for x = 0 and 1 due to similarities in integrated absorption coefficients [11]; however, a similar expression can be derived for x = 2.

By using this process, relative concentrations of non-hydrogen bonded water species (S_0), self-associated water-water hydrogen bonded species (S_1), and water-polymer (polar sites) hydrogen bonded species (S_2), were obtained via NIR spectroscopy for all the specimens at different moisture-contaminated conditions [11].

3.2.6 Microwave Relative Permittivity Measurement

To accurately measure dielectric properties at microwave frequencies, a split post dielectric resonator (SPDR)—fabricated by QWED© of Warsaw, Poland—was coupled with an Agilent programmable vector network analyzer (VNA) as shown in Figure 15. This setup enabled measurement of bulk relative permittivity and tracking of small changes in relative permittivity on the order of 10^{-3}. The SPDR utilizes low loss dielectric materials in its construction, allowing the device to resonate at a specific frequency with a very high quality factor (Q-factor). Measurement uncertainty using this setup is 0.3 % in relative permittivity, while loss tangent can be measured with resolutions as low as 2 x 10^{-5} [106]. To calibrate the 2-port system, the scattering parameters S11, S22 and S21 were adjusted. These represent the magnitudes of reflected signal at port 1, reflected signal at port 2, and the signal transmitted from port 1 to port 2 of the SPDR respectively. These were adjusted manually by carefully changing the location of the coupling loops within the resonant cavity. The minimum gain in S11 and S22 were adjusted to be equal prior to adjusting

the gain in S21 to -40 dB. For the -3 dB bandwidth calculation, values for resonant frequency and quality factor of the empty resonator were first recorded at 2.48 GHz. Insertion of the specimen under test into the resonant cavity of the SPDR causes a shift in resonant frequency measured using the VNA [36,107]. This resonant frequency shift is used to calculate the real part of relative permittivity (ε'_r) of the specimen according to Equation 3 [106].

$$\varepsilon'_r = 1 + \frac{f_0 - f_s}{h\, f_0\, K_\varepsilon(\varepsilon'_r, h)} \tag{3}$$

Where

f_0 is resonant frequency of empty SPDR

f_s is resonant frequency with the dielectric specimen inserted

h is sample thickness

K_ε is a function of ε'_r and h, documented in a table unique to each SPDR, provided by the manufacturer

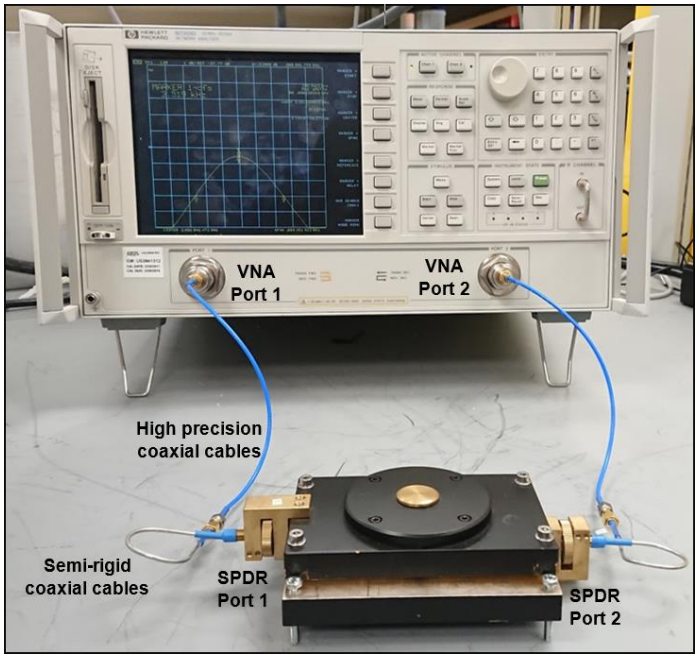

Figure 15: Split post dielectric resonator (SPDR) coupled to a vector network analyzer (VNA)

3.3 Results

3.3.1 Optical Microscopy

Micrograph sections from the undamaged and damaged specimens obtained via the optical microscope described in Section 3.2.4 are shown in Figure 13. A typical undamaged specimen viewed by the naked eye has a uniform light green color, while its micrographs show complete and uniform bonding between the fiber roving and polymer matrix. In contrast, unpainted damaged specimens exhibit a white discoloration at and around the impact point. This discoloration was similarly discernable on Section B-B cut through the impact point, with its radius increasing with depth. This is consistent with results reported from previous studies [35]. Micrographs for the damaged specimen show the discoloration to be representative of the damaged area. Within this damaged region, instances of damage-induced new free volume were identified as illustrated in Figure 13.

3.3.2 Gravimetric Moisture Uptake

The gravimetric moisture uptake data is presented in Figure 16, where moisture content by weight is plotted against the square root of immersion time. The moisture uptake profiles show a generally linear trend when the early data points of the damaged specimens are excluded. The initially steeper slopes for both damaged specimens likely indicates the preferential diffusion of moisture to occupy voids created by delaminations and matrix cracks within the laminate, both resulting from impact [35,108,109]. The plots also show an increase in the rate of moisture uptake with increasing damage—a result of the increase in potential diffusion pathways in the damaged areas. Gravimetric analysis is a useful tool but is incapable of identifying differences in local moisture concentration compared to bulk water content. Thus, its utility as a damage characterization method is very limited.

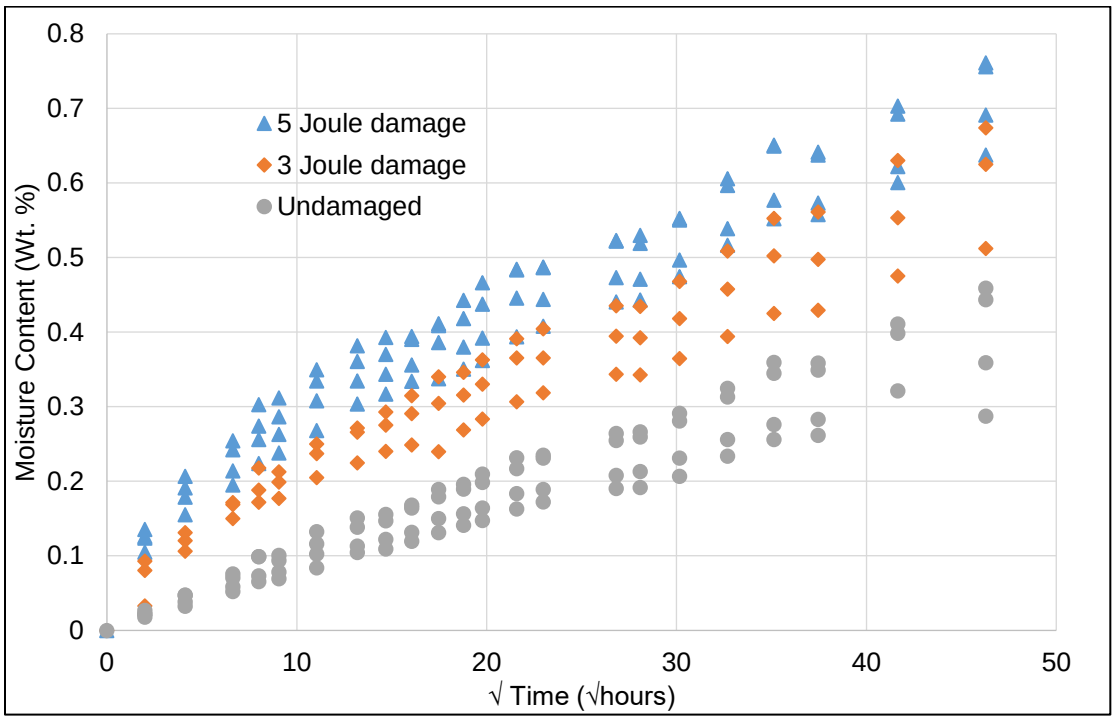

Figure 16: Plot of moisture content with immersion time

3.3.3 Near-Infrared Spectroscopy

The full NIR spectra obtained is shown in Figure 17. From this, spectral response for the relevant frequency band (between 6000 and 8000 cm^{-1}, where water can be separated into its free and bound states) was extracted [11]. Analysis of the data involved three major steps: baseline subtraction, subtraction of the initial dry spectra, and fitting a model comprised of a combination of peaks to the obtained spectra [11].

An objective baseline correction algorithm based on a previous study was applied to the spectral data [110]. This involved fitting an *n*-degree polynomial to the data and then eliminating points that were more than one standard deviation above the fitted line. This process was repeated until the curve converged to the bottom of the peak forming the required baseline. Preliminary results suggested the ideal baseline for this spectral range would be linear [110] (see insert in

Figure 17). Using this algorithm, a linear function fitted to points on both ends of the relevant spectral range was obtained for all conditions; the resulting linear baseline was then subtracted from the spectra. The bounds of the linear function obtained for the 0 % moisture (dry) condition formed the basis for the spectral limits adopted for subsequent moisture-contaminated spectra of the tested specimen.

To eliminate the spectral contributions from epoxy and glass fiber constituents of the polymer matrix composite, the baseline-corrected dry spectra was then subtracted from all subsequent baseline-corrected moisture-contaminated spectral conditions [11,111]. Figure 18 shows spectral curves obtained for increasing levels of moisture contamination after baseline correction and dry spectra subtraction. The various spectra shown in Figure 18 indicate the occurrence of distinct peaks in the vicinity of 7000 cm^{-1}, 6800 cm^{-1}, and a broad peak at 6600 cm^{-1} representing the presence of S_0, S_1, and S_2 species of water molecules [11,41,105].

Knowing the approximate peak positions, the spectra obtained for the various moisture-contaminated conditions were deconvoluted into three peaks, all close to the expected frequencies [11,41,105]. The deconvolution was achieved by minimizing the sum of residuals (error squared). The total residual for each fit was generally of the order 10^{-5} or lower. The summation of these three peaks produced a model that provided a close fit to the measured spectra, as shown in Figure 14. The area bounded by peaks S_0, S_1, and S_2 were estimated and relative concentration of each species calculated by applying Equation 2.

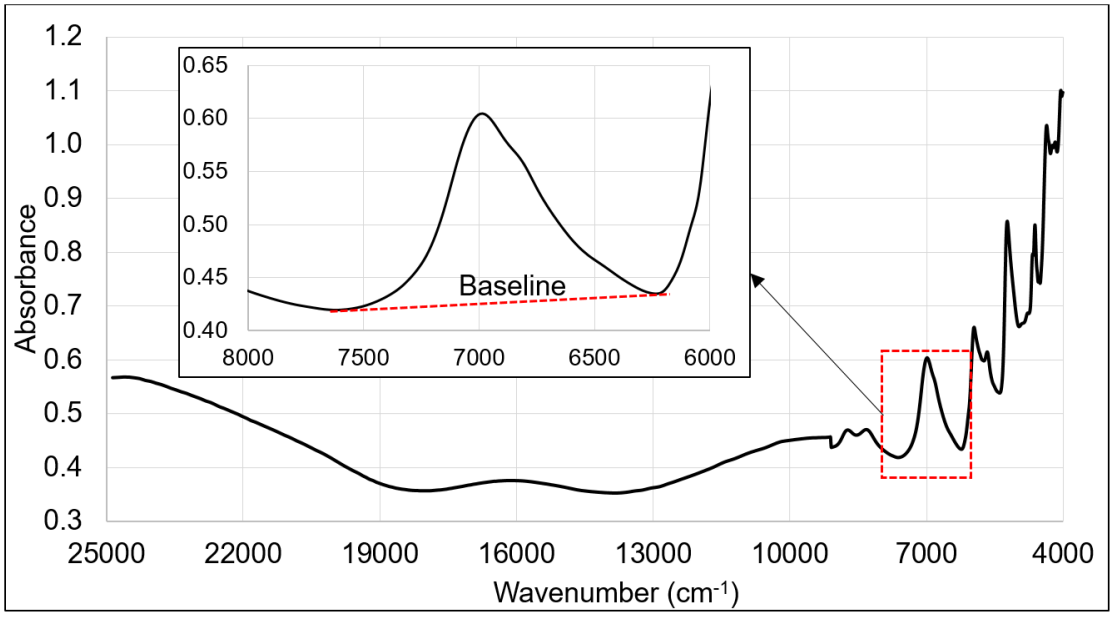

Figure 17: Typical NIR spectra for moisture contaminated epoxy/glass fiber composite laminate. Insert: Spectral region of interest showing linear baseline to be subtracted.

In estimating relative concentrations of free and bound water, S_0 and S_1 species are designated as free water molecules while S_2 is designated as bound water, consistent with previous studies [11,41,105]. Figure 19 (a) & (b) shows the relative concentration variation of free and bound water with moisture content for an undamged and damaged specimen respectively. In previous studies [11], linear functions provided an adequate fit to the free and bound water fraction data. However, to accommodate the damaged specimens in this study—which had a much higher fraction of free water at low moisture content—a more accurate function was needed. Hence, a second-order polynomial fit was adopted. Relative to the linear function, this doubled the correlation coefficient squared (R^2) of the fit to the damaged data, while the fit to the undamaged specimen data remained close to linear even when the higher order function was adopted, consistent with previous studies [11]. Using data from lines of best-fit in Figure 19 (a) & (b), the ratio of free to bound moisture content—eta (η), is plotted for all three cases (undamaged, 3 Joule, and 5 Joule damage) as shown in Figure 20. Error bars shown indicate twice the standard deviation

(± standard deviation); these are obtained when data from all specimens within the same group are considered. In all cases, results show an initially higher proportion of free-to-bound water at low moisture content. This ratio gradually decreases with increasing levels of moisture. Results also show a general increase in η with incresing levels of damage. From this plot a clear distinction can be seen between the proportion of free to bound water in the undamaged specimen compared to the damaged specimens. This is again indicative of free water occupying delaminations and matrix macro and micro-cracks in the damaged specimen (see micrographs for damaged specimen in Figure 13). The decrease in η suggests a gradual increase in bound water content, indicative of a much slower process of binding water molecules to polar sites within the polymer matrix [57].

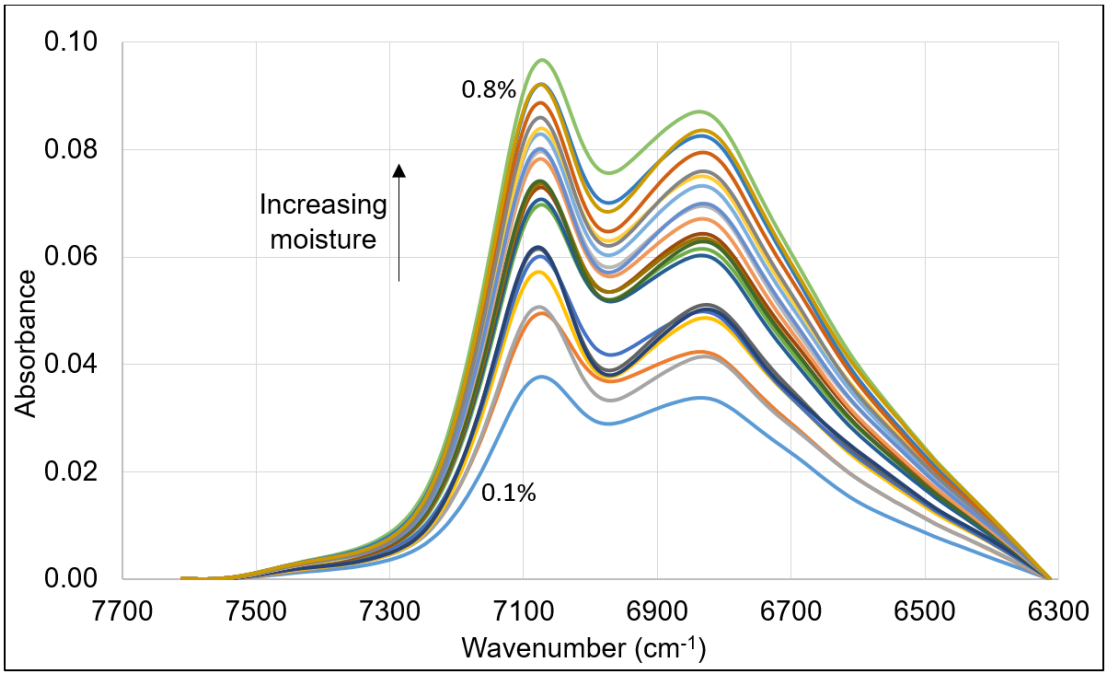

Figure 18: Typical NIR spectra after baseline correction and subtraction of dry spectra showing effect of increasing levels of moisture contamination from 0.1 to 0.8 %.

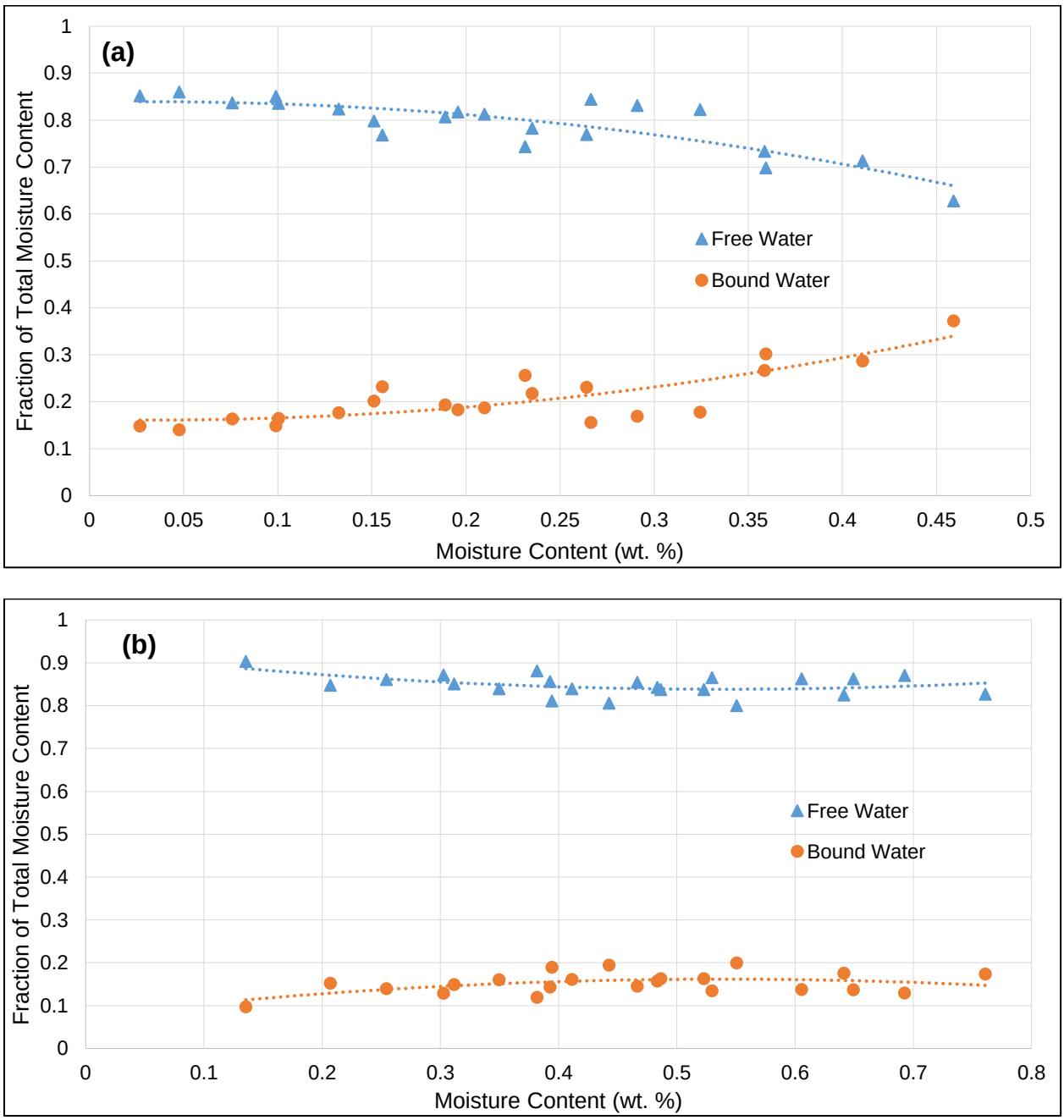

Figure 19: Plot showing free and bound water relative concentrations for (a) Undamaged (b) 5 Joule damaged specimen as a function of total moisture content by weight.

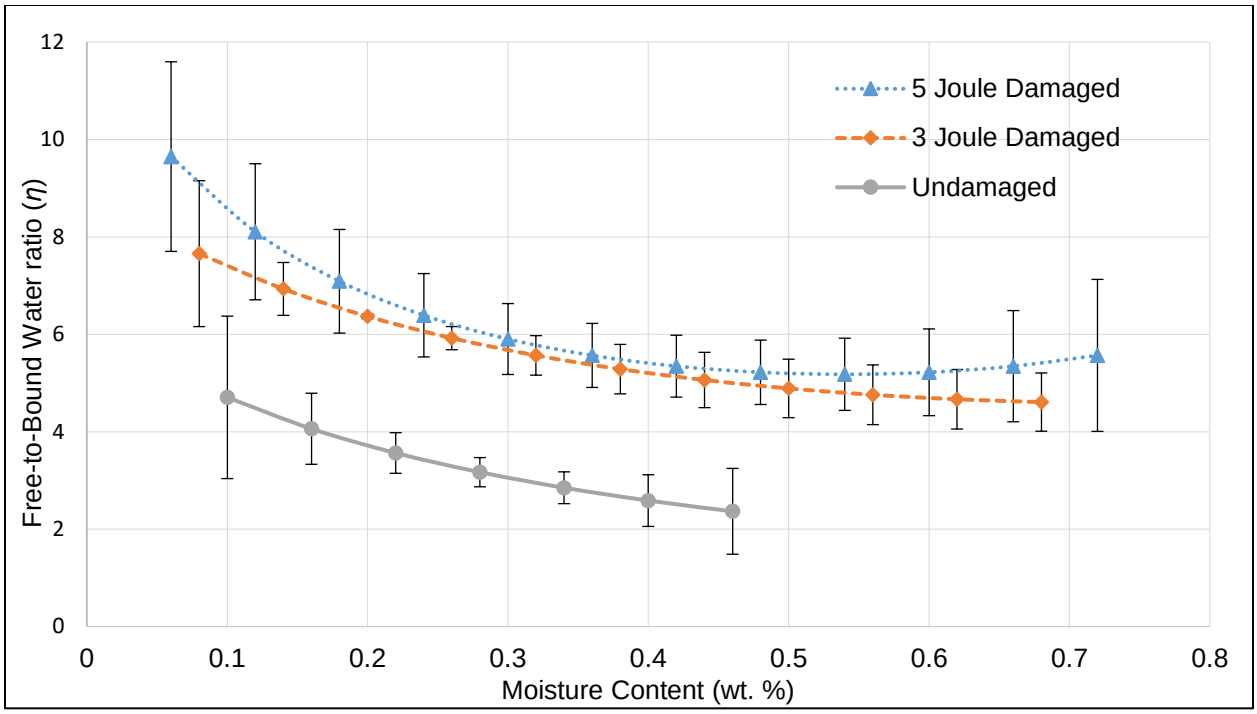

Figure 20: Plot showing ratio of free to bound water concentration (η) variation with moisture content for epoxy/glass fiber composite when undamaged and damaged at different levels.

3.3.4 Microwave Relative Permittivity

The distribution of free and bound water was also investigated through analysis of microwave frequency dielectric properties. The relationship between bulk relative permittivity and immersion time (see Figure 21) follows a trend similar to the gravimetric uptake curves in Figure 16. However, relative permittivity is also sensitive to the state of absorbed water in addition to the volume, showing much clearer distinctions between damage levels. This is even more evident when the response in relative permittivity is plotted against moisture content by weight as seen in Figure 22. This figure clearly demonstrates that relative permittivity is not only a function of the amount of absorbed moisture but also the nature of restriction to dipolar rotation imposed by virtue of its interactions with the polymer matrix (e.g., its state). The change in bulk relative permittivity of the laminate is much more pronounced for the damaged specimen, even when the total volume

of absorbed water is equivalent between the undamaged and damaged laminates. We can reasonably infer, then, that the higher relative permittivity in damaged specimens at equivalent total water content is the result of higher η. This is consistent with NIR results, and consistent with microscopy results in Figure 13 that illustrate a higher availability of internal free volume with increased damage.

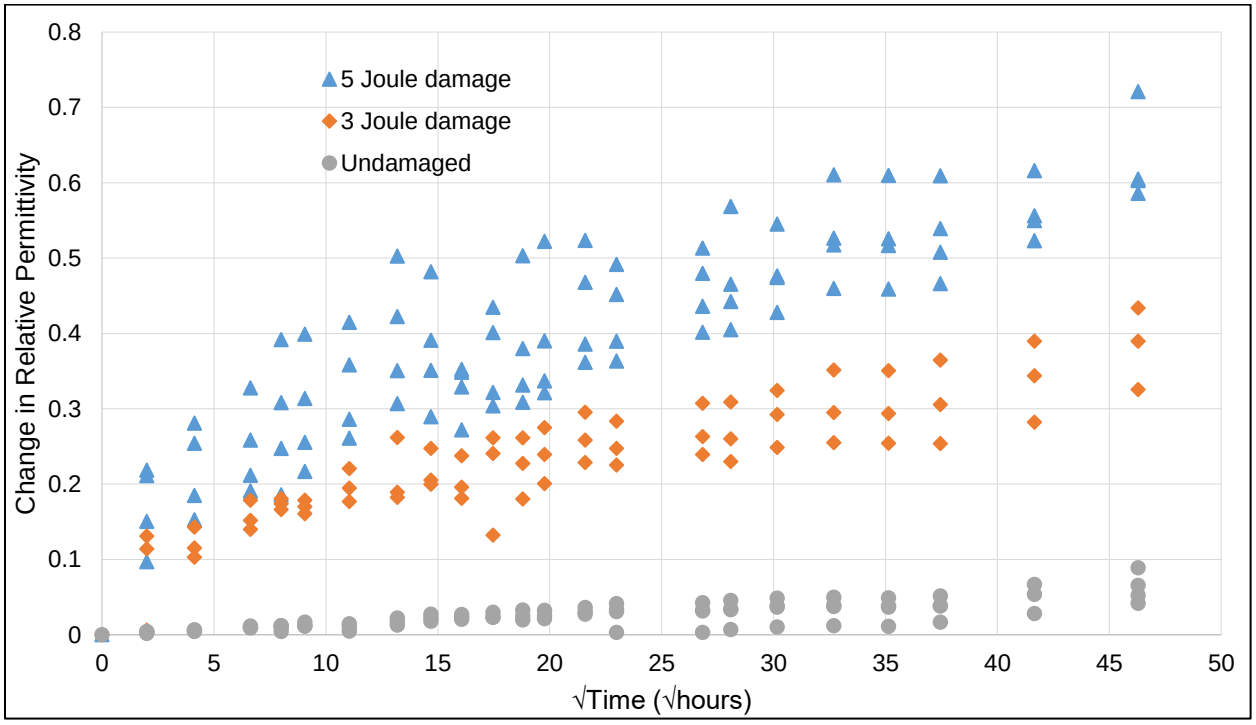

Figure 21: Plot of change in relative permittivity with immersion time

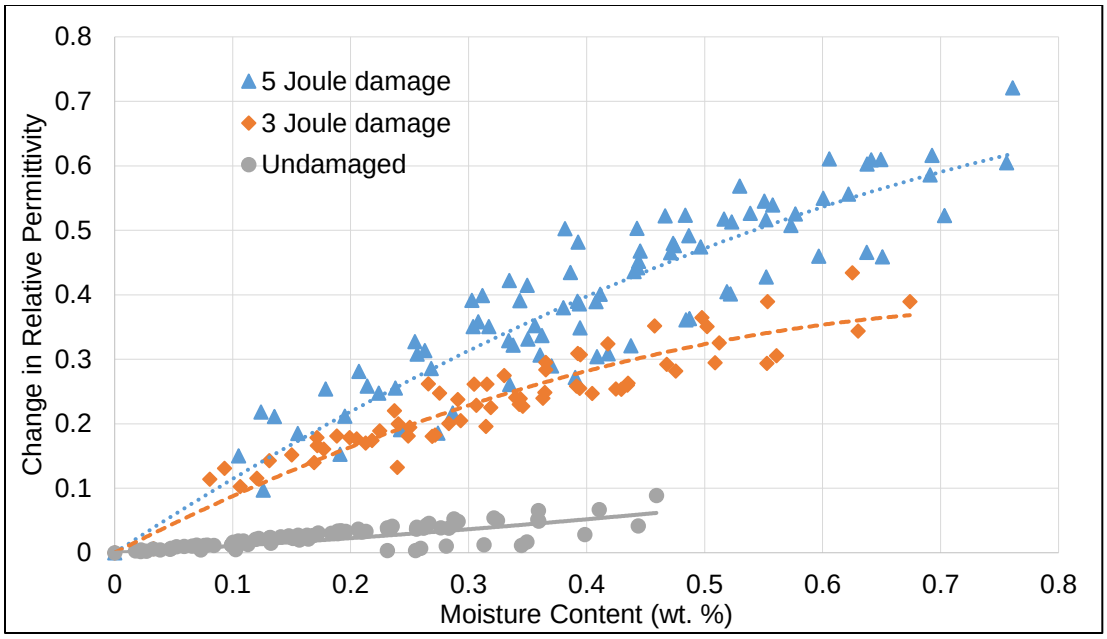

Figure 22: Plot of change in relative permittivity with moisture content

3.4 Discussion

3.4.1 NIR Spectroscopy and Microwave Relative Permittivity Comparisons

Data obtained from both NIR spectroscopy and microwave frequency relative permittivity show a similar change in absorbed water state in response to damage. Comparing results from both methods, we can infer that at lower levels of moisture the undamaged specimen contains significantly less free and more bound moisture relative to the damaged specimens. This is evident from its lower η (see Figure 20) and the significantly slower rise in relative permittivity for the undamaged specimen relative to the damaged specimens at lower moisture levels (see Figure 22).

This trend changes with increasing moisture, showing a gradual decline in η as well as a less steep increase in relative permittivity. This implies a higher concentration of moisture in the bound state relative to the free state with increasing moisture content. This also implies an initial preferential diffusion of moisture in the free state to occupy macro and micro-voids created as a result of laminate damage. When the influence of dynamic moisture concentration profiles on

unsaturated polymer matrix composites is considered, the same conclusions are reached. Studies that investigated the dynamic moisture concentration profile in polymer matrix composites, suggest a much higher concentration of moisture closer to the edges than at the center of the specimen during the early stages of moisture uptake [112]. Since the damaged region is at the center, water would rapidly migrate to the voids in the damaged region through a network of microcracks and exist in the free state; hence, resulting in higher η. At saturated moisture levels, similar logic would apply resulting in higher levels of bound water overall but still a locally higher level of free water at the damaged regions.

Both methods also showed sensitivities to the magnitude of damage induced in the laminates. Although NIR spectroscopy generally showed higher η for increasing levels of damage as seen in Figure 20, the distinction between 3 and 5 Joule damage was not as pronounced as in the microwave relative permittivity data. This limitation in sensitivity to damage magnitude when applying NIR spectroscopy could result from a number of factors such as the small difference in damage level (3 Joule vs 5 Joule), the non-uniform damage area, and the limited size of sampling area (aperture size of approx. 20 mm diameter) tested relative to the much larger damage-affected region. Hence, NIR absorbance due to moisture at a highly damaged local area may be similar or even higher for a 3 Joule damaged specimen compared to absorbance at a less damaged local region in a 5 Joule damaged specimen. This was much less of a problem with the dielectric data as the 2.48 GHz SPDR had an apperture size of over 50 mm in diameter. Hence, an electric field was being applied to over 90% of the specimen area during each measurement. This meant that virtually all of the damage-affected regions contributed to the increase in relative permittivity, thereby capturing the overall effect of 3 Joule or 5 Joule damage and giving a more accurate represenation of the damage magnitude. This clear distinction in relative permitttivity between 3

and 5 Joule damage specimen is shown in Figure 21 and Figure 22. However, this would be less of a limitation in practical applications where spatial variations of η or relative permittivity over a wide area would be collected and used to create a damage map of the laminate [107]. In such an application, a smaller apperture such as in NIR spectroscopy may provide more accurate results and probably better damage mapping and identification resolutions.

3.4.2 Feasibility and Limitations of Water Interaction-Enabled Non-Destructive Examination (WINDE)

The use of water as a type of 'imaging agent' for NDE can be implemented in a variety of characterization techniques that are sensitive to the free and bound state of water [11,60,92,93]. The characterization techniques utilized in this study have demonstrated this possibility. However, limitations of each technique may impede its application to specific conditions. In the case of microwave dielectric properties, a theoretical limitation may result from its insensitivity to free water that is physically bound. This may limit its detection to flaw sizes above length scales at which the chemically-free water begin to act as bound water due to physical confinement [97,98]. Another limitation of applying the microwave-frequency dielectric properties as a characterization method is its limitation to only non-conductive materials. Unlike non-conductive dielectric materials that retain their outer shell valence electrons when an electric field is applied and are restricted to polarization only, conductors allow their outer shell valence electrons to migrate throughout the material, hence invalidating the polarization concept [113]. Similarly, characterization depth limitations exist for NIR spectroscopy in diffuse reflectance mode. Sensitivity of the technique may be limited when damage is beyond the maximum penetration depth for infrared radiation in the medium [114], or when strongly absorbing materials such as carbon fiber is used as polymer reinforcement [115].

Additionally, the sensitivity of the method is a function of the total moisture content as well as the relative amount of free and bound water in the system. The total moisture content of a polymer composite changes with the humidity level of its surroundings based on moisture concentration differences and diffusion laws. However, there is also a higher tendency to lose and gain free water compared to bound water, which requires a higher activation energy due to hydrogen bonding to polar sites [93,116]. This behavior may cause a decrease in the amount of free water residing in the damaged region, thereby affecting sensitivity to damage [117]. Initial sensitivity immediately after damage may also be affected by dependence on the natural process of moisture diffusion. The time required before the method can detect damage may range from a few hours post-impact to a few days. This would depend on the matrix polarity [118], humidity of the operating environment, and the amount of moisture absorbed in the material before damage occurs [107]. Further investigations could examine the influence humidity level of the operating environment would have on sensitivity and the delay in damage detection.

For safety critical systems, early detection of damage at the initiation stage plays an important role in estimation of the remaining useful life of a component. This early stage of composite damage initiation involve matrix micro-cracking. However, detection of micro-cracks at such early stages of damage currently poses a challenge for existing composite NDE methods [35,76]. Of the well-established methods, few can provide useful details about the state of the materials at and below the micro-scale; acoustic emission, x-ray radiography & computed tomography, non-linear acoustics, and resistivity have the capacity to detect matrix micro-cracks but not without limitations [35,76]. These limitations have been reported in previous studies and generally include safety concerns and non-suitability for field use (in the case of x-rays), inability to provide flaw size information (acoustics), and requirements for multiple electrodes or limitation

to conductive materials (resistivity). The proposed method of analyzing the nature of moisture interaction may provide a suitable way to characterize these micro-cracks without the highlighted limitations.

3.5 Conclusion

This study investigated the possibility of leveraging the effects of damage on the nature of polymer-water interaction in the detection of local damage within a polymer matrix composite. Barely visible damage was induced in 16-ply epoxy/glass fiber laminate specimens via impact at 0 (undamaged), 3 Joule, and 5 Joule energy levels before moisture exposure. Gravimetric, near-infrared (NIR) absorption and microwave-frequency dielectric properties were measured periodically within a 3-month period during which the specimens were exposed to moisture. Analysis of results obtained via gravimetric moisture uptake indicate the possibility of detecting the presence of damage within a composite structure but with limited information on spatial distribution or location of damage. Results from NIR spectroscopy indicate higher amounts of free water relative to bound water in damaged specimen, showing as much as a 2-fold higher free-to-bound water ratio in 5 Joule damaged specimen when compared to an undamaged specimen. Similarly, results from microwave dielectric analysis show as much as an 8-fold higher change in relative permittivity for the same level of damage compared to an undamaged specimen and within the same range of moisture content. Both characterization methods also indicate sensitivity to the magnitude of damage, with microwave relative permittivity showing better differentiation between 3 and 5 Joule damage, likely due to the larger aperture size of the split post dielectric resonator. These results indicate a higher proportion of bound water in the undamaged laminate, while free water preferentially migrates to voids created by matrix cracking and delaminations within damaged regions. Hence, the study has shown that analysis of polymer-water interactions within

a polymer matrix may provide an opportunity to accurately detect low levels of damage and estimate its magnitude and location. Leveraging such molecular-level interactions within the polymer matrix may enable detection of damage at length scales beyond current polymer matrix composite non-destructive examination methods. It may also enable characterization of combined physical-chemical damage modes such as hygrothermal loading and physical damage.

CHAPTER 4: INVESTIGATING THE EFFECT OF MOISTURE ABSORPTION AND DESORPTION HISTORY ON SENSITIVITY OF POLYMER-WATER INTERACTIONS TO DAMAGE

4.1 Rationale

Polymer matrix composites continue to supplant traditional materials across a wide range of industries due to their high strength-to-weight ratio, corrosion resistance, and other desirable properties. However, polymer composites remain susceptible to water absorption from atmospheric moisture in the form of humid air or precipitation. It is widely accepted that polymer composites can absorb a significant amount of moisture in typical service environments [25,27], leading to changes in material properties and performance [92,119]. Numerous studies have been performed to understand the mechanisms of moisture diffusion in polymer matrix composite systems in an effort to map moisture content to material properties and performance. While most models simplify the interaction between penetrant (water) and host (polymer), several have accounted for more complex and realistic interactions. Among these are a dual-mode sorption model accounting for the presence of immobilization sites [15,26], a new hindered diffusion model extending the classical Langmuir-type and Fickian theories to consider effects of both chemical and physical structure of polymeric composites [27,28], and modifications to the Fickian model to account for hygro-elastic relaxations and polymer-water interactions [29]. In general, the studies demonstrate the need for other considerations in predicting moisture absorption behavior in polymer matrix composites beyond the classical Fickian diffusion process.

Based on the dual-sorption model, the concept of two concurrent diffusion processes—an initial fast process in which water migrates to voids and matrix cracks within the laminate, then a slow process representing the intrinsic diffusion in the polymer itself—can be extended to moisture

diffusion in undamaged and damaged regions [15,22]. In the undamaged region, moisture migrating through the matrix is much slower due to physical constraints resulting from navigating the relatively tightly-packed polymer network. In addition, these water molecules have to overcome secondary binding forces such as hydrogen bonding, van der Waals forces, and dipole-dipole interactions associated with polar functional groups and polymer chains within the network [20,41,120]. The combination of physical constraints and chemical interactions restrict a water molecule's migration and rotation, a condition referred to as the 'bound' state [96,97,121]. Water without such constraints is regarded as 'free' [11,56]. Voids and matrix cracks—which may result from damage—provide ideal sites where water may exist in the free state due to their relatively large physical separation from the polymer network itself [122].

The effect of damage on moisture diffusion mechanisms in polymer composites has been investigated in a number of studies [24,34,36,51]. These studies conclude that damage creates new and less restrictive pathways within the polymer matrix for additional moisture diffusion, which preferentially migrates to the newly-created free volume. This leads to a higher equilibrium moisture content and an increased rate of absorption [24,36,37]. While previous studies have investigated these mechanisms that drive moisture diffusion within damaged composites, no attempt has been made to elucidate the state of absorbed moisture based on the nature of its interaction with the polymer matrix, nor has there been any experimental study on the variation in spatial distribution of these moisture states within a laminate with localized damaged. This study addresses these gaps while also investigating how the free and bound water distribution within a damaged laminate changes with moisture absorption and desorption.

In our previous work, changes in free and bound water distribution as a result of damage within a polymer matrix composite laminate were leveraged to detect low levels of impact damage

[5,36,37,60]. Here, the effect of changes in absorbed moisture levels on the sensitivity of this technique and on the spatial distribution of water states is investigated. This is achieved by monitoring the distribution of free and bound water in undamaged, 2-Joule, and 3-Joule impact-damaged polymer composite laminates as they are subject to moisture absorption and desorption. To detect these changes, free and bound water are characterized using microwave-frequency relative permittivity, which is sensitive to the dipolar rotational polarization mechanism of water. Within the microwave frequency range, the relative permittivity is closely related to the ability of the molecule to rotate without restrictions [38,70]. Due to the absence of physical and chemical restraining forces, water in the free state rotates unimpeded in the presence of a changing electromagnetic field [123]. This leads to free water having a high relative permittivity of approximately 80 [71], while bound water (primarily hydrogen bound) is restricted in its ability to rotate with a changing electromagnetic field, which results in a relative permittivity close to 3 [72]. The various less-firmly-bound states resulting from other secondary bonding interactions have a relative permittivity between these two extremes [41,52].

4.2 Materials and Methods

4.2.1 Materials

Test samples were made from a polymer composite commonly used in the aerospace industry; an epoxy/glass fiber composite laminate consisting of a Hexcel F161 epoxy resin and a crowfoot weave glass fabric, Style 120. Twenty-two plies of prepreg with dimensions 305 x 178 mm were laid up, ensuring alignment of 0° and 90° directions for all plies. This was cured in a hot press at 772 kPa. Starting at room temperature, the stacked prepreg under pressure was heated at a steady rate of 10 °C/minute to 180 °C. The prepreg was then maintained at 180 °C for 2 hours before pressure was released. The formed laminate was then cooled to room temperature at an

average rate of 2 °C/minute. Properties of the laminate were determined by resin burn-off in accordance with ASTM D3171 [102]. Six undamaged laminate specimens of size 20 x 50 mm were used in the resin burn-off exercise. The process was carried out in a high-temperature furnace maintained at 800 °C until elimination of all epoxy residue. Resin, void, and fiber content were determined from pre and post-burn-off weight measurements. The average laminate thickness was 1.7 mm with a standard deviation of 0.1 mm. Other laminate properties are given in Table 2.

Table 2: Average epoxy/glass fiber laminate Properties

Property	Mean (%)	Standard Deviation (%)
Fiber volume fraction	51.36	0.72
Resin volume fraction	43.32	0.63
Void volume fraction	5.32	0.58

4.2.2 Sample Conditioning

Smaller test specimens of dimensions 100 x 55 mm were cut from the larger cured laminates using a wet diamond saw. The specimens were then dried at 65 °C in a vacuum oven until a stable weight was achieved per ASTM D5229 [103]. During the absorption process, the test specimens were immersed in de-ionized water to accelerate moisture uptake. The temperature was maintained at 25 °C using a water bath. During the desorption process, test specimens were placed in a low humidity chamber maintained at room temperature and below 10% relative humidity using an 8% indicating t.h.e.® desiccant. Specimen weights were measured using a Mettler-Toledo high-precision analytical balance.

4.2.3 Impact Setup

Low velocity out-of-plane impacts at 2 and 3 Joule were applied at the center of corresponding test specimens. This induced barely-visible damage in the form of matrix cracks,

fiber/matrix debonding, and delaminations in a localized area of the laminate [104]. This type of damage is consistent with small-diameter hail or tool damage (e.g. a dropped tool during aircraft maintenance—a common cause of this type of damage). At such levels, damage is often difficult or impossible to detect visually when a coat of paint has been applied (see Figure 23). Paint, even when applied prior to the damage, often masks the telltale discoloration associated with impact damage of this type. To achieve this type of damage, an impact setup consisting of a drop tower equipped with a double-column-impactor guide mechanism and a crosshead-mounted hemispherical striker tip of radius 9.4 mm was used [124]. The total drop-weight was 4.29 kg. Before impact, each specimen was firmly secured within two 3-mm-thick steel fixture plates. Each plate had a 35 mm diameter cut-out which exposed the intended impact location of the secured specimen. The amount of damage induced was varied by adjusting the drop height of the crosshead. Three undamaged specimens and four specimens each of 2 and 3-Joule damage levels were used in the experiment.

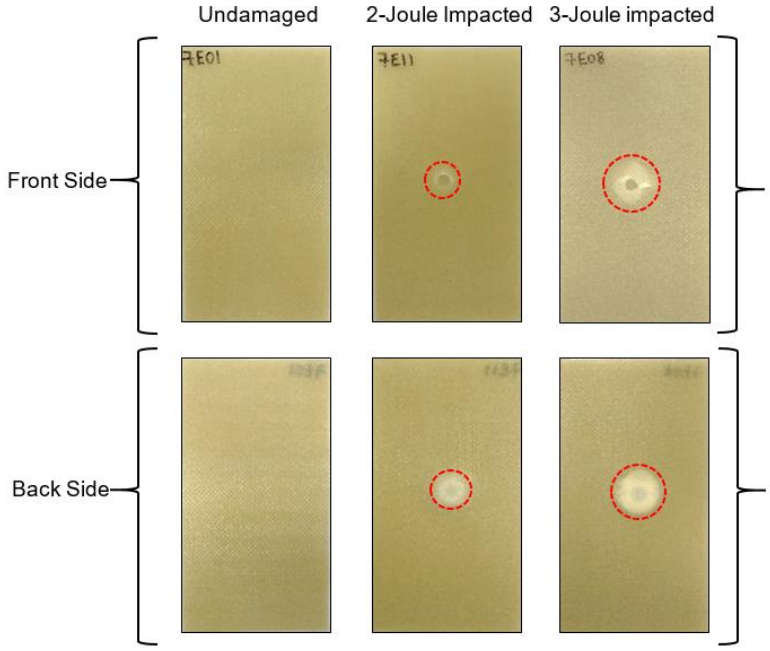

Figure 23: Front and back sides of undamaged, 2 and 3-Joule impact-damaged laminates

4.2.4 Split-Post Dielectric Resonance Technique

There are numerous techniques for characterizing dielectric properties. These vary in accuracy, complexity, specimen material type, and applicable frequency range [74]. To accurately measure the dielectric properties of an epoxy/glass fiber laminate within the microwave frequency range, a split post dielectric resonator (SPDR) manufactured by QWED© of Warsaw, Poland was employed. The SPDR was coupled with an Agilent programmable vector network analyzer (VNA) as shown in Figure 24. The setup enables accurate measurement of relative permittivity with only 0.3% uncertainty; detecting small changes on the order 10^{-3} [106]. Details of the measurement and calibration process are provided in Section 3.2.6 and our previous study [5].

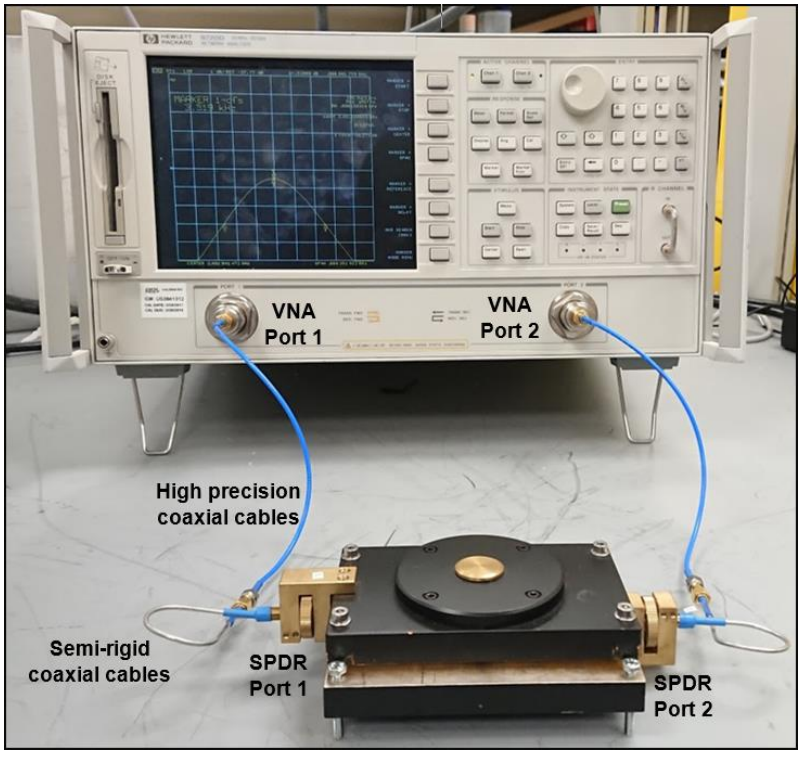

Figure 24: Split post dielectric resonator (SPDR) coupled to Vector Network Analyzer (VNA)

4.2.5 Experimental Procedure

During the absorption and desorption process, moisture content by weight and spatial variation in relative permittivity at 5 GHz were measured at specific time intervals. At each measurement, wet specimens were first carefully dried using a lint-free cloth. Effects of residual surface moisture were mitigated by allowing the specimens to dry further at room conditions for 10 minutes until the weight stabilized. To ensure accuracy in such sensitive weight measurements, static electric charges on the specimen surface were removed by exposure to pressurized ionized air immediately prior to weighing. Specimen weights were recorded before and after each 15-minute dielectric scan. An average of both weights was used to calculate the percentage moisture concentration for that measurement. A discussion of moisture loss during testing is included in the Section 4.3.1 related to potential confounding factors.

To accurately move the specimen within the resonant cavity of the SPDR, a custom setup employing NEMA-17 stepper motors and A4988 motor drivers controlled by an Arduino MEGA 2560 board was utilized (see Figure 25 (a)). MATLAB® scripts were developed which simultaneously controlled the VNA and accurately moved the specimen to specified grid points. A virtual grid of 61 by 3 points was created across the sample surface (see Figure 25 (b)). This was chosen to maximize coverage of the entire area around the damaged region while limiting test time to minimize moisture loss during the test. The grid had step sizes of 1 mm for the long axis (61 points) and 12.5mm for the short axis (3 points). To eliminate specimen edge effects, the grid points at the margins were at least 15 mm from any edge of the specimen (see Figure 25 (b)). On each step, a measurement was obtained for the local bulk dielectric properties (relative permittivity and loss tangent) of an approximately 30 mm diameter area (aperture of the resonant cavity) centered at that grid point.

The two-dimensional scan data was plotted using the MATLAB® shading option 'interp'. This performs a linear interpolation to calculate the values for missing pixels between defined data points. Hence, a full heat map representing relative permittivity variation across the specimen could be generated from 183 (61 x 3) data points. Results obtained were comparable to much more time consuming but higher resolution scans having a 0.5 mm step size for both axes.

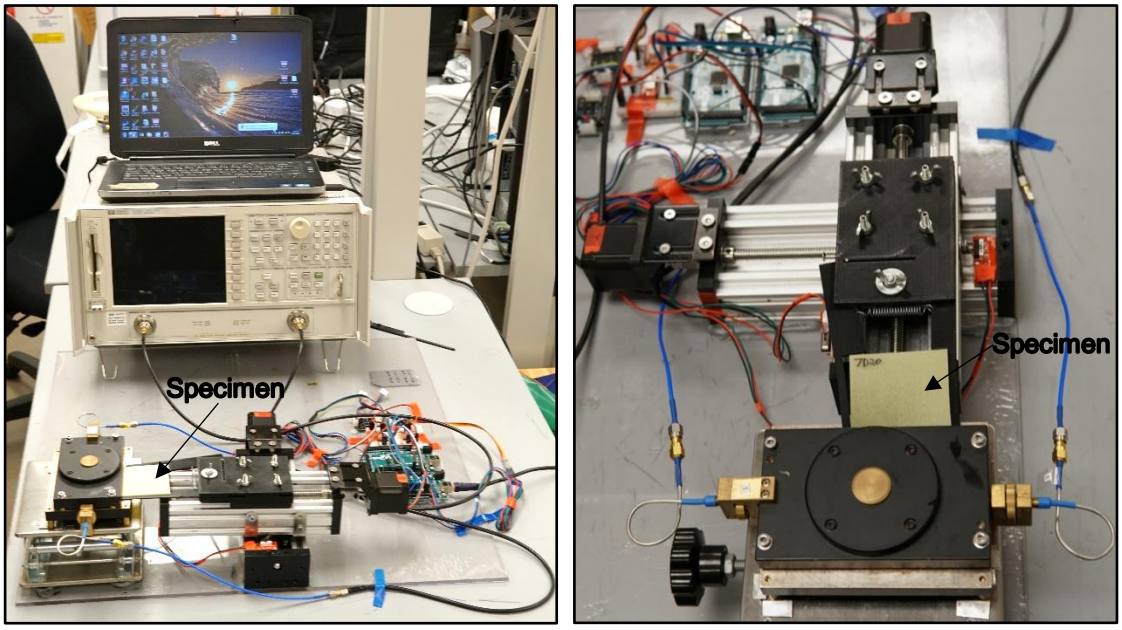

(a)

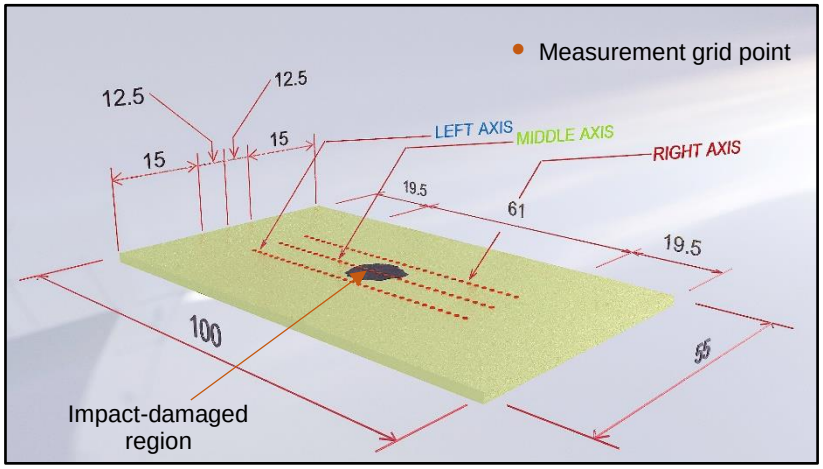

(b)

Figure 25: Experiment setup showing (a) complete system setup (b) typical measurement grid points on specimens

4.3 Results and Discussion

4.3.1 Mitigation of Confounding Factors

A few factors which could influence accuracy of relative permittivity measurements required consideration and mitigation. These include changes in environmental conditions, moisture content, and thickness variation across the specimen [72,107].

Relative permittivity calculations using the SPDR technique are primarily based on the shift in resonant frequency resulting from insertion of a specimen in the resonant cavity. Hence, to achieve accurate measurements, the resonant frequency of the empty cavity at the same environmental condition is required. Since measuring this for each grid point during the scan was not feasible, it was collected at the end of each test. Therefore, during each scan, variations in temperature and relative humidity were maintained within 0.1 ℃ and 1 % respectively. This limited changes in relative permittivity resulting from environmental factors to a maximum of 0.1 % [36].

Another important factor to consider during scans is loss or gain of moisture by the specimen. This was mitigated by allowing immersed specimens to achieve a stable weight prior to tests as described in Section 4.2.5. Additionally, the test duration was limited to 15 minutes by minimizing the number of grid points measured and maximizing step size. This limited moisture lost from specimens during scans to approximately 0.005% by weight; equivalent to a relative permittivity change of 0.02% for an undamaged specimen.

Localized thickness variations could also affect relative permittivity measurements. Thickness was measured at nine points across each laminate and a mean was calculated. This was then used for relative permittivity calculations. To mitigate the effects of thickness fluctuation about the mean, a baseline undamaged and completely dry relative permittivity map was first

created. This was then subtracted from corresponding grid points of subsequent scans for that specimen [107]. After performing this subtraction, any relative permittivity obtained is therefore a function of damage or changes in moisture content, rather than potential thickness variations.

The need to actively control these mitigating factors would severely limit the utility of the method if deployed in-service without improvement. Therefore, future research will focus on methods of accounting for variability in moisture content during a test, variable specimen thickness, and changing environmental conditions, rather than actively controlling them.

4.3.2 Results

As demonstrated in Figure 26, the specimen moisture uptake shows a linear relationship between moisture content by weight and the square root of exposure time for all damage levels, consistent with prior studies [15,51]. The uptake curves suggest sensitivity of gravimetric moisture uptake rate to damage levels, with the undamaged specimen absorbing water at the slowest rate and the most severely damaged specimen absorbing water at the highest rate. The linear relationship between moisture uptake and the square root of time indicates the absorption process remained below equilibrium water content (saturation) levels. The desorption process—which follows immediately after absorption—shows initial rapid loss of moisture followed by a slower rate of moisture loss which appears to decrease with time (see Figure 27). As was the case in absorption, the rate of moisture loss shows correlation with damage level. The curves indicate slower moisture loss for the undamaged specimens and faster loss for the damaged specimens, as expected.

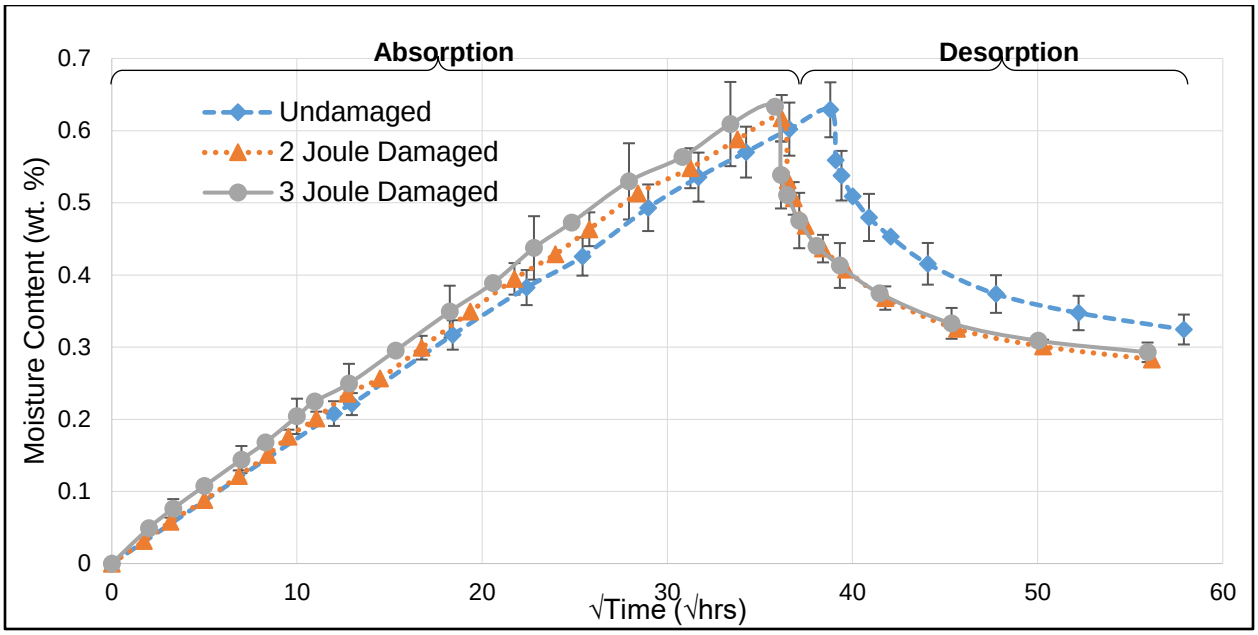

Figure 26: Plot of moisture uptake with square root of time for undamaged, 2-Joule, and 3-Joule damaged specimens. Error bars represent 95% confidence interval. Note that some error bars are not shown to improve readability.

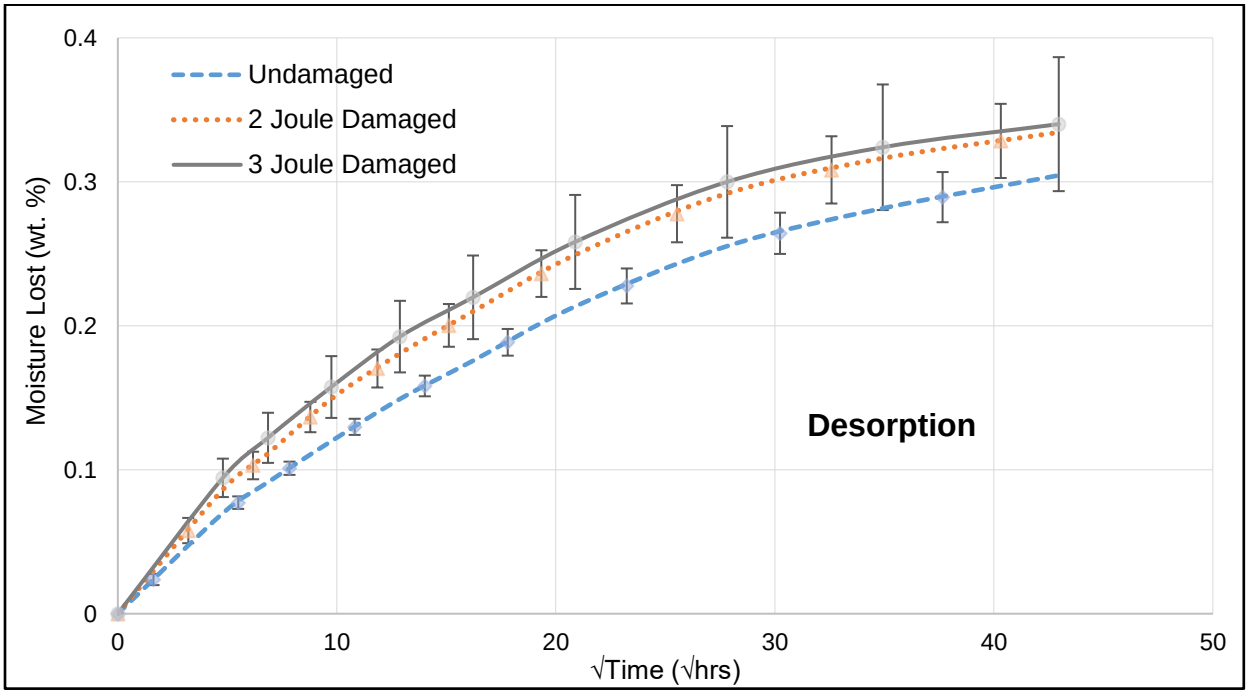

Figure 27: Plot of moisture lost with time for undamaged, 2-Joule, and 3-Joule damaged specimens during the desorption process. Error bars represent 95% confidence interval.

The effect of moisture uptake on the spatial variation of relative permittivity was also considered for all groups of specimens (undamaged, 2 and 3-Joule damaged). Figure 28 shows the spatial variation of relative permittivity across these specimens. The scans were taken during the absorption process at approximately the same moisture content of 0.45 % by weight. The relative permittivity map shows sensitivity to the damaged region, with significantly higher relative permittivity at the impact location compared to undamaged areas. This rise in relative permittivity in the damaged region also increases with damage levels, with the 2 and 3-Joule impact locations having as high as 2.8 and 3 times the relative permittivity of undamaged areas, respectively.

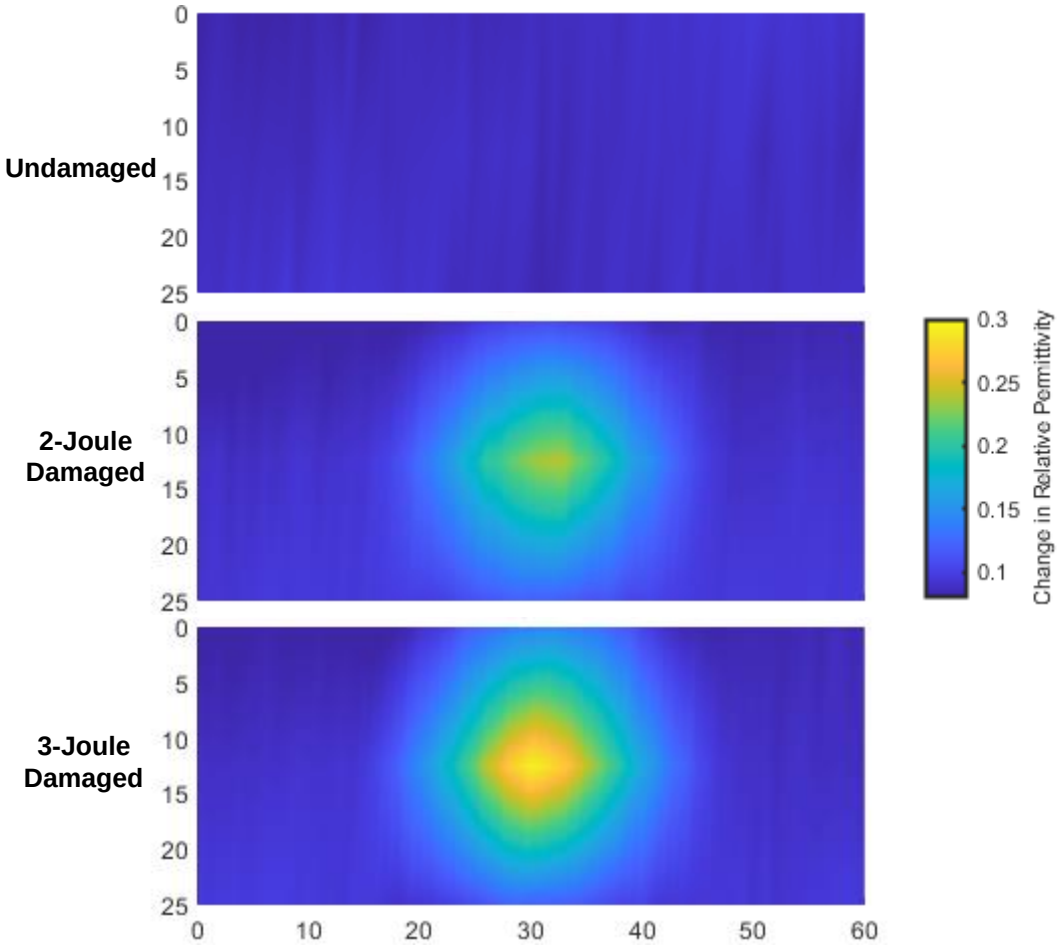

Figure 28: Two-dimensional spatial variation of relative permittivity for Undamaged (top), 2-Joule damaged (middle), and 3-Joule damaged (bottom) specimens all at 0.45% moisture content by weight during the absorption process.

To examine the effect of water content (measured as weight percentage of the total sample) on the spatial variation of relative permittivity, data for the middle axis grid points was considered (see Figure 25 (b)). The spatial variation plots in Figure 28 show that the maximum relative permittivity changes occur along this central axis, making it the best axis to observe the effects of varying moisture content, as expected. The middle axis curves, overlaid together in Figure 29 (a), show the variation in relative permittivity change for an undamaged specimen at various moisture contents during absorption. These curves remain essentially flat at the various moisture levels, suggesting no measurable damage. Curves for the 2 and 3-Joule damaged specimens in Figure 29 (b) and (c) show a subtle initial depression in relative permittivity at the damage site, followed by a significant rise in relative permittivity with increasing moisture levels. The relative permittivity rise was also sensitive to the impact energy level (extent of damage), with results for higher damage levels showing consistently higher increase at the damage site relative to increase at the undamaged regions.

For the desorption process, the spatial variation in relative permittivity was also obtained for the different damage states at the same moisture content of 0.45% by weight (see Figure 30), after having reached a maximum moisture content of 0.63%, 0.64%, and 0.65% for the undamaged, 2-Joule, and 3-Joule damaged laminates respectively. This is equivalent to the moisture content of scans in Figure 28, obtained during the absorption process. However, in this case, the results are very different. The undamaged and 2-Joule damaged specimen shows almost no variation in relative permittivity across the laminate. The 3-Joule damaged specimen shows only minor relative permittivity depression in the damaged region.

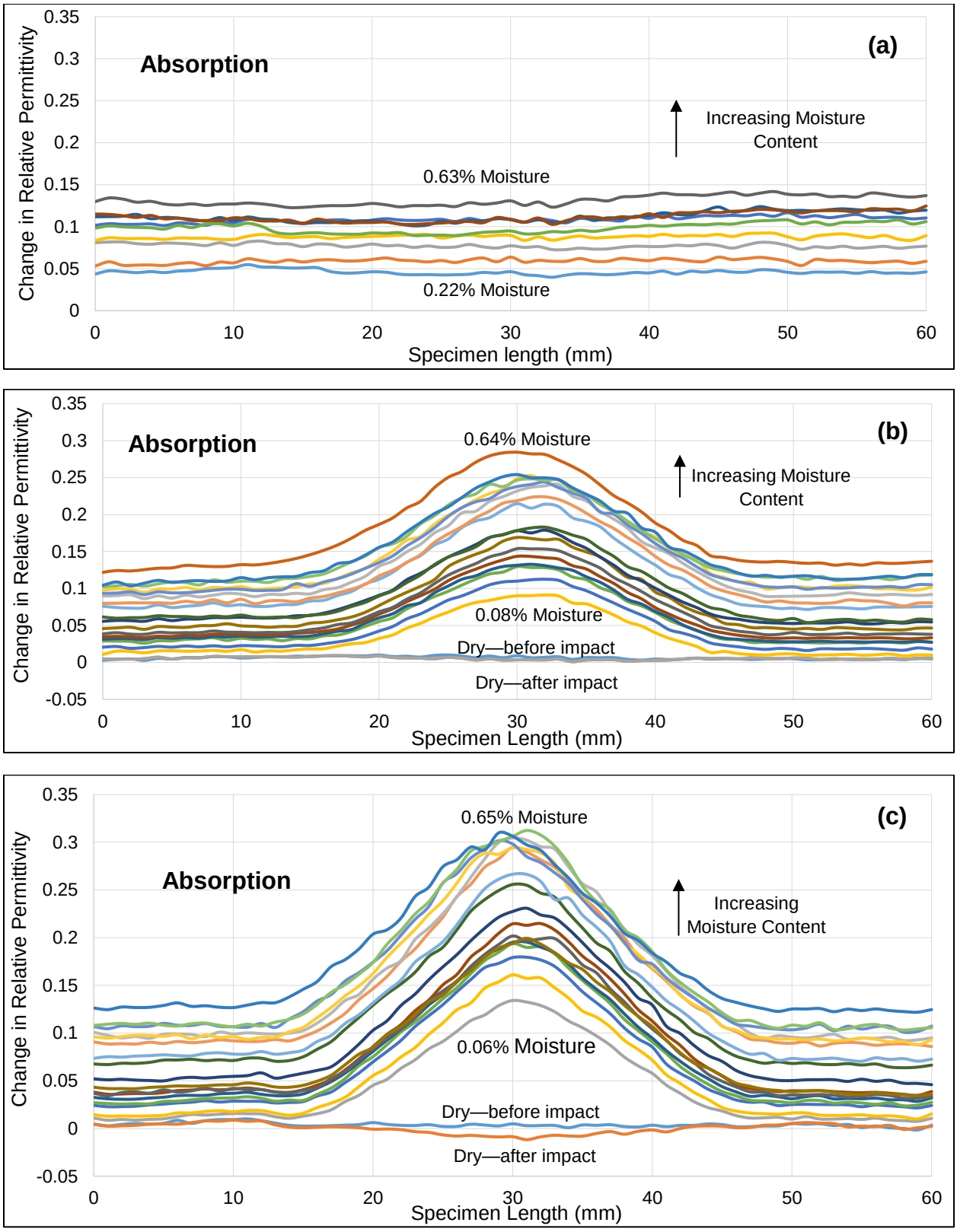

Figure 29: Plot of middle axis variation of relative permittivity with moisture content by weight for (a) Undamaged, (b) 2-Joule damaged, and (c) 3-Joule damaged specimens during the absorption process.

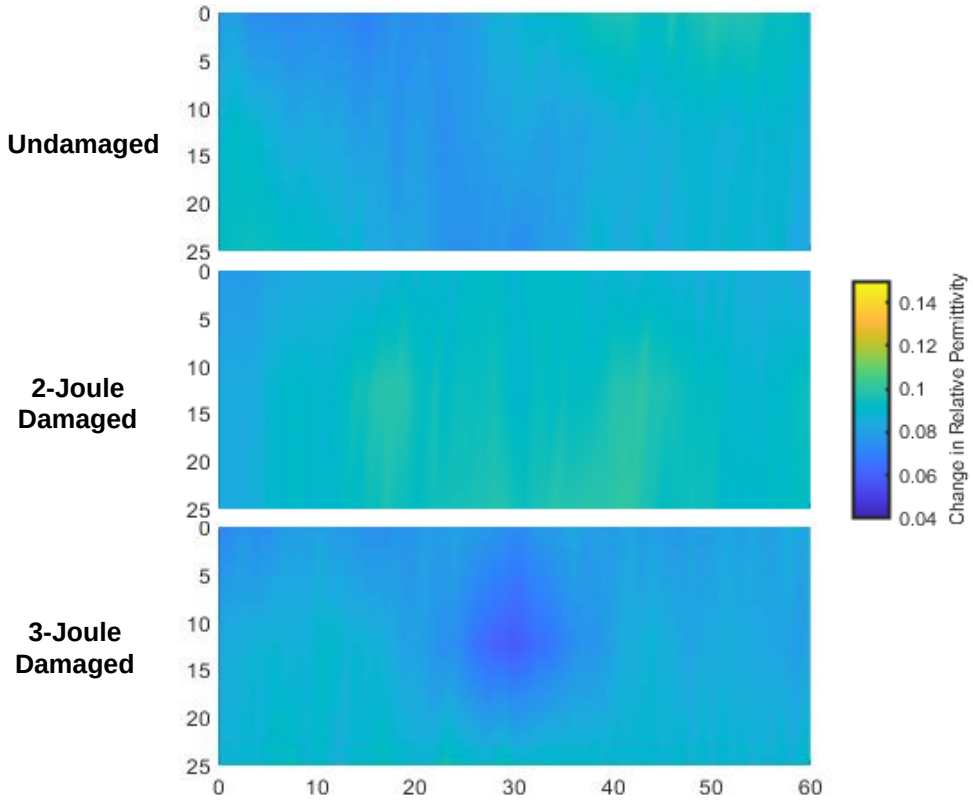

Figure 30: Two-dimensional spatial variation of relative permittivity for undamaged (top), 2-Joule damaged (middle), and 3-Joule damaged (bottom) specimens all at 0.45% moisture content by weight during the desorption process.

For the desorption process, the middle axis variation of relative permittivity with moisture content was also obtained (see Figure 31). For the undamaged specimen, results show a uniform reduction in relative permittivity with moisture content, with each curve remaining essentially flat. This is similar to the behavior observed during the absorption process. In the case of damaged specimens, a greater reduction in relative permittivity was observed at the damage site during the early stages of desorption. The reduction was more significant in the specimens with higher damage levels. Also, below 0.4% moisture in the 2-Joule and 0.5% moisture in the 3-Joule damaged specimens (curves labelled ‘A’), a depression in relative permittivity is observed at the impact location.

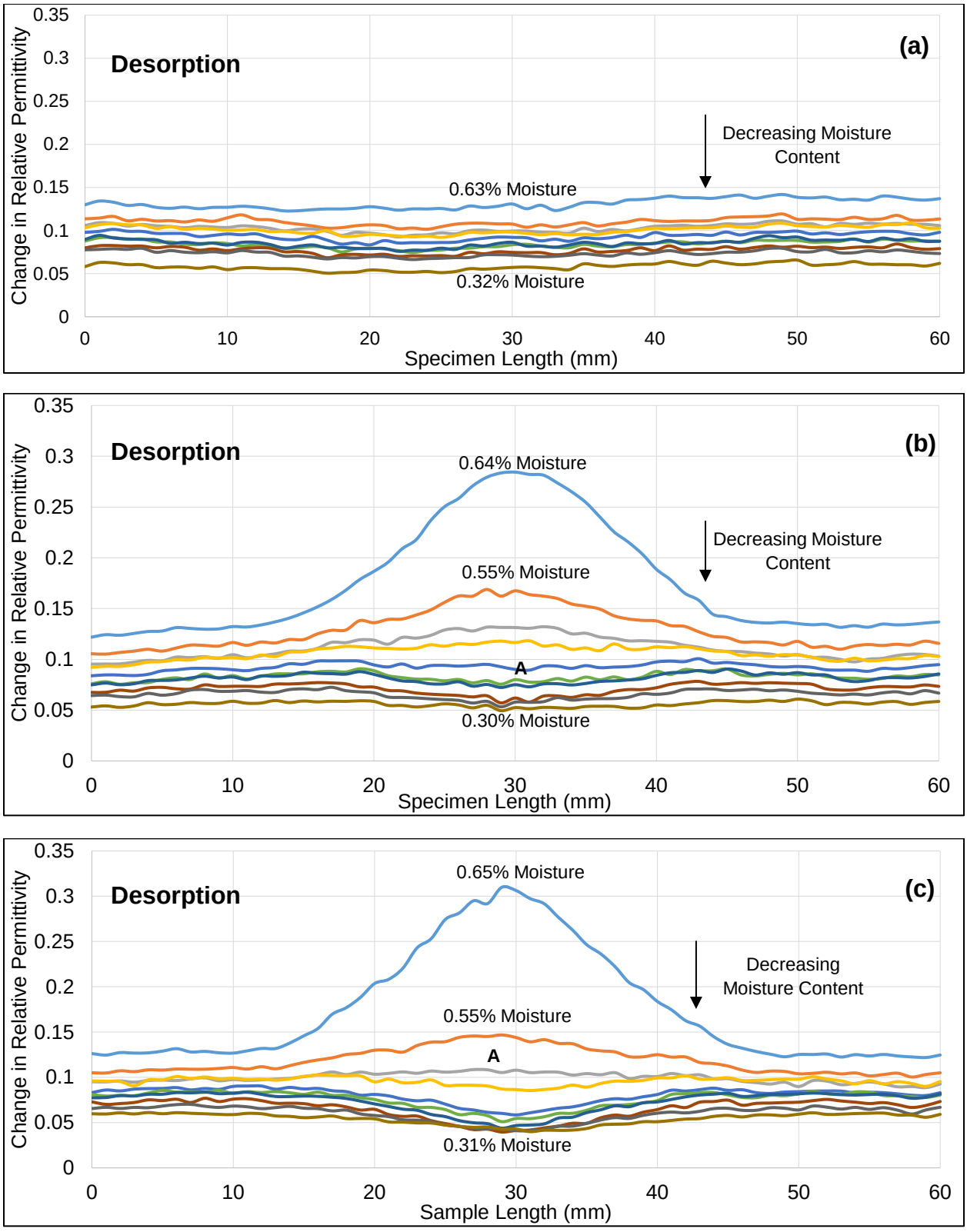

Figure 31: Plot of middle axis variation of relative permittivity with moisture content for (a) Undamaged, (b) 2-Joule damaged, and (c) 3-Joule damaged specimens during the desorption process.

4.3.3 Dual-Mode Sorption and Damage-Dependent Hysteresis

For a clearer understanding of the observed behavior, dual-mode sorption theory can be applied. Previous studies have described the moisture diffusion in a polymer composites to consist of two diffusion processes—a fast and a slow process, with both processes having different diffusivities and equilibrium uptakes. The slow process represents Fickian diffusion within the matrix, while the fast process is a function of the physical flaws [22]. At very low damage levels, these processes are barely distinguishable by gravimetric moisture uptake data as shown in Figure 26. However, due to water existing in the free state within flaws but being much more constrained as it navigates the undamaged polymer network, these processes are even more prominent in the relative permittivity data and could be correlated with polymer-water interaction mechanisms. Figure 32 (a) and (b) show the relative permittivity desorption curves specific to an undamaged and damaged region for the 3-Joule damaged specimen. For both regions, a line of best fit is obtained by considering only data points below 0.45% moisture. In both cases, a linear relationship is observed between relative permittivity change and moisture content. This line is then extrapolated to predict the change in relative permittivity at higher moisture levels (> 0.45%). For the undamaged region, the prediction is quite accurate, signifying a predominantly single-mode diffusion process making up the desorption curve. Conversely, the linear extrapolation for the damaged region significantly under predicts the change in relative permittivity at higher levels, suggesting the presence of an additional diffusion process. To address this difference, a 2^{nd} order polynomial curve is added representing the second component (predominantly free water). The free water component rapidly decreases to zero while the bound water component gradually decreases in a linear fashion. Similar analysis and decomposition can be performed for the

absorption process to show rapid increase in relative permittivity in the damaged region due to free water, and a gradual linear increase due to physically constrained and chemically bound water.

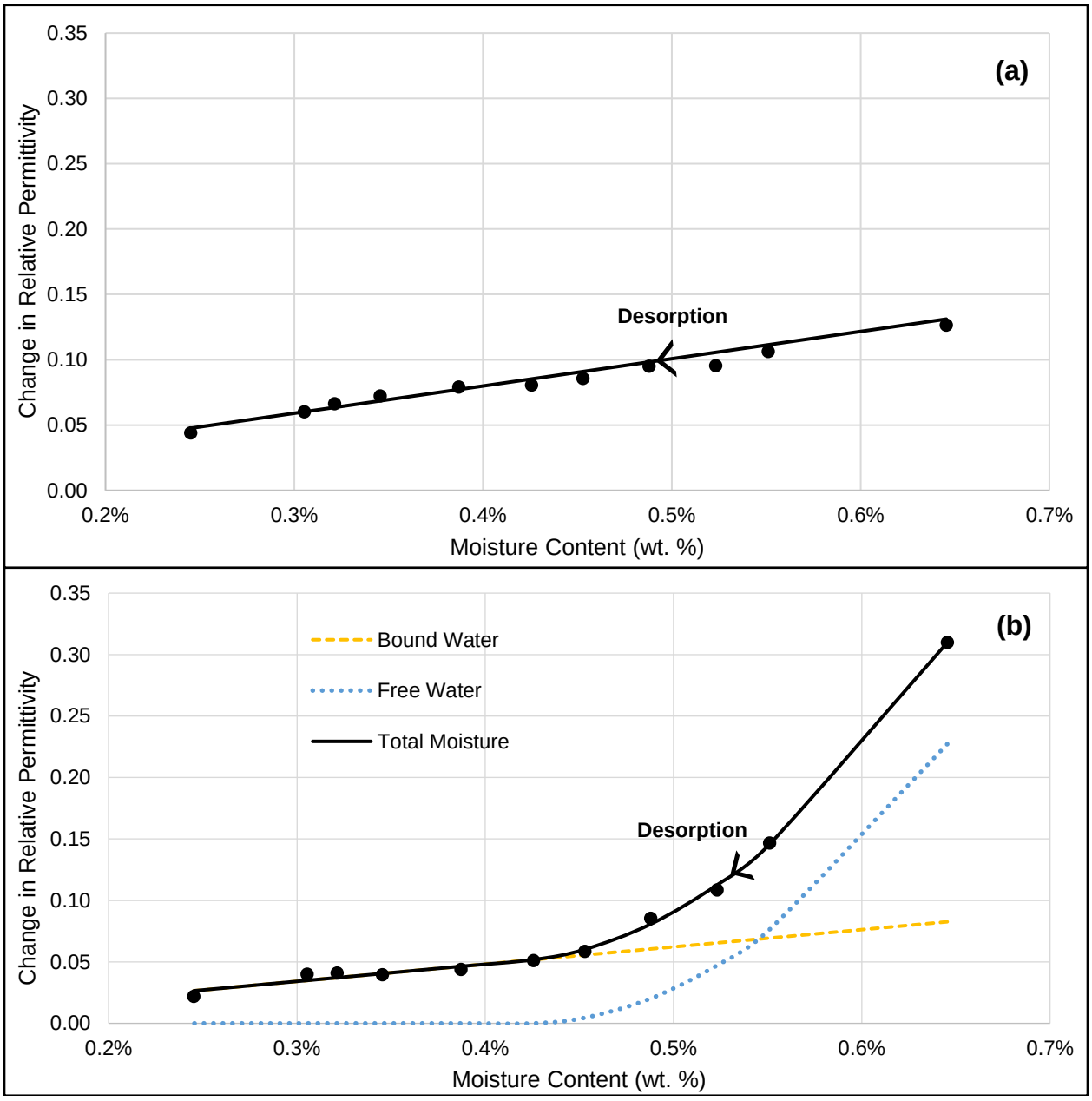

Figure 32: Plot showing (a) Single-phase desorption in undamaged region and (b) two-phase desorption in damaged region of a 3-Joule damaged specimen.

By combining the relative permittivity curves for the absorption and desorption process at the damaged region, an interesting distinction is observed in the form of a hysteresis loop (see Figure 33). For the damaged specimens, significant hysteresis is observed during absorption and desorption at the damage location. The size of the loop is also correlated with the magnitude of damage, with higher damage levels producing larger hysteresis loops. Further, the absorption and desorption curves for the undamaged specimens (or undamaged regions in damaged specimens) both indicate a linear relationship between relative permittivity and moisture content. They show essentially no hysteresis, with absorption and desorption paths appearing approximately coincident.

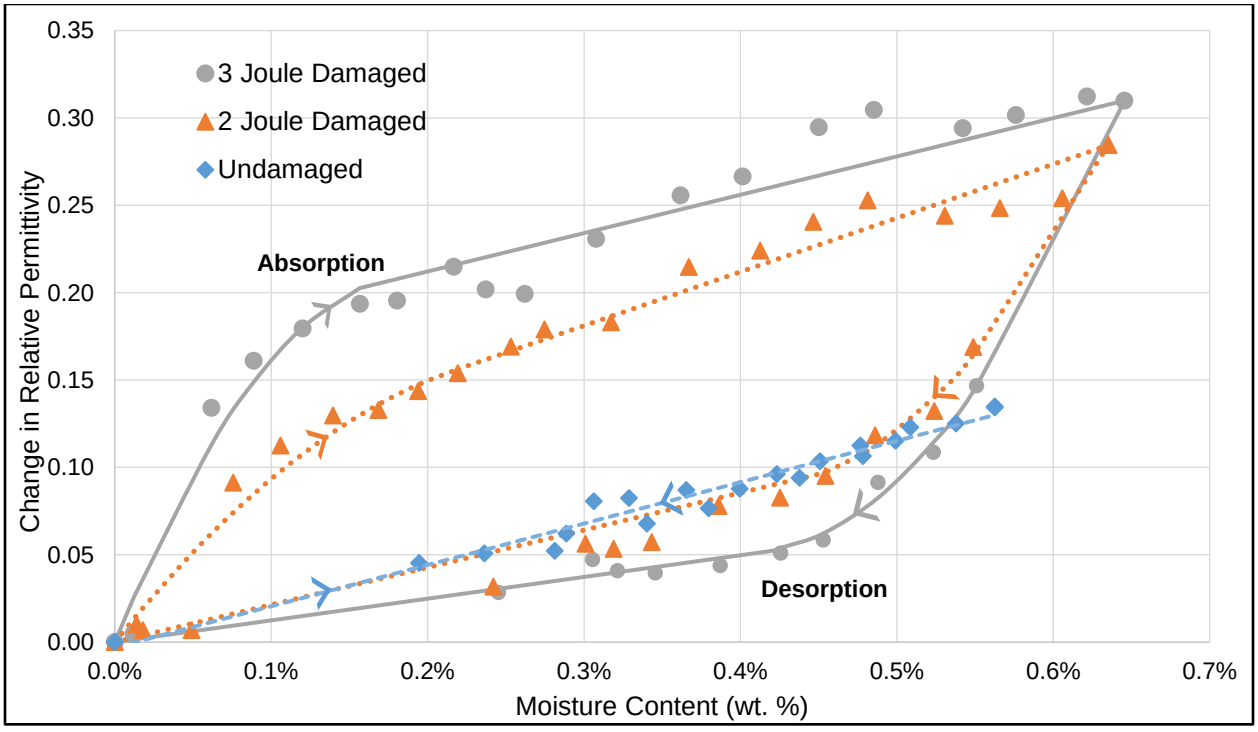

Figure 33: Plot showing damage-dependent hysteresis in relative permittivity during absorption and desorption for undamaged, 2-Joule, and 3-Joule damaged specimens.

4.3.4 Discussion

The different results during absorption and desorption clearly demonstrate that spatial variation of relative permittivity across a damaged specimen is a complex phenomenon involving not only magnitude of damage and total water content, but also the direction of the moisture concentration trend. Identifying damage locations, then, is not a simple exercise in finding areas of higher relative permittivity, but in finding areas that are more sensitive to changing external moisture conditions such as humidity or precipitation fluctuations.

Subtraction of each specimen's relative permittivity in its dry and undamaged state from subsequent moisture-contaminated states allows isolation of the effect of moisture-related changes to relative permittivity. These moisture-driven changes in relative permittivity are due to contributions from three potential effects: differences in local concentration of total water content, differences in local ratio of free to bound water states, or local changes in specimen thickness due to swelling. Though the method is sensitive to thickness variation and the contribution of thickness changes from the dry to moisture-contaminated state cannot be entirely discounted, we believe the low moisture content and exposure time preclude measurable swelling. Manual thickness measurements support this conclusion, having shown no change from dry to moisture-contaminated state. The presence of additional diffusion pathways related to physical damage and additional free volume likely contribute significantly to local relative permittivity in damaged areas due to higher water volume in these areas.

With this understanding, we can deduce from the results that water exists in the free state within the relatively large voids in the form of matrix cracks and delaminations created due to impact damage. The sharp rise and drop in relative permittivity at the damaged region—during the early absorption and desorption process respectively—is indicative of free water migrating

between the damaged site and the external environment. This migration of water to and from the damage site is likely enhanced by fractures in the polymer matrix creating easier pathways for moisture intrusion. Meanwhile, moisture migration to the undamaged areas is driven largely by traditional diffusion kinetics [22], indicated by the gradual rise in relative permittivity.

Another peculiar feature of the relative permittivity curves for the absorption and desorption process is the depression in relative permittivity at the damage location (see Figure 29 (b) & (c) and Figure 31 (b) & (c)). Immediately following impact and before moisture diffusion to the damage site, the bulk relative permittivity includes some contribution from initially empty space within newly created voids. Therefore, the relative permittivity within these voids would, initially, be close to unity (the relative permittivity of free space and air) [38,125], resulting in a reduction in the local bulk relative permittivity [126]. A similar outcome is observed during the desorption process, where free water in the voids desorbs much faster from the damaged region, leaving dry air. The relative permittivity within these voids again would be closer to unity compared to that of constrained and bound water in the undamaged region, leading to a reduction in the bulk relative permittivity and a depression of the curve at the damaged region.

This result is consistent with the mobility of free versus bound water; the latter requires substantial energy to break the hydrogen bond or other secondary bonding interaction with the water molecule [55,93,116,127]. Even in the absence of chemical polymer-water interaction, a water molecule with direct access to the outside environment will obviously more easily migrate and evaporate when compared to a free water molecular that must first navigate a more tortuous path through the polymer network.

From the results obtained we can infer that when polymer-water interactions are leveraged as a basis for non-destructive examination, moisture desorption may cause a loss in sensitivity to

damage, as shown in Figure 31 (b) and (c). Further, there exists the potential for temporary moisture states where the damaged region is indistinguishable from the undamaged region. For example, Figure 30 (middle) or the curve labelled 'A' in Figure 31 (b) & (c) show that the relative permittivity change is uniform across the specimens. To account for such scenarios, the use of moisture absorption-desorption hysteresis loops as a basis for damage detection may be a more accurate approach. The hysteresis loops could be used to not only identify the damage location but also estimate the extent of damage, while eliminating uncertainties due to prior moisture absorption or desorption states. This is particularly important as the loop size appears to be dependent on the extent of damage as shown in Figure 33. In addition, sensitivity to smaller levels of damage could be enhanced by achieving higher levels of moisture content before start of desorption. In such a case, at least two scans would be required and a small natural fluctuation in the total moisture content, driven by variations in the environment, would be necessary. The level of damage and environmental variations required, along with the likelihood of finding damage based on measurement intervals, is a subject of future study.

4.4 Conclusion

The effect of moisture absorption/desorption history on sensitivity to damage of water state distributions in a polymer composite, was investigated. Water molecules, normally in the 'free' state, become 'bound' due to physical constraints or chemical interactions. While our previous studies showed how these interactions can be leveraged for damage detection in polymer composites, this study investigates how free and bound water distributions across a damaged laminate change during absorption and desorption processes. Experiments involved inducing barely-visible damage—up to 3 Joules impact—in 22-ply epoxy/glass fiber composite laminates. The dry laminates were first exposed to moisture, absorbing up to 0.65 % by weight, prior to

desorption in a low humidity chamber. Polymer-water interactions, associated with microwave-frequency relative permittivity, were characterized using a split post dielectric resonator at 5 GHz. Results obtained show rapid non-linear changes in relative permittivity, proportional to the level of damage, during the early stages of absorption and desorption at the damaged region. This was then followed by a steady linear behavior. While in undamaged regions, only this steady linear behavior was observed. Further analysis of these results suggest a linear single-mode sorption process in the undamaged regions, due to traditional diffusion kinetics; this comprises largely moisture in the bound state. While in damaged regions, a dual-mode sorption process exists, having an additional non-linear component made up of free water occupying impact-induced cracks within the polymer matrix. Results also indicate damage-dependent hysteresis behavior in relative permittivity, with hysteresis loop size directly correlated with the extent of damage.

Understanding how the sensitivity to damage of water state distributions is affected by moisture absorption/desorption history, is important in achieving accurate damage prediction using polymer-water interactions. For nondestructive examination, additional uncertainty is introduced by having no knowledge of the absorption/desorption history of the polymer composite structure. This uncertainty and any loss in sensitivity could be mitigated by adopting an approach based on the size of the relative permittivity hysteresis loop, generated by variation in moisture content.

CHAPTER 5: LEVERAGING POLYMER-WATER INTERACTIONS AND DAMAGE-DEPENDENT HYSTERESIS FOR QUANTITATIVE DAMAGE DETECTION

5.1 Rationale

Polymer composites are becoming widely adopted in engineering applications. As they replace metals in various safety-critical moderate temperature service environments [10,12], ascertaining their damage state and fitness for service becomes more crucial. This is confounded by the difference in behavior of these layered materials with regards to damage. Unlike metals, internal damage may be present in the absence of visible surface damage [35,109], especially when paint or coatings are applied. Such damage may be induced during routine operations such as thermal cycling, hail or dropped-tool impact, and cyclic loading leading to matrix cracking, fiber-matrix debonding, and delaminations which may weaken the structure without any warning signs [77,104].

All current nondestructive examination (NDE) techniques for polymer matrix composites have various limitations. These include: inability to characterize beyond a certain depth, limitation to flaws of specific orientation, challenges in flaw localization and characterization, limitations to materials of specific electrical conductivity, and system complexity—requiring a skilled operator [77,81,82]. Hence, many NDE procedures for safety critical parts have adopted the use of multiple techniques to ascertain structural integrity or they simply incorporate larger design safety factors to compensate for these shortcomings [3]. Therefore novel approaches to NDE of polymer composites are still required to provide reliable, simple, and cost effective solutions. One such approach which may provide a viable solution to many of these challenges is the use of naturally absorbed water as an ‘imaging agent’ for damage detection in these materials [5,36,37,107].

Polymer matrix composites have a tendency to absorb measurable moisture in nearly all operating environments. Studies have shown as much as 2% by weight moisture being absorbed in epoxy based polymer matrix composites [17], and over 0.4% absorbed at steady state for environments with relative humidity as low as 21.5% [128]. This absorption is typically driven by traditional diffusion kinetics [18,27,28,31,129–131], polymer polarity [19,20], and damage state of the material [21,22]. Studies have shown the effective diffusion process could be deconvoluted into a combination of these multiple independent diffusion processes [22], providing an opportunity to focus on moisture diffusion due to damage state as a means for damage detection [117].

Water absorbed by the polymer matrix has been reported to exist in the 'free' state—having no interaction with the polymer matrix, or 'bound' state—interacting with the polymer matrix via secondary bonding interactions such as hydrogen bonding with polar functional groups, dipole-dipole attractions, or van der Waals forces with polymer chains [21,41,132,133]. These interactions restrict the mobility of the water molecules, limiting their ability to rotate with an electromagnetic field at microwave frequencies and also influencing the resonant frequency of the oxygen-hydrogen bond vibrations [11,36,52]. These effects have enabled the ability to characterize these polymer-water interactions using near-infrared spectroscopy [11,37] and microwave-frequency dielectric properties [36,51,134], amongst other techniques [41,50,135].

Damage which creates voids within the polymer matrix in the form of matrix cracks, fiber-matrix debonding, and delamination create ideal sites for water to exist in the free state [41,120,122]. While, in undamaged regions water molecules behave differently due to their close proximity to the polymer network, leading to interactions that limit it to the bound state [41,60,122]. Hence, a higher concentration of free water could be an indication of damage.

Furthermore, leveraging such a molecular level phenomenon for NDE could enable damage detection at sub-micron-scale levels—a limitation of current techniques [5].

In our previous work, we demonstrated how polymer-water interactions can be characterized and the effects of localized impact damage on the water state distribution [5]. We further investigated humidity fluctuations in the ambient environment leading to loss or gain of total moisture and its effect on the water state distributions in a damaged polymer composite laminate [117]. We concluded that such variations in moisture content had a significant effect on the sensitivity to damage of polymer-water interactions. Single-mode sorption was also observed in undamaged regions and dual-mode sorption in damaged regions. This led to the discovery of damage-dependent hysteresis in polymer composites, providing a reliable basis for nondestructive damage detection [117]. However, in these studies, only a qualitative determination of damage state based on polymer-water interactions and damage-dependent hysteresis was outlined. Hence, an approach to map the location of damaged areas in polymer composites is required.

This study builds on knowledge gained in behavior of polymer-water interactions and explores ways to quantitatively define the extent of localized damage in a polymer matrix composite. Polymer-water interactions are characterized using microwave-frequency dielectric properties by coupling a split post dielectric resonator to a vector network analyzer [75]. Similar to scans in our previous work [117], water state distributions are obtained by 2-dimensional scans showing spatial variation in relative permittivity (real part of dielectric constant) across the polymer matrix composite laminate. The first method explored is based on a single scan taken during the absorption process, while the second method is based on multiple scans taken during the absorption and desorption processes—an approach based on damage-dependent hysteresis. To map out the damaged regions and demonstrate predictability, a machine learning based approach

is adopted. Finally, progress towards a highly sensitive generalized approach is discussed, and further considerations required to achieve this are presented.

5.2 Materials and Methods

5.2.1 Experimental Details

A detailed description of the experimental procedure used in this study has been provided in our previous work [117]. These include a description of materials used, fabrication processes, material properties, sample conditioning, impact setup, dielectric measurement, and the data collection process at each measurement interval. Reference should be made to Section 4.2 of this work or Section 2 (Experimental) of the publication for these details [117]. Also, a discussion on how confounding factors were mitigated has been provided in Section 4.3.1 [117]. Hence, the rest of this section will focus on details relevant to data processing that would enable successful damage prediction.

5.2.2 Machine Learning Model

In order to determine the damage state across the laminate, a prediction of ‘undamaged’ or ‘damaged’ would be required at all points. This can be interpreted as a binary classification problem which can be solved using various machine learning models, i.e. neural network, logistic regression, clustering, etc. Due to the fairly low number of predictive features, a logistic regression model is employed. The machine learning model is implemented using MATLAB® and optimization is achieved using the ‘fminunc’ (function minimization unconstrained) advanced optimization function. The fminunc function requires a cost function as the main input. The cost function outputs the prediction error for a set of model parameters (weights) and their gradients. Other inputs required include optimization options such as maximum number of iterations and

'GradObj' which is set to 'on'—specifying that the gradient would be provided at each iteration. Initial parameter values are also required.

The logistic regression cost function is composed of two parts—a log-loss cost term and a regularization term (see Equation 4) [136,137]. The log-loss cost term is ideal to avoid local minimums during optimization of the logistic regression model. The regularization term is included to avoid over-fitting the data by adjusting the regularization parameter λ. This parameter determines how much effect the term has on the cost function [136]. The gradient function is the partial derivative of the cost function with respect to the parameters (see Equation 5) [136]. This helps point the algorithm in the direction of minimum cost for subsequent iterations. Note that the derivative of the cost function with respect to the first parameter (θ_j) is not regularized (hence Equation 5a) [136].

Cost:

$$J(\theta) = \frac{1}{m}\sum_{i=1}^{m}\left[-y^{(i)}\log\left(h_\theta\left(x^{(i)}\right)\right) - \left(1-y^{(i)}\right)\log\left(1-h_\theta\left(x^{(i)}\right)\right)\right] + \frac{\lambda}{2m}\sum_{j=1}^{n}\theta_j^2 \quad (4)$$

Gradient:

$$\frac{\partial J(\theta)}{\partial \theta_j} = \frac{1}{m}\sum_{i=1}^{m}\left(h_\theta\left(x^{(i)}\right) - y^{(i)}\right)x_j^{(i)} \qquad \text{for } j = 0 \qquad (5a)$$

$$\frac{\partial J(\theta)}{\partial \theta_j} = \left(\frac{1}{m}\sum_{i=1}^{m}\left(h_\theta\left(x^{(i)}\right) - y^{(i)}\right)x_j^{(i)}\right) + \frac{\lambda}{m}\theta_j \qquad \text{for } j \geq 1 \qquad (5b)$$

Where,

i is the example number

j is the parameter number

m is total number of examples

n is the total number of parameters

θ_j is the weight for the j^{th} feature

$x^{(i)}$ is the input feature of the i^{th} example

$y^{(i)}$ is the output for the i^{th} example

h_θ is the predicted output for an example based on a set of θ parameters

λ is the regularization parameter

5.3 Results and Discussion

5.3.1 Effect of Moisture on Damage Sensitivity

Gravimetric moisture uptake and moisture loss behavior with time has been provided in our previous study showing how absorption/desorption history affect the sensitivity to damage of polymer-water interactions [117]. Figure 34 shows the effect of moisture content on polymer-water interactions by observing the spatial variation in relative permittivity with increasing moisture content for a 2 and 3-Joule impact-damaged specimen. An increased sensitivity to damage is observed with increasing moisture content. Also, with increasing moisture content a subtle increase in relative permittivity is observed in the undamaged regions. This is indicative of a higher proportion of free water relative to bound water migrating to the damaged region, while the gradual increase in relative permittivity in the undamaged region is primarily driven by a higher proportion of physically or chemically bound water [5]. This therefore establishes that the sensitivity to damage is not only a function of the extent of physical damage but also the moisture content, forming a sensitivity triangle comprising moisture content, extent of damage, and relative permittivity as the three main influences. Thus, the relative permittivity and moisture content could serve as ideal predictors of the damage state of a moisture contaminated polymer composite laminate.

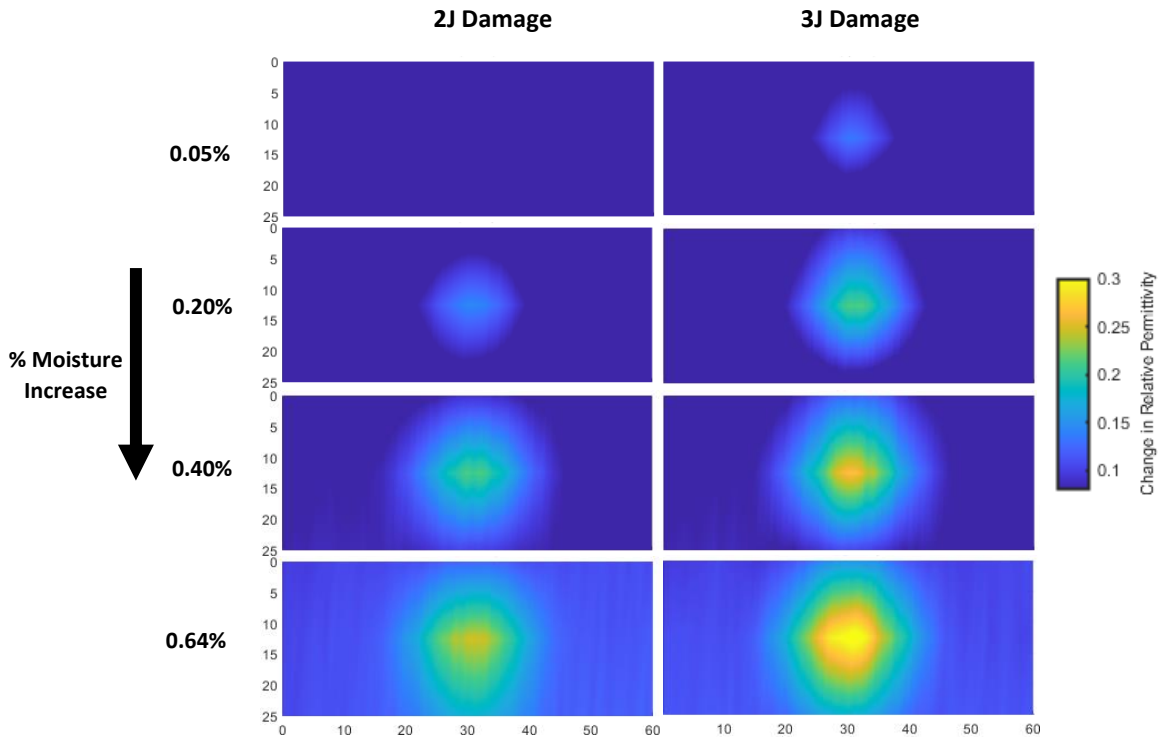

Figure 34: Effect of moisture content on sensitivity of polymer-water interactions to damage. Length measurements in mm.

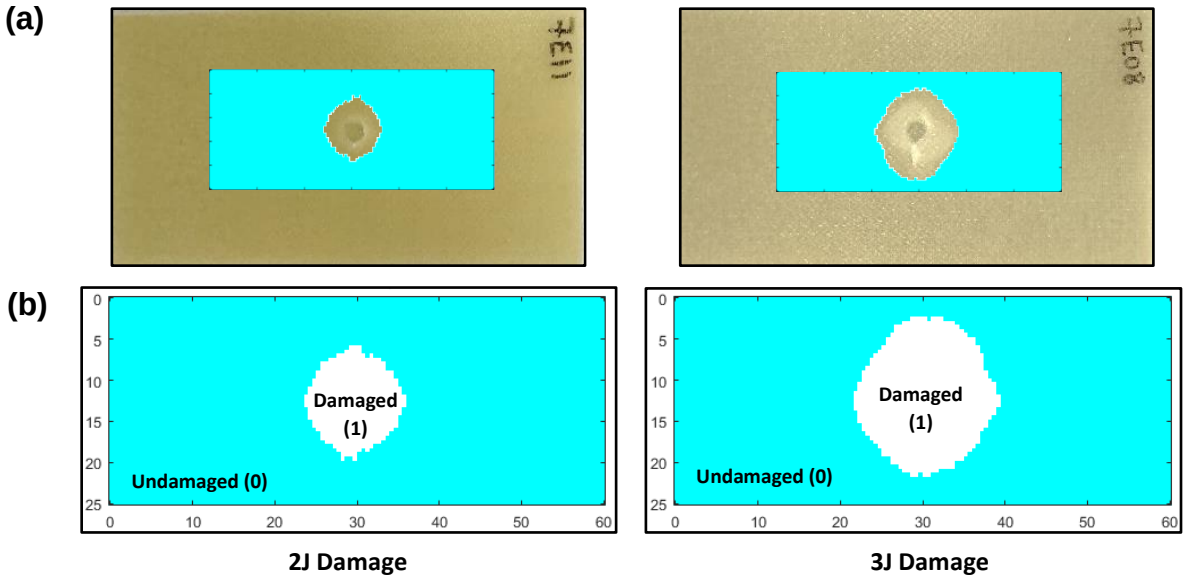

Figure 35: (a) Representative scans superimposed on test specimens to mark damaged regions (b) Labelled representative scans used as training examples. Length measurements in mm.

5.3.2 Input Features for Machine Learning Model

Based on conclusions from Section 5.3.1 above, the total moisture content along with the relative permittivity at the various points across the laminate would be ideal input features in a machine learning model for determining the damage state at each point across a laminate. These are designated as features x_1 and x_2 respectively, while $\boldsymbol{x}$ is the feature vector. The first step is to label the example data which would serve as input for training the logistic regression model. To achieve this, a representative scan image with pixel sizes of 0.5 mm is superimposed on an actual specimen. The relative permittivity at the edge of the damaged region is then determined as the threshold relative permittivity, above which any point would be labelled as damaged (see Figure 35 (a)). Since the output label ($\boldsymbol{y}$) can only be undamaged or damaged, this can be modelled as a binary classification problem [136], where the undamaged regions have an output label of '0' and the damaged regions '1'. Therefore, the final labelled examples would be as shown in Figure 35 (b).

To achieve a non-linear decision boundary with just two features, a combination of various powers of x_1 and x_2 up to the 6th power is used to generate the feature vector ($\boldsymbol{x}$) [138]. This results in a feature vector comprising 28 elements (see Equation 6). Since the desired output is either a '0' or '1', a sigmoid function is employed according to Equation 7 to limit the predictions from this vector to between 0 and 1 [136].

Feature vector:
$$\boldsymbol{x} = [1 \;\; x_1 \;\; x_2 \;\; x_1^2 \;\; x_1x_2 \;\; x_2^2 \;\; x_1^3 \;\; . \;\; . \;\; . \;\; x_1x_2^5 \;\; x_2^6] \tag{6}$$

Sigmoid Function:
$$h_\theta(\boldsymbol{x}) = \frac{1}{1 + \; e^{-\boldsymbol{\theta}^T \boldsymbol{x}}} \tag{7}$$

5.3.3 Training the Machine Learning Model

The total sample consists of four 2-Joule and 3-Joule impact damaged specimens (total of eight specimens). The training data set comprises 75% of the total sample size (three 2-Joule and 3-Joule impacted specimens—total of six), while 25% (a 2-Joule and 3-Joule specimen—total of two) is reserved for the test data set. To eliminate any bias in test set selection, all 16 possible groupings of the specimens into training and test sets were evaluated. Results in Table 3 shows variation in training set accuracy of only 0.15% between upper and lower 95% confidence bounds for the 16 possible combinations, indicating a high level of predictability regardless of grouping. Figure 36 (a) shows a distribution of undamaged and damaged data points as a function of relative permittivity and moisture content for a typical grouping. An interface between the undamaged and damaged data points can be observed. The goal of the model training process is to identify the ideal interface, or decision boundary, between the undamaged and damaged regions. To determine this ideal decision boundary, the model weights (θ) for the input parameters at the minimum cost is required. Equations 4 and 5 provides the cost and gradient functions to be computed at each iteration, where a unique set of θ is tested. The effect of the regularization parameter remained negligible even when reduced to the adopted value of 0.0001, indicating minimal effect of the regularization term in preventing over-fitting. This is simply due to the large number of data points (~ 550,000) used in training the model. Therefore, an additional cross-validation set to optimize this parameter is not required. After training the model, the optimum decision boundary is obtained as shown in Figure 36 (a); this is used in developing the prediction model in Figure 36 (b). The boundary appears to be fairly linear; therefore, a linear model would be a reasonable approximation for prediction of damage based on only moisture content and relative permittivity.

Table 3: Training and Test Set Accuracy

	95% Confidence Interval (%)	
	Upper Bound	Lower Bound
Training Set Accuracy	97.35	97.20
Test Set Accuracy – 2-Joule Impact	98.22	96.88
Test Set Accuracy – 3-Joule Impact	96.78	95.36

5.3.4 Damage Predictions

Using the prediction model developed in Figure 36 (b), each pixel in the 2-dimensional relative permittivity scan is evaluated and—depending on where it falls on the prediction model—is classified as an undamaged or a damaged point. Figure 37 shows predictions on a typical test set for a 2-Joule and 3-Joule impact-damaged specimen at various moisture contents. When compared to scans in Figure 34 where the relative permittivity increased with moisture content, the prediction model compensates for this and effectively predicts the damaged regions at different moisture content. Table 3 shows the associated accuracies in predicting damaged areas in a 2-Joule and 3-Joule damaged specimen. A severe under-prediction is observed for the 2-Joule specimen at and below 0.1% moisture by weight. This indicates that detecting lower levels of damage require higher amounts of moisture to increase sensitivity of the technique. Therefore, a minimum level of moisture content could be established based on the desired level of damage to be detected.

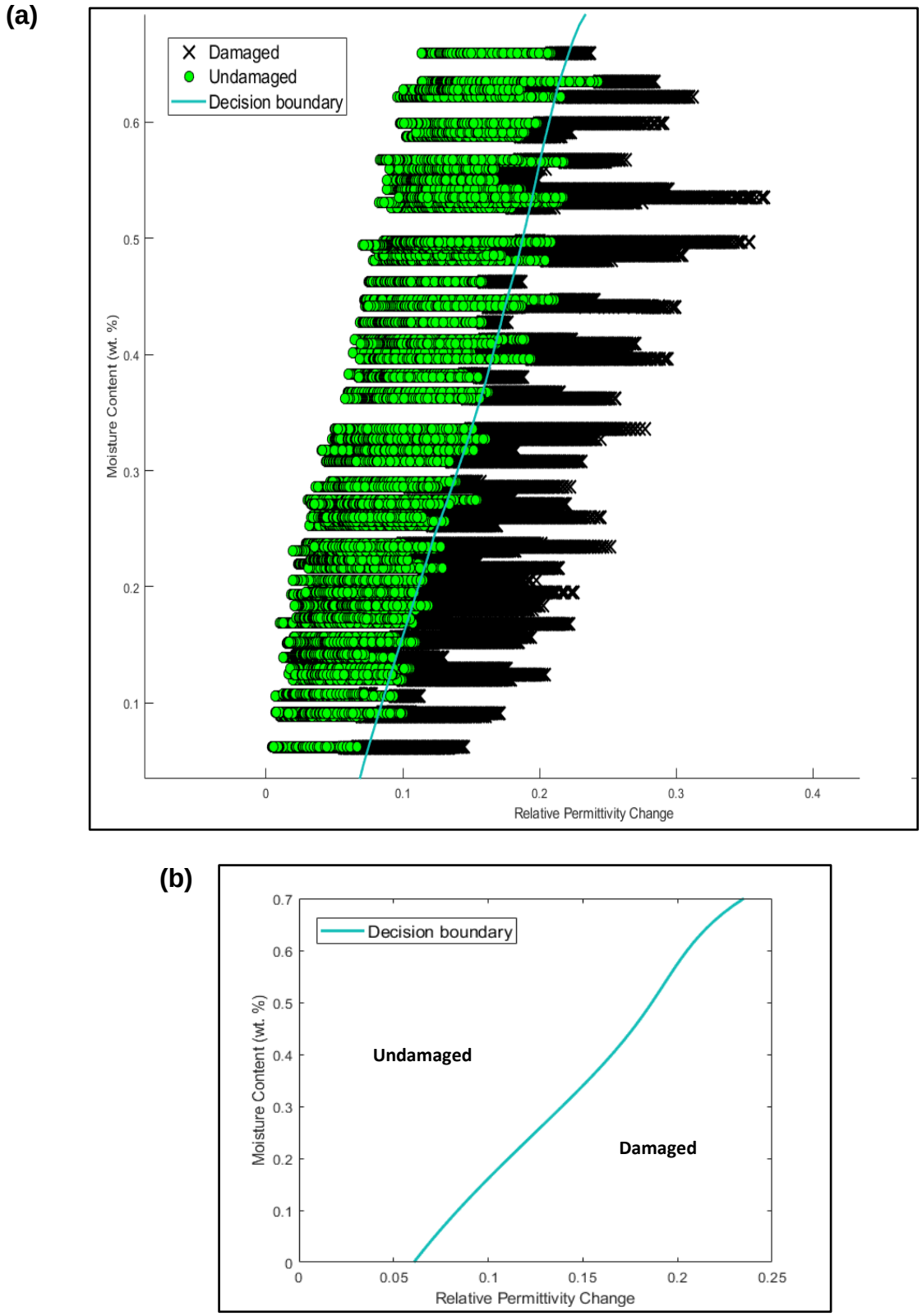

Figure 36: (a) Plot of example data showing undamaged and damaged data points. (b) Final prediction model.

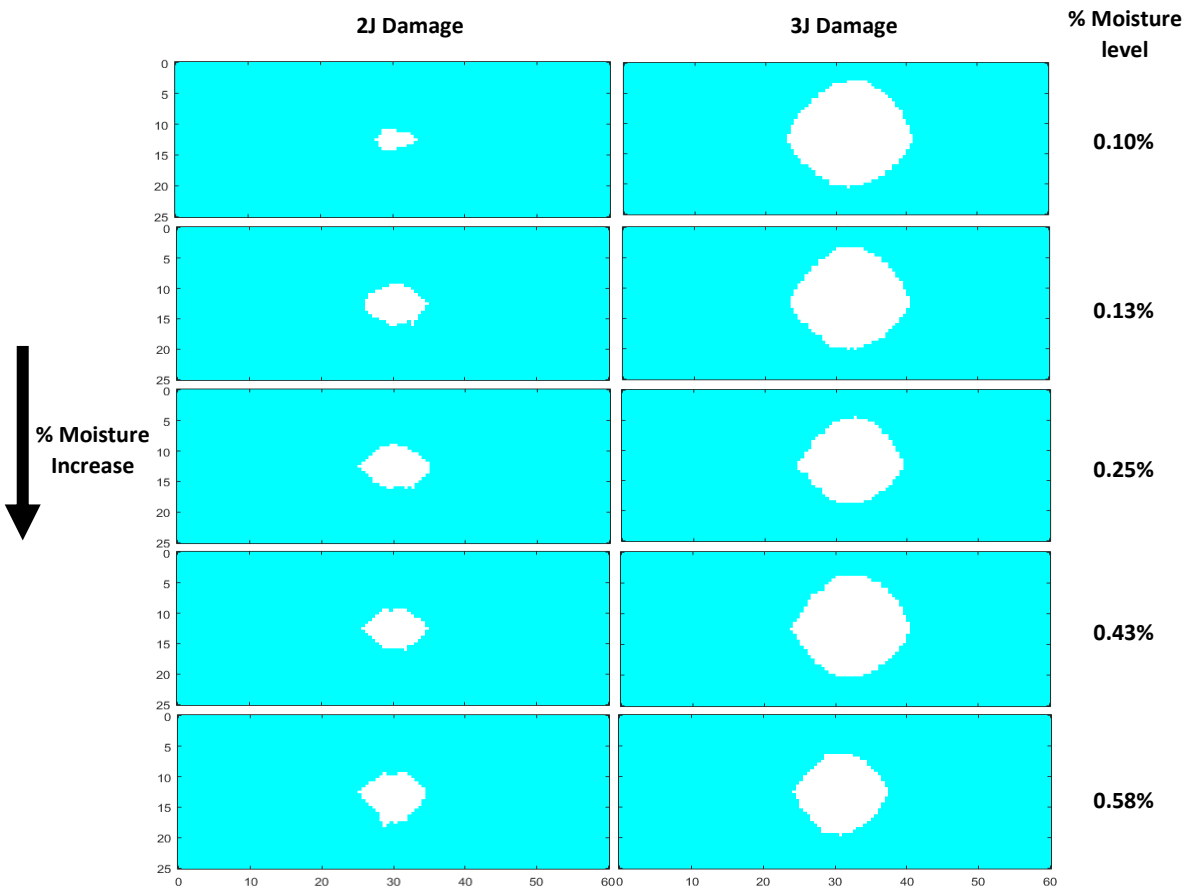

Figure 37: Damage predictions on test set. Length measurements in mm.

5.3.5 Limitations of Damage Detection Based on Absorption Process Scans

The damage detection approach described so far is based on absorption process scans and relative differences in relative permittivity. It has the advantage of requiring only one scan and being simple to implement by training a machine learning model. However, it also has some limitations which could hamper deployment as a damage detection technique for polymer composites. Firstly, the need to subtract the relative permittivity response of the initial dry-pristine condition from subsequent moisture contamination states is not very practical for many field applications where no prior knowledge exists of the dielectric response of the composite part [77]. Secondly, there is some uncertainty due to possible desorption before or during scanning, which

could lead to decreased sensitivity to damage [117]. Thirdly, in the presence of signal noise due to confounding factors [117], relatively low damaged-to-undamaged ratios as shown in Figure 38 may result in difficulty in detecting relative permittivity change as a result of damage. Here we define the damaged-to-undamaged ratio as the largest change in relative permittivity at the damaged region divided by the average relative permittivity change of the undamaged regions. This provides an idea of how sensitive the technique is to damage. Finally, the prediction model developed would be specific to only a unique combination of materials and moisture absorption process. Hence, different models would be required for other material systems or test specimens which undergo a different moisture absorption process and produce a different dielectric response.

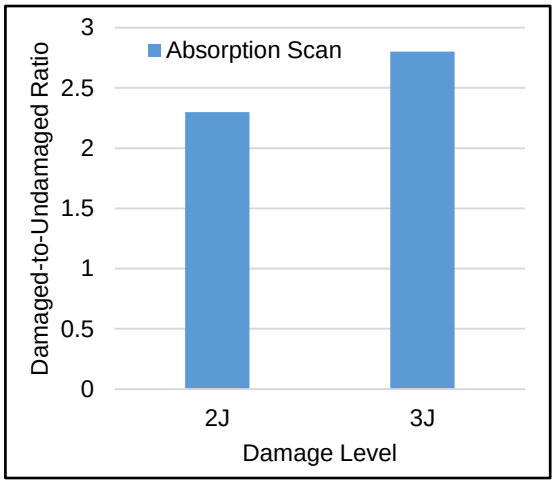

Figure 38: Damaged-to-undamaged ratio for 2 and 3-Joule impact damaged specimens at 0.6% moisture by weight.

5.3.6 Damage-Dependent Hysteresis

The adoption of a damage detection technique based on the damage-dependent hysteresis behavior in polymer composites could provide a viable solution to many of the challenges identified in Section 5.3.5 using absorption process scans. The possibility of leveraging the hysteresis effect as a reliable basis for damage detection was proposed in our previous work

(Chapter 4) [117], where we showed how it can be used to eliminate the uncertainty resulting from fluctuations in total moisture content. We also showed that the size of the hysteresis loops can be correlated to the extent of physical damage within the polymer composite (see Figure 39). Therefore, a way to quantify the size of the hysteresis loop to determine the damage state is required. One way to achieve this is to fit a linear trend line to the absorption-desorption data and calculate the residual sum of squares (RSS). For an undamaged region, the linear trend would fit closely, generating a relatively low RSS. While for a damaged region, a poor linear fit would be achieved leading to a significantly higher RSS (see Figure 40 (a) and (b)).

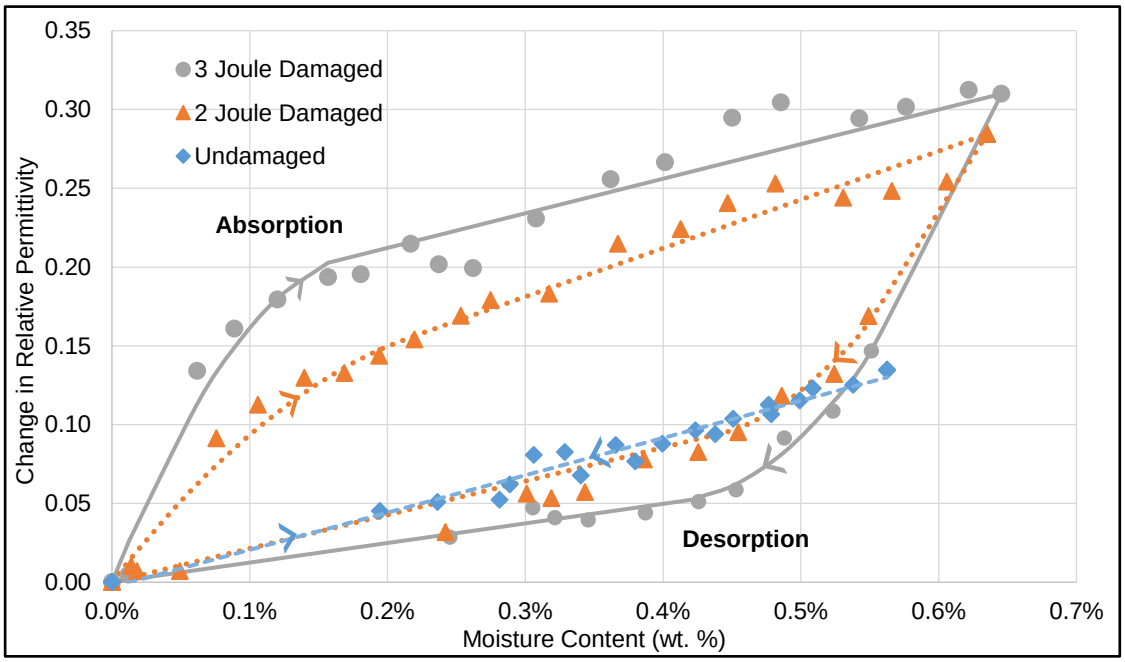

Figure 39: Plot showing damage-dependent hysteresis in relative permittivity [117].

The use of damage-dependent hysteresis also presents an opportunity to eliminate the need for subtraction of the dry-pristine relative permittivity baseline, which may be impractical in many scenarios. By excluding the starting data point at the origin and introducing an intercept term for the linear fit, the use of absolute values of relative permittivity becomes possible. Figure 40 (c)

and (d) shows the plots achieved by incorporating these changes. The undamaged region plot in Figure 40 (c) remains almost identical to Figure 40 (a) due to their close linear fit. While for the damaged region absorption-desorption plot in Figure 40 (d), more flexibility is provided to the linear fit with introduction of an intercept term—enabling a better fit relative to that in Figure 40 (b). Since our damage quantification metric is based on RSS, a better linear fit would lead to a lower RSS and hence less sensitivity to damage.

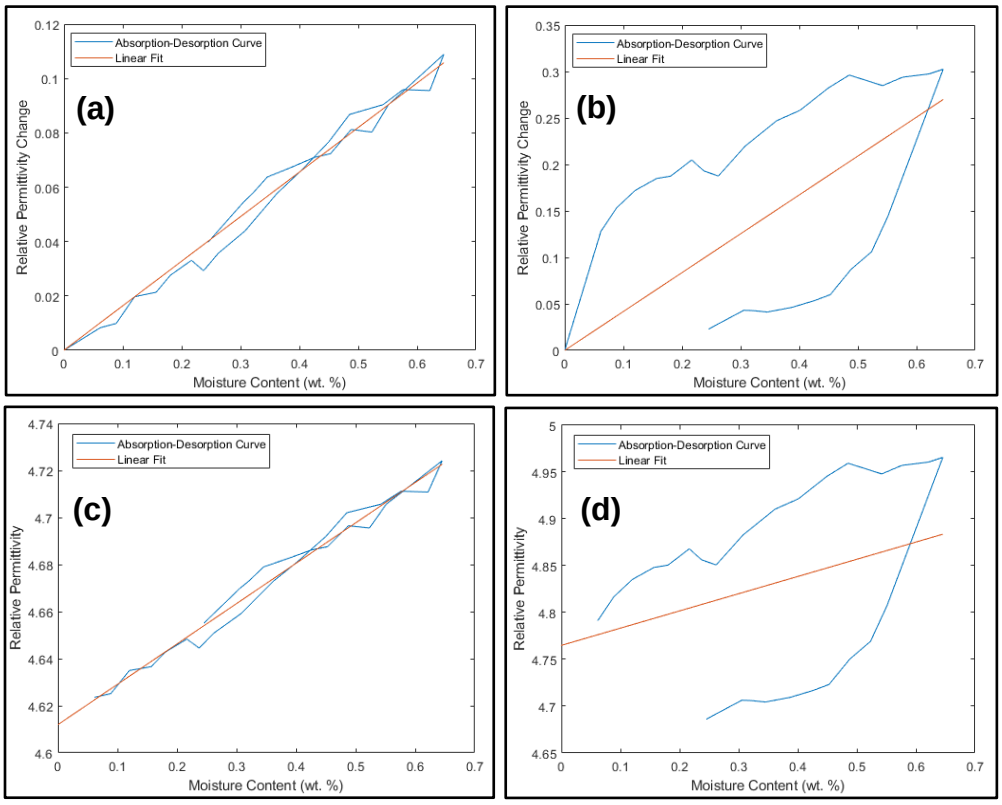

Figure 40: Linear fit to absorption-desorption data for a 3-Joule impact damage specimen in (a) an undamaged region for specific case (b) a damaged region for specific case (c) an undamaged region for generalized case (d) a damaged region for generalized case.

A 2-dimensional plot showing variation in RSS can be produced by generating an absorption-desorption plot for each point on the laminate and then fitting a linear trend line to the plot (see Figure 41). The result obtained is similar to the change in relative permittivity variation

scans in Figure 34, with the RSS scans also showing significantly higher RSS at the damaged regions. However, the RSS scan has some key advantages. Unlike the absorption process scans where the relative permittivity of the undamaged region also increases gradually with moisture content (see Figure 34), for damage-dependent hysteresis the undamaged region remains essentially flat and close to zero for any scenario. This can be clearly seen in Figure 42, which shows the variation in RSS for the middle axis (a horizontal line through the middle) of scans in Figure 41. Also, the sensitivity to the extent of damage is much more pronounced as seen in Figure 41 and Figure 42, showing much better distinction between damage levels. The magnitude of this difference is appreciated when we compare the undamaged-to-damaged ratio for damage-dependent hysteresis and absorption process scans as shown in Figure 38 and Figure 43. Damage-dependent hysteresis shows undamaged-to-damaged ratios close to 400 for the 3-Joule damaged specimens, compared to just 2.8 for the absorption process scan. This is over two orders of magnitude greater, which suggests sensitivity improvements of similar magnitude. Consequently, training a machine learning model based on damage-dependent hysteresis data should produce more accurate predictions with fewer limitations.

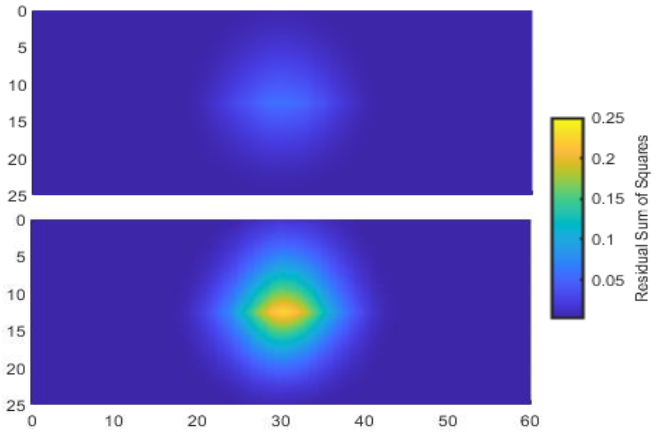

Figure 41: 2-dimensional spatial variation in residual sum of squares for a 2-Joule and 3-Joule impact damaged laminate. Length measurements in mm.

Also, the loss in sensitivity in moving to a generalized process, described earlier, can be observed from Figure 43. This loss appears to be tolerable considering the very high sensitivity levels being achieved with damage-dependent hysteresis.

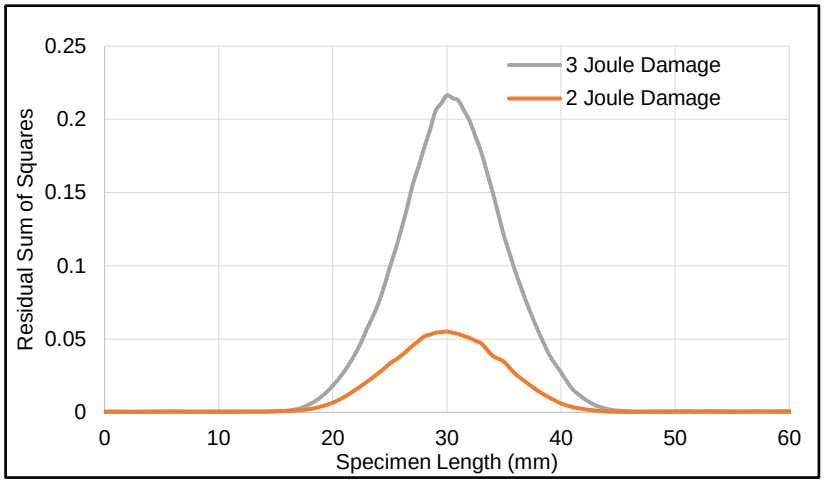

Figure 42: Residual sum of squares variation along the middle axis of a 2-Joule and 3-Joule impact damaged laminate.

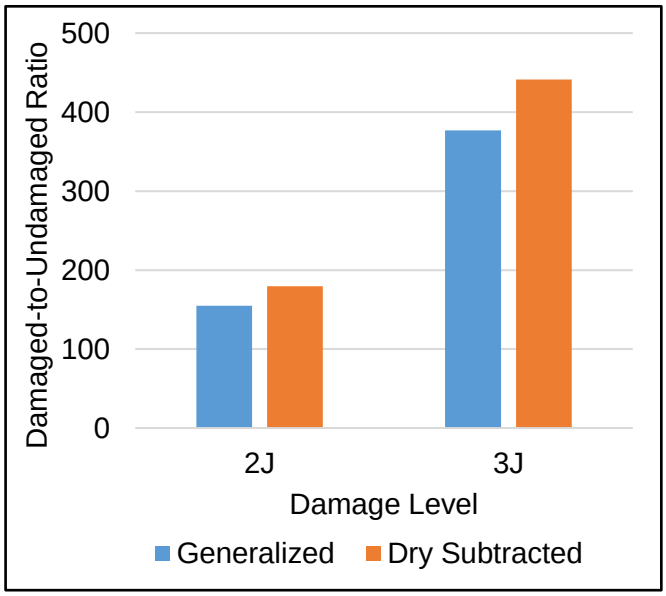

Figure 43: Damaged-to-undamaged ratio for 2 and 3-Joule impact damaged specimens using damage-dependent hysteresis.

5.3.7 New Possibilities with Damage-Dependent Hysteresis

With significantly higher levels of sensitivity now achievable with damage-dependent hysteresis, new possibilities in the development of a nondestructive examination technique based on polymer-water interactions may become feasible; thus providing additional flexibility in factors that influence sensitivity to damage such as moisture variation range, detectable level of damage, number of scans required, sensitivity of dielectric characterization technique, and effects of confounding factors.

A smaller moisture variation range may now be adequate to observe the hysteresis effect. The method could simply take advantage of the rapid non-linear increase during absorption and similar decrease during desorption [5,117], rather than waiting for much slower moisture up-take in the undamaged region. This could lead to a faster damage detection process. Alternatively, the higher sensitivity would allow for detection of lower damage levels, which could enable sub-micron scale damage detection in polymer composites. Such resolution is necessary for detecting damage at the initiation phase [76], which could enable better prediction of yield point and remain useful life in polymer composites.

The number of scans required to generate adequate number of data points for the hysteresis loop could also be reduced since the sensitivity is also closely related to the number of points used in calculating the RSS. Increasing the number of data points would add smaller RSS values to undamaged regions but much larger values to damaged regions, leading to increased sensitivity. Hence depending on the level of sensitivity required, the number of required scans could be optimized. Interpolations between scans to generate additional data points could be another potential means for increasing sensitivity.

Another factor which affects sensitivity is the dielectric characterization method. The use of more robust but less sensitive dielectric characterization techniques could now be possible with the higher sensitivity. The currently used split post dielectric resonance technique for dielectric property characterization is the most accurate technique, with only 0.3% uncertainty [74,106]. However, it has very limited specimen size requirements—0.95 mm, 1.95 mm, and 3.1 mm maximum thickness for 10 GHz, 5 GHz, and 2.4 GHz. Also they work in transmission mode [5,117], requiring access to both sides of a laminate. The less restrictive free space technique could be used in reflectance mode, allowing one-sided characterization in applications where only one side of the laminate is accessible. The downside of the free space technique is its reduced accuracy [74], which could be compensated for by the high sensitivity of the damage-dependent hysteresis technique.

Further studies are required to confirm how each of these newly unlocked possibilities can be leveraged in developing this method from the current laboratory scale to suitability for field applications. Field deployment studies could begin with marine applications, which may be a natural fit for the damage-dependent hysteresis technique. During service, the extreme exposure to moisture can accelerate the absorption phase, while desorption can be achieved naturally during dry docking for maintenance. It would also be necessary to investigate how paint and coating on the polymer composite surface could affect the ability to detect damage. Since majority of polymer composites in service are painted and coated, it would be useful to know how these affect moisture uptake, microwave signal degradation, and distribution of the various water states in a damaged polymer composite.

5.4 Conclusion

This study provides an avenue for the nondestructive detection of damage in polymer matrix composites by analysis of polymer-water interactions and damage-dependent hysteresis. We build on our prior studies which investigated the effect of damage on water state distribution and the role fluctuations in total moisture content plays in determining their degree of sensitivity to damage. These studies concluded that a higher proportion of free water exists in voids created due to damage in a moisture-contaminated polymer composite, and that damage-dependent hysteresis exists for absorption and desorption processes. In this study, a machine learning approach for quantifying damaged regions in a polymer composite is presented. A logistic regression model is trained and evaluated, showing satisfactory performance in mapping out damaged regions in a polymer matrix composite laminate. Furthermore, a generalized basis for nondestructive examination of polymer composites based on damage-dependent hysteresis is demonstrated. This is shown to achieve sensitivity levels which are over two orders of magnitude greater than results obtained by leveraging polymer-water interactions through a single absorption process scan. This improvement in sensitivity enables new possibilities which would allow further development of the technology and scale-up from the lab to a system ready to be applied in the field.

CHAPTER 6: INVESTIGATING THE EFFECT OF PAINTING AND COATINGS ON SENSITIVITY OF POLYMER-WATER INTERACTION NONDESTRUCTIVE EXAMINATION

6.1 Rationale

The surface of polymer matrix composites are typically finished by application of a gel coat, surface veil, primer and/or paint; each compound serving specific purposes. The gel coat is used for contact molding, providing a smooth surface finish, fire retardancy [139], and wear resistance. The surface veil contains compounds which provide ultraviolet protection, corrosion inhibitors, and a weather barrier. Primer and then paint is applied to provide aesthetic value. These possess various compounds which may disrupt moisture diffusion into the polymer composite or degrade microwave-frequency signal. Also, near-infrared light may not be able to penetrate beyond the surface of these coatings. Since in-service polymer matrix composites would typically be coated and painted, it's necessary to evaluate the effect these added layers may have on the sensitivity of polymer-water interactions to damage either by simple absorption process scans or damage-dependent hysteresis.

This work involves evaluating the effect of commercially available paint and coating systems on the ability to detect low levels of damage. The effects of moisture contamination and damage on polymer-water interactions within uncoated and one-side coated polymer matrix composite laminates is investigated. The chosen variants are representative of how polymer matrix composite surfaces are finished for in-service structures. The selected surface finish is identical to typical military aircraft specifications and is fabricated by a certified shop (VX Aerospace) to ensure compliance with industry standards.

6.2 Materials and Methods

6.2.1 Sample Preparation

The test plaques are made with 7 plies of MTC412-G300-8HS-38%RW-OST-50 prepreg, which is a G300 glass, 8-harness plain weave, and a mix of 38% resin by weight applied to one side of the fabric. The resin system is proprietary to SHD^{TM} composites and was designed with the intent of being a replacement to MTM45-1, a Solvay^{TM} resin, which is industry standard on many aerospace production parts.

Each plaque is laid up on a glass substrate material to ensure overall laminate flatness with peel ply underneath and on top of the laminate during the cure cycle. The peel ply not only ensures that the part surface is acceptable for primer/paint adhesion without much preparation, but also promotes the removal of air during the vacuum bagging process. All plies are a 0/90° fabric which are laid down in alternating warp/weft directions to minimize any inconsistencies within the plies themselves.

Vacuum bagging is done via standard practices, applying layers of peel ply, non-perforated release, breather material, and a plastic vacuum bagging material surface bagged down to the glass substrate with tacky tape. Two vacuum ports are utilized, one used as a gage and the other for a vacuum line. The assembly is leak checked to ensure it holds a minimum of 85 kPa without any leaks.

The prepreg requires a cure cycle which ramps at a rate of 1-2 °F/min and a pre-soak at 140 °F for 3 hours. This is followed by a curing soak at 270 °F for an additional 3 hours with a slow ramp down to room temperature at 1-2 °F/min. The first soak is done to promote resin fluidity by reducing the overall viscosity.

Once the laminate is produced, the final dimensions are cut on a band-saw to 1/8” outside of the overall part lines, then finally trimmed down with grit blocks increasing in grit number until the desired dimensions are achieved.

Surface preparation is done by sanding with 180 grit sandpaper to remove any small resin buildup due to wrinkles in the release or bagging material (minimal on a flat layup). A skim coat of aeropoxy (lightweight aerospace filler) is applied and is sanded down for flatness, leaving the filler in low spots. The surface is then prepared for painting with a 220 grit wet sandpaper.

The primer applied is MIL-PRF-23377 Class N primer, which is a non-chromate primer for non-ferrous substrates; this is allowed to cure before the paint is applied. For the coated laminates, one coat of MIL-DTL-64159 Type II federal color standard 30051 [140], typically used on military helicopters and airplanes, is applied on the side to be coated.

6.2.2 Sample conditioning and Measurement Procedure

The two types of laminates (uncoated and coated) were further cut into 55 x 100 mm specimens using a wet diamond-tipped saw. Groups included three specimens each for undamaged-uncoated, damaged-uncoated, undamaged-coated, and damaged-coated variants (total of 12 specimens).

The damaged specimens were impacted at 5 Joules as described in Section 4.2.3. Moisture contamination was achieved by exposure to a humid environment, having greater than 85% relative humidity at room temperature. The specimens were placed in a low humidity chamber for desorption. The chamber achieved less than 10% relative humidity using 8% indicating t.h.e.® desiccant.

Note that all gravimetric and dielectric data were collected according to procedures described in Section 4.2.5.

6.3 Results and Discussion

The plot in Figure 44 (a) shows moisture uptake behavior for undamaged and impact-damaged uncoated and coated polymer matrix composite laminates. A clear distinction between the moisture absorption rate for the uncoated and coated is observed, with the coated absorbing significantly more moisture than the uncoated specimens. In Figure 44 (b) a similar behavior is observed during desorption. This highlights the effect of the coating which is composed of filler, primer, and paint. The actual content of these resins are proprietary, but they primarily comprise epoxy and polyurethane. Therefore, this additional resin has an effect of decreasing the fiber volume fraction, which studies have reported leads to higher diffusivities and equilibrium moisture content [14].

Effects of the coating on sensitivity to damage is investigated by observing the change in relative permittivity at the middle-axis (see Section 4.3.2 and Figure 25 (b)) of the specimen at various moisture levels. Figure 45 (a) shows a higher increase in relative permittivity at the damage location compared with the undamaged region as moisture levels increase. During desorption (Figure 45 (b)) a similar trend is observed, with the relative permittivity of the damaged region reducing faster than the undamaged regions. At lower moisture levels (<0.37%) this difference disappears, with the curves becoming essentially flat. This is consistent with hysteresis behavior observed in Section 4.3.3 [117].

Figure 46 shows similar plots for the coated specimen. The behavior is similar to that observed in the uncoated specimens but with less sensitivity to the damaged region, indicating the coating has an effect of reducing sensitivity to damage.

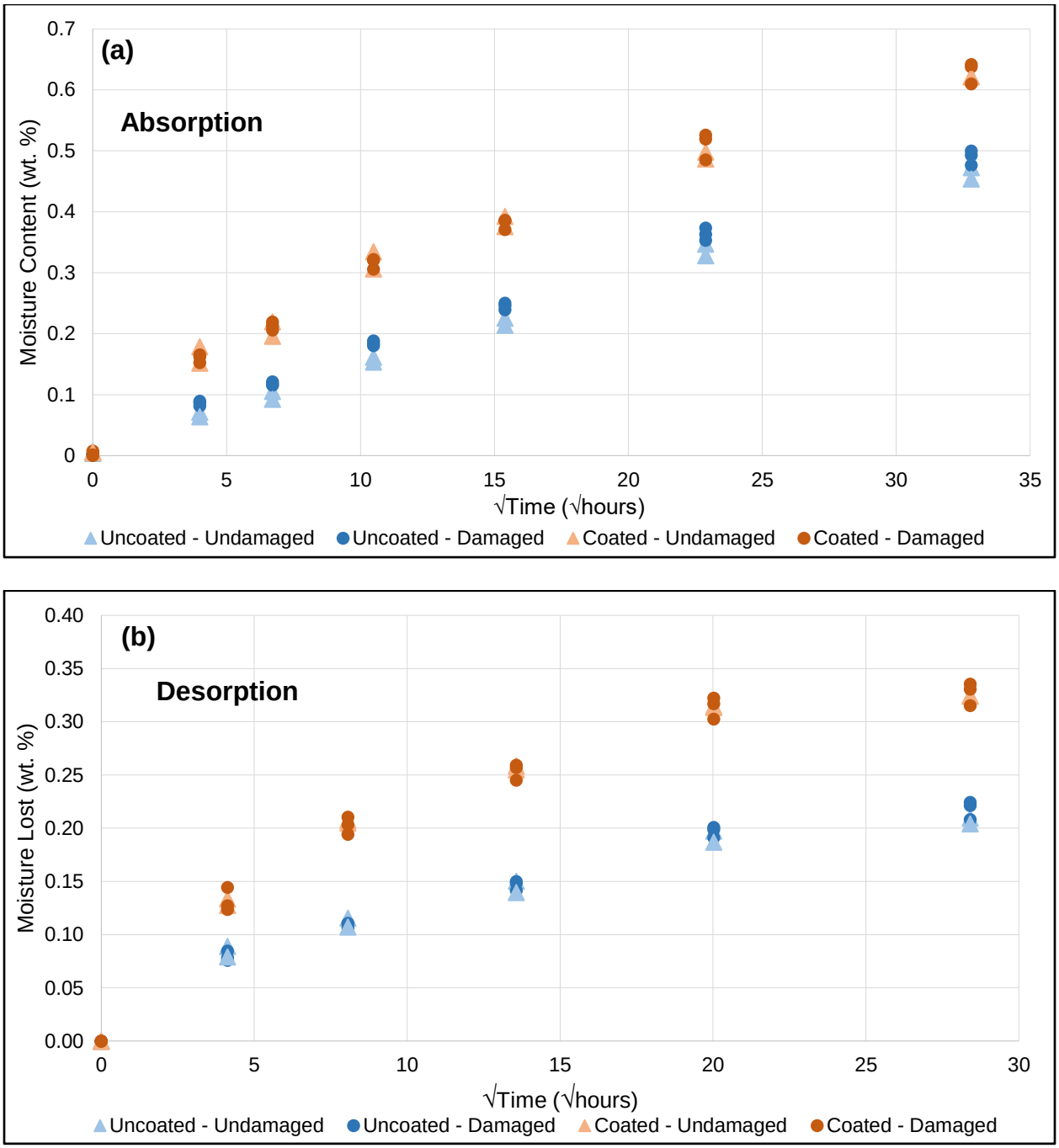

Figure 44: Change in % moisture content by weight with root of time for damaged and undamaged variants of uncoated and coated polymer matrix composite laminates during (a) moisture uptake (b) moisture loss.

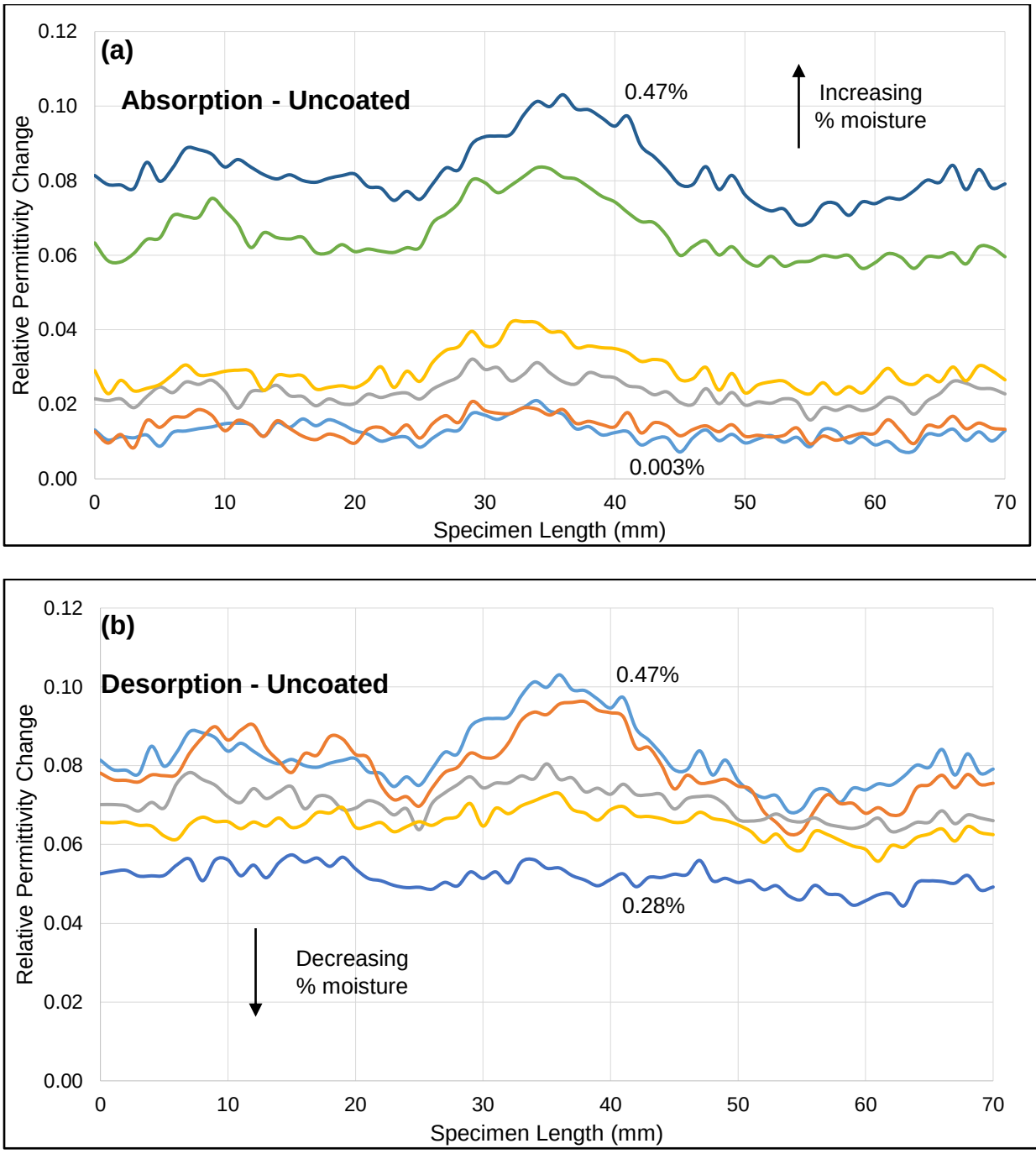

Figure 45: Relative permittivity change with wt. % moisture content for middle-axis scans across an uncoated impact-damaged polymer matrix composite laminate during (a) absorption (b) desorption.

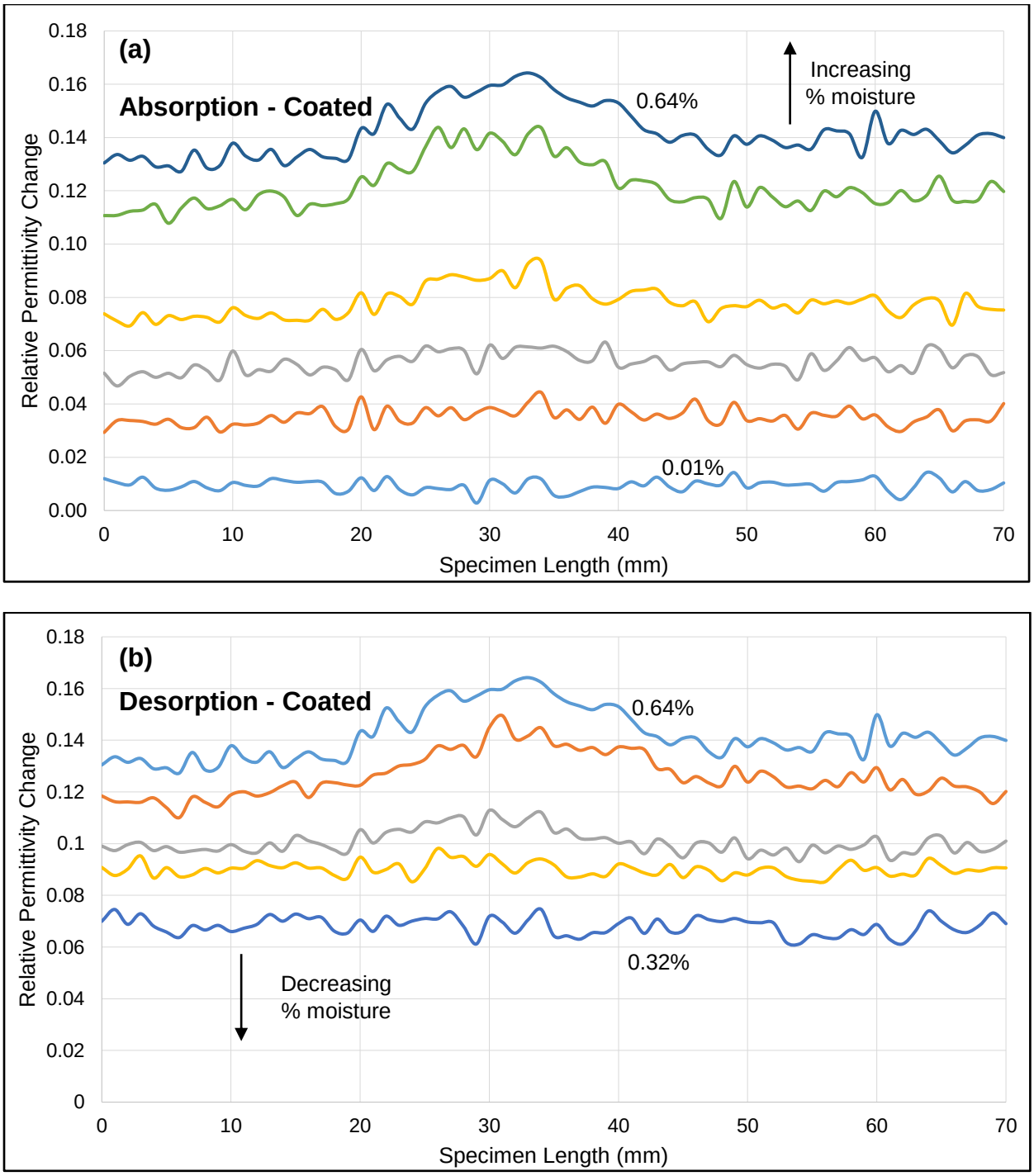

Figure 46: Relative permittivity change with wt. % moisture content for middle-axis scans across a coated impact-damaged polymer matrix composite laminate during (a) absorption (b) desorption.

The higher moisture content achieved in the coated specimens does not lead to a higher increase in relative permittivity at the damaged region—as would be expected from our previous work on polymer-water interactions described in Section 5.3.1—but leads a more general increase. This suggests the additional water is absorbed by the polyurethane and epoxy coating layer only [128], and not into the voids and fractures created as a result of impact-damage. The interaction of water with polyurethane and epoxy has been studied using differential scanning calorimetry and infrared spectroscopy, and the findings published in literature [41]. Results from these studies indicate that strong hydrogen bonds are formed between water molecules and active functional groups contained in the coating such as ether, secondary and tertiary amine, carbonyl, epoxide, isocyanate, and hydroxyl [41]. These are polar in nature and have a tendency to partake in hydrogen bonding. The studies also show that water in the free state exists between the polyurethane-epoxy interface.

Figure 47 and Figure 48 shows how the additional layer of coating tends to decrease the sensitivity to damage. The extent of damage can be quantified by applying the highly sensitive damage-dependent hysteresis technique described in Section 5.3.6 to the absorption-desorption plots in Figure 47, for uncoated and coated specimens. Figure 47 (a) and (b) show an increase in slope with damage due to water in the free state at the damaged region. Furthermore, the relatively higher slopes in the coated specimens again indicate higher free water levels, but in this case resulting from free water absorbed within the coating only. Free water is known to degrade microwave signals due to its lossy nature [51,52]; this could lead to difficulty in characterizing effects of moisture in the coated laminate, leading to loss in sensitivity to damage. To measure this sensitivity loss, the technique of comparing the deviation from a linear-fit with increasing damage—demonstrated in Section 5.3.6—can be employed. The deviation from linear-fit is

measured by calculating the residual sum of squares (RSS). For the uncoated and coated specimens, the RSS are computed for both undamaged and damaged regions; then the damaged-to-undamaged ratio (see Section 5.3.5) is then computed, providing an indicator of sensitivity to damage. A smaller difference in deviation from the linear-fit is observed between the undamaged and damaged areas in the coated laminate compared to the uncoated.

Figure 48 (a) and (b) shows the effect of the coating on sensitivity to damage for the absorption process scans and the damage dependent hysteresis scans, indicating approximately 6% and 40% loss in sensitivity respectively, due to the coating.

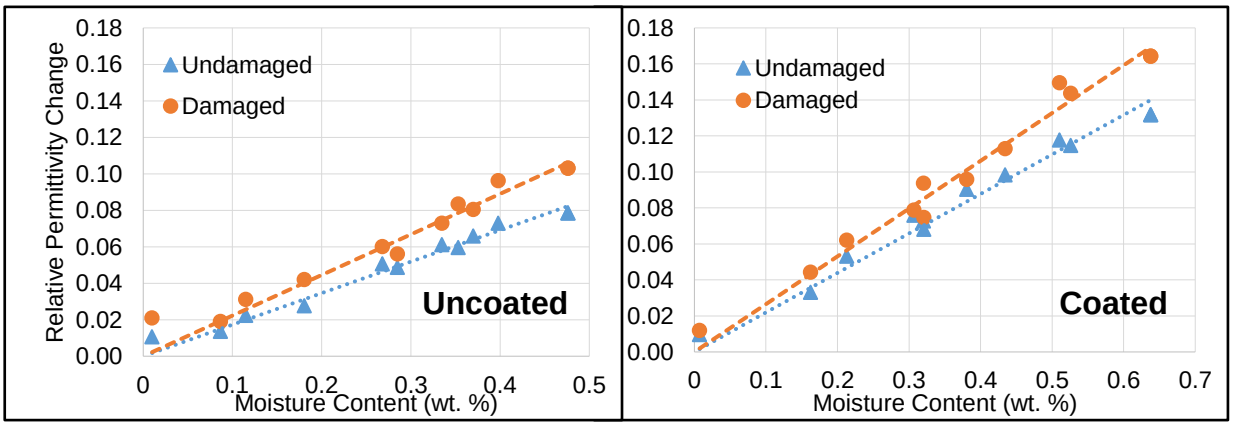

(a) (b)

Figure 47: Absorption-desorption plots of relative permittivity change in an undamaged and damaged region of (a) an uncoated (b) a coated polymer composite laminate.

When the sensitivity obtained in this study is compared to prior work in Section 5.3.6 [117], significantly lower sensitivity to damage is observed. This is likely due to two factors—moisture exposure method and lower moisture level. The prior study exposed the specimens to moisture via immersion in water. This enabled much higher moisture diffusivity into the specimen [25], especially in the damaged region. That led to much better contrast between the damaged and

undamaged regions. The moisture level also has a significant effect on sensitivity to damage. As shown in Section 5.3.1, an increase in moisture level increases sensitivity to damage. The apparently higher moisture levels achieved by the coated composites was due to the strong affinity for moisture of the coating. Therefore, much higher levels of moisture would be required for coated composites to compensate for this effect of the coating.

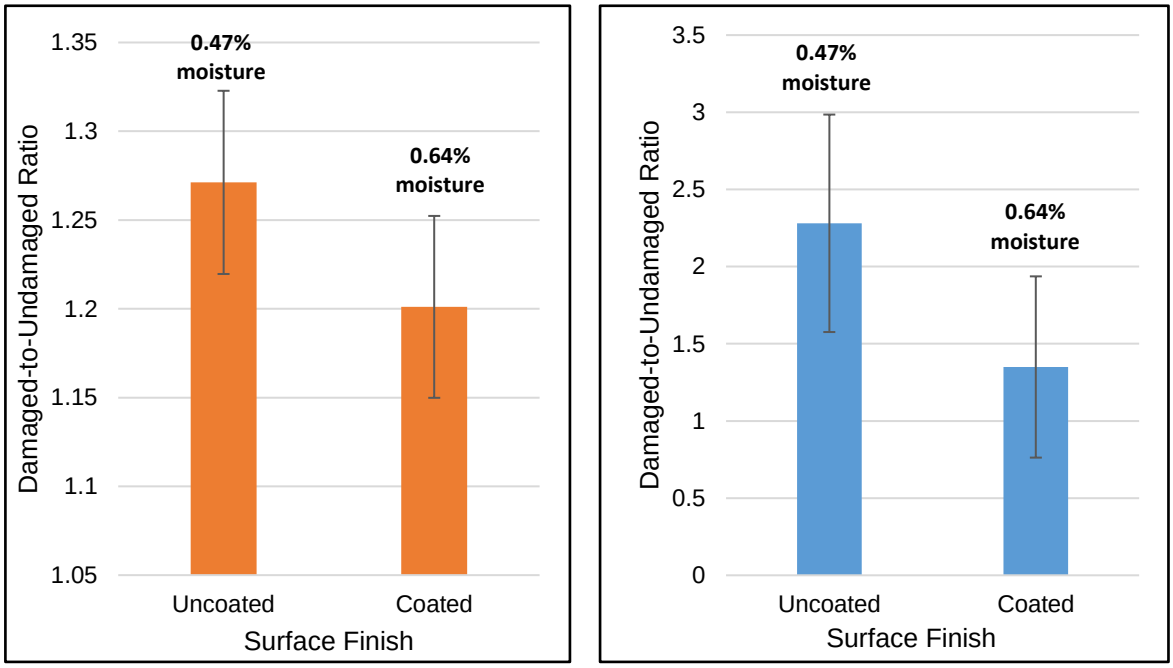

(a) (b)

Figure 48: Effect of surface coating on sensitivity to damage by applying (a) absorption process scans (b) damage-dependent hysteresis techniques.

Further studies are required to investigate how specific filler, primer, and paint combinations affect moisture absorption and the corresponding mitigation actions required. This could provide guidance on minimum levels of moisture which must be attained to provide adequate sensitivity to detect damage of a particular minimum size.

6.4 Conclusion

Polymer composites in service are used with various surface finishes applied to serve various functions, such as weather barrier, wear resistance, and for aesthetic value. This study investigates the effect that a widely used aerospace coating combination has on sensitivity of polymer-water interactions to damage. Results show higher moisture absorption in the coated specimens compared to uncoated. It also suggests the additional moisture has a higher proportion of water in the free state and is absorbed to the coating and paint layer only. They show as much as 40% loss in sensitivity to damage with coatings applied, when damage-dependent hysteresis—based on polymer-water interactions—is applied as a nondestructive examination technique. Further studies focused on the effect of specific filler, primer, and paint combinations are required to establish minimum moisture content levels that provide adequate sensitivity to damage for desired length scales.

CHAPTER 7: CONCLUSION

7.1 Major Findings

Through an experimental approach, an understanding of the dynamic behavior of water in a damaged polymer composite laminate was achieved. This led to the discovery of damage-dependent hysteresis behavior during absorption and desorption processes. This dissertation 'Leveraging Polymer-Water Interactions for Damage Detection in Polymer Composites' contributes several novel findings to the body of knowledge; these are highlighted below by chapter.

Chapter 3 explored ways polymer-water interactions could be characterized with emphasis on near-infrared spectroscopy and dielectric spectroscopy. The goal was to understand how damage in polymer composites could affect the water state distribution.

- Results from NIR spectroscopy indicate as much as a 2-fold increase in free-to-bound water ratio in 5-Joule damaged specimen compared to an undamaged specimen. Similarly, results from microwave dielectric analysis show as much as an 8-fold higher change in relative permittivity for the same level of damage compared to an undamaged specimen. These results were observed at the same moisture content for damaged and undamaged specimens.
- Both characterization methods also indicate sensitivity to the magnitude of damage, with microwave-frequency relative permittivity showing better differentiation between 3 and 5-Joule damage. Its superior performance is likely due to the larger aperture size, which enables a more holistic characterization of the damaged regions compared to near-infrared spectroscopy.

- The results indicate a lower proportion of free water in the undamaged laminate and higher free water levels in damaged laminates, primarily due to preferential migration of free water to voids created by matrix cracking, debonding, and delaminations within damaged regions.
- The study showed that analysis of polymer-water interactions within a polymer matrix may provide an opportunity to accurately detect low levels of damage and estimate its magnitude and location.

Chapter 4 investigated how sensitivity to damage of polymer-water interactions could be affected by precipitation or humidity driven fluctuations in total moisture content of a polymer composite laminate.

- Results indicate the absorption and desorption history of polymer composites has a significant impact on sensitivity to damage when applying polymer-water interactions as a nondestructive examination technique.
- Undamaged areas were shown to exhibit linear single-mode sorption. While damaged regions exhibit dual-mode sorption comprising an initial rapidly increasing or decreasing non-linear process, and a steady linear behavior. The linear and non-linear components demonstrate bound and free water behavior, respectively.
- Results also indicate damage-dependent hysteresis behavior in relative permittivity with moisture content, showing the hysteresis loop size is directly correlated with the extent of damage. A damage detection technique based on this provides a way to mitigate the uncertainty or sensitivity lost when applying polymer-water interactions in damage detection.

Chapter 5 demonstrated how polymer-water interactions can be utilized in localized damage detection. The aim of the study was to understand the relationship between relative permittivity, total moisture content, and sensitivity to damage level. Then based on this understanding, develop algorithms for localized damage detection based on polymer-water interactions.

- Results demonstrated that a machine learning approach based on logistic regression can be used to develop an effective localized damage predictive model with moisture content and relative permittivity as predictive features. Results indicated a linear decision boundary can be used to define the undamaged-damaged interface in the moisture content vs relative permittivity change plot.
- A generalized basis for nondestructive examination of polymer composites which requires no knowledge of the dielectric response of the pristine-dry state can be achieved by using damage-dependent hysteresis.
- Results also show much higher sensitivity to damage can be realized by adopting damage-dependent hysteresis. Over two orders of magnitude increase in damage sensitivity levels can be achieved by measuring the degree of hysteresis effect (extent of damage) through a linear fit and calculating the residual sum of squares.
- Damage-dependent hysteresis attaining such high sensitivity levels can enable further development of the technique into a viable method for damage detection suitable for industrial and field applications.

Chapter 6 investigated how coating and paint applied on a polymer composite surface may affect the ability to detect damage based on polymer-water interactions. The aim of this study was to compare sensitivity to localized damage in an uncoated and coated composite laminate.

- Results show a faster rate of moisture absorption in coated specimens compared to uncoated, indicating additional affinity for moisture due to the epoxy and polyurethane compounds in the coating.
- Results from relative permittivity response indicates higher levels of free water in the additional moisture absorbed due to the coating; and this additional moisture is not absorbed to the damaged region but to the coating layer.
- Coatings on polymer matrix composites can lead to as much as a 40% loss in sensitivity to damage when damage-dependent hysteresis—based on polymer-water interactions—is applied as a nondestructive examination technique. This can be mitigated by increasing the moisture content to compensate for the damage sensitivity loss.

7.2 Future Work

For continued development of the nondestructive examination technique, a number of future research directions that would enable further understanding and adaptation of the system for industry use have been identified. Some of these would require additional experimental studies, development of data processing algorithms, advancements in spectroscopic techniques, cross-disciplinary collaborations, and further understanding of the underlining physics. These are highlighted briefly below:

- A study to investigate the effects of specimen immersion in water compared to exposure to a high humidity environment during moisture uptake is required. Some loss in sensitivity to damage may be observed due to the higher diffusivity achieved when immersed in water compared to when exposed to humid environments. This effect needs to be taken into consideration when determining the sensitivity levels based on moisture content required to detect a certain level of damage (as described in Section 5.3.1).

- Advances in spectroscopic techniques would be required to extend the suitability of the technique to conductive and strongly absorbing reinforcements such as carbon fibers. As a wide range of aerospace applications for safety-critical components involve the use of carbon fibers, the ability to apply polymer-water interactions for damage detection in such materials would significantly broaden the impact of the technique.
- A key advantage of this technique is it being based on a molecular level phenomenon. This enables its application across a wide range of length scales, from sub-micron to macro scale. Atomic force microscopy Infrared spectroscopy (AFM-IR) has been shown to achieve nano-scale resolutions in characterization. AFM-IR would be useful in applying the technique to damage detection at nano-scale levels. This would be particularly important for very thin polymer composites required in sub-micron sized components.
- In *Chapter 5*, a generalized method for damage detection based on damage-dependent hysteresis capable of identifying hotspots in a polymer composite laminate was demonstrated. Further development of this into a generalized quantitative damage mapping technique was limited by inadequate data points required to clearly define a model which could predict the effective resonant cavity size at a particular moisture content. A similar experiment should be developed with adequate damage levels which would enable this prediction.
- In this work a majority of epoxy resin system was employed. The result is expected to be similar for different resin systems, but with some variations in dielectric and near-infrared responses. Experimental studies on various widely used thermoset and thermoplastic resin systems is required to validate this assumption.

- Further experimental studies on damage-dependent hysteresis is required to determine the optimum moisture variation range and number of scans needed to detect damage at a particular level. This would allow for optimization of these test parameters, minimizing scan time and resources.
- A study to compare the capabilities of the method to current nondestructive examination techniques is required to show areas of superiority, especially in characterization of current hard to detect flaws due to orientation, zero volume disbonds, and flaw size.
- In this work, the effects of short-term moisture contamination on damage and polymer-water interaction was investigated. It is believed that even at higher moisture levels, locally higher amounts of free water would still enable sensitivity to damage; however, validation of this is required by investigating the effects of longer term moisture-contamination.
- Damage-dependent hysteresis behavior was characterized in *Chapters 4 and 5* using microwave-frequency relative permittivity. Further validation of the conclusions reached could be achieved by applying near-infrared spectroscopy in damage mapping. Also, due to its smaller aperture size better resolutions scans could be obtained through this method.
- A preliminary investigation of the effect of coating and painting on sensitivity to damage was performed in *Chapter 6.* Quantitative details on the loss of sensitivity to damage due to specific filler, primer, and paint combinations is required. This could provide guidance on minimum levels of moisture which must be attained to provide adequate sensitivity for detecting damage of a particular minimum size, when specific coatings are used.
- Development of simulation models can eliminate limitations of experimental setups. The use of ANSYS-HFSS (High Frequency Structural Simulation) software in modeling microwave environments has gained popularity in recent times. Developing a model which

would simulate the interactions between resonant cavities, dielectric materials, free and bound water, and environmental conditions would eliminate the physical, economic, and time constraints associated with performing hands-on experiments. This could drastically accelerate the pace of innovation.

REFERENCES

[1] Kaware K, Kotambkar M. Low velocity impact response and influence of parameters to improve the damage resistance of composite structures/materials: a critical review. Int J Crashworthiness 2021:1–25. https://doi.org/10.1080/13588265.2021.1914985.

[2] Schaff JR, Technologies U. Fatigue and Life Prediction. Composites, vol. 21, ASM International; 2001, p. 252–8. https://doi.org/10.31399/asm.hb.v21.a0003382.

[3] Zhu TL. A reliability-based safety factor for aircraft composite structures. Comput Struct 1993;48:745–8. https://doi.org/10.1016/0045-7949(93)90269-J.

[4] Callister Jr., 1940- WD. Materials science and engineering : an introduction 8e. Hoboken, New Jersey: Hoboken, New Jersey : John Wiley & Sons, ©2012.; 2012.

[5] Idolor O, Guha RD, Berkowitz K, Geiger C, Davenport M, Grace L. Polymer-water interactions and damage detection in polymer matrix composites. Compos Part B Eng 2021:108637. https://doi.org/10.1016/j.compositesb.2021.108637.

[6] Wallenberger FT, Watson JC, Li H, Industries PPG. Glass Fibers. Composites, vol. 21, ASM International; 2001, p. 27–34. https://doi.org/10.31399/asm.hb.v21.a0003353.

[7] Chang KK, Nemours EIDP De. Aramid Fibers. Composites, vol. 21, ASM International; 2001, p. 41–5. https://doi.org/10.31399/asm.hb.v21.a0009242.

[8] Peterlik H. Carbon Fibers. Ceram. Matrix Compos., vol. 9781118231, Hoboken, NJ, USA: John Wiley & Sons, Inc.; 2014, p. 27–39. https://doi.org/10.1002/9781118832998.ch2.

[9] Wallenberger FT, Industries PPG. Introduction to Reinforcing Fibers. Composites, vol. 21, ASM International; 2001, p. 23–6. https://doi.org/10.31399/asm.hb.v21.a0003352.

[10] Boyle MA, Martin CJ, Neuner JD, Corporation H. Epoxy Resins. Composites, vol. 21, ASM International; 2001, p. 90–6. https://doi.org/10.31399/asm.hb.v21.a0003363.

[11] Musto P, Ragosta G, Mascia L. Vibrational spectroscopy evidence for the dual nature of water sorbed into epoxy resins. Chem Mater 2000;12:1331–41. https://doi.org/10.1021/cm9906809.

[12] Stenzenberger H, Gmbh T. Bismaleimide Resins. Composites, vol. 21, ASM International; 2001, p. 97–104. https://doi.org/10.31399/asm.hb.v21.a0003364.

[13] Mills A, Manufacturing C, Kingdom U. Manual Prepreg Lay-Up. Composites, vol. 21, ASM International; 2001, p. 470–6. https://doi.org/10.31399/asm.hb.v21.a0003409.

[14] Hurdelbrink KR, Anderson JP, Siddique Z, Altan MC. The coupled effect of fiber volume fraction and void fraction on hydraulic fluid absorption of quartz/BMI laminates. AIP Conf Proc 2016;1713. https://doi.org/10.1063/1.4942325.

[15] Pillay S, Vaidya UK, Janowski GM. Effects of moisture and UV exposure on liquid molded carbon fabric reinforced nylon 6 composite laminates. Compos Sci Technol 2009;69:839–46. https://doi.org/10.1016/j.compscitech.2008.03.021.

[16] Akay M, Kong Ah Mun S, Stanley A. Influence of moisture on the thermal and mechanical properties of autoclaved and oven-cured Kevlar-49/epoxy laminates. Compos Sci Technol 1997;57:565–71. https://doi.org/10.1016/S0266-3538(97)00017-1.

[17] Zafar A, Bertocco F, Schjødt-Thomsen J, Rauhe JC. Investigation of the long term effects of moisture on carbon fibre and epoxy matrix composites. Compos Sci Technol 2012;72:656–66. https://doi.org/10.1016/j.compscitech.2012.01.010.

[18] Fan Y, Gomez A, Ferraro S, Pinto B, Muliana A, Saponara V La. Diffusion of water in glass fiber reinforced polymer composites at different temperatures. J Compos Mater 2019;53:1097–110. https://doi.org/10.1177/0021998318796155.

[19] Soles CL, Yee AF. A Discussion of the Molecular Mechanisms of Moisture Transport in

Epoxy Resins. J Polym Sci Part B Polym Phys 1999;38:707–15. https://doi.org/10.1002/(SICI)1099-0488(20000301)38.

[20] Guha RD, Idolor O, Grace L. An atomistic simulation study investigating the effect of varying network structure and polarity in a moisture contaminated epoxy network. Comput Mater Sci 2020;179:109683. https://doi.org/10.1016/j.commatsci.2020.109683.

[21] Vuković F, Walsh TR. Moisture Ingress at the Molecular Scale in Hygrothermal Aging of Fiber–Epoxy Interfaces. ACS Appl Mater Interfaces 2020:acsami.0c17027. https://doi.org/10.1021/acsami.0c17027.

[22] Bao LR, Yee AF. Moisture diffusion and hygrothermal aging in bismaleimide matrix carbon fiber composites: Part II-woven and hybrid composites. Compos Sci Technol 2002;62:2111–9. https://doi.org/10.1016/S0266-3538(02)00162-8.

[23] Ishai O. Environmental Effects on Deformation, Strength, and Degradation of Unidirectional Glass-Fiber Reinforced Plastics. I. Survey. Polym Eng Sci 1975;15:486–90.

[24] Berketis K, Tzetzis D, Hogg PJ. Impact damage detection and degradation monitoring of wet GFRP composites using noncontact ultrasonics. Polym Compos 2008;30:1043–9. https://doi.org/10.1002/pc.20652.

[25] Jiang X, Kolstein H, Bijlaard FSK. Moisture diffusion in glass-fiber-reinforced polymer composite bridge under hot/wet environment. Compos Part B Eng 2013;45:407–16. https://doi.org/10.1016/j.compositesb.2012.04.067.

[26] Vieth WR, Howell JM, Hsieh JH. Dual sorption theory. J Memb Sci 1976;1:177–220. https://doi.org/10.1016/S0376-7388(00)82267-X.

[27] Grace LR, Altan MC. Non-fickian three-dimensional hindered moisture absorption in polymeric composites: Model development and validation. Polym Compos 2013;34:1144–

57. https://doi.org/10.1002/pc.22523.

[28] Grace LR, Altan MC. Characterization of anisotropic moisture absorption in polymeric composites using hindered diffusion model. Compos Part A Appl Sci Manuf 2012;43:1187–96. https://doi.org/10.1016/j.compositesa.2012.03.016.

[29] Bond DA. Moisture diffusion in a fiber-reinforced composite: Part I - Non-Fickian transport and the effect of fiber spatial distribution. J Compos Mater 2005;39:2113–42. https://doi.org/10.1177/0021998305052030.

[30] Zhou J, Lucas JP. Hygrothermal effects of epoxy resin. Part II: variations of glass transition temperature. Polymer (Guildf) 1999;40:5513–22. https://doi.org/10.1016/S0032-3861(98)00791-5.

[31] Rodriguez LA, García C, Grace LR. Long-term durability of a water-contaminated quartz-reinforced bismaleimide laminate. Polym Compos 2018;39:2643–9. https://doi.org/10.1002/pc.24255.

[32] Guermazi N, Ben Tarjem A, Ksouri I, Ayedi HF. On the durability of FRP composites for aircraft structures in hygrothermal conditioning. Compos Part B Eng 2013;85:294–304. https://doi.org/10.1016/j.compositesb.2015.09.035.

[33] Soles C, Chang F, Bolan B, Hristov H, Gidley A, Yee A. Contributions of the nanovoid structure to the moisture absorption properties of epoxy resins. J Polym … 1998;36:3035–48. https://doi.org/10.1002/(SICI)1099-0488(199812)36:17<3035::AID-POLB4>3.3.CO;2-P.

[34] Berketis K, Tzetzis D. Long-term water immersion ageing characteristics of GFRP composites. J Mater Sci 2009;44:3578–88. https://doi.org/10.1007/s10853-009-3485-9.

[35] Bossi RH, Giurgiutiu V. Nondestructive testing of damage in aerospace composites. Polym

Compos Aerosp Ind 2014:413–48. https://doi.org/10.1016/B978-0-85709-523-7.00015-3.

[36] Idolor O, Guha R, Grace L. A Dielectric Resonant Cavity Method for Monitoring of Damage Progression in Moisture-Contaminated Composites. Am. Soc. Compos. 2018, vol. 2, Lancaster, PA: DEStech Publications, Inc.; 2018. https://doi.org/10.12783/asc33/25963.

[37] Idolor O, Guha R, Berkowitz K, Grace L. Damage Detection in Polymer Matrix Composites by Analysis of Polymer-Water Interactions Using Near-Infrared Spectroscopy. Am. Soc. Compos. 2020, Lancaster, PA: DEStech Publications, Inc.; 2020. https://doi.org/10.12783/asc35/34874.

[38] Zoughi R. Microwave non-destructive testing and evaluation. Dordrecht ; Boston : Kluwer Academic Publishers, [2000]; 2000.

[39] Abdessalem A, Tamboura S, Fitoussi J, Ben Daly H, Tcharkhtchi A. Bi-phasic water diffusion in sheet molding compound composite. J Appl Polym Sci 2020;137:1–12. https://doi.org/10.1002/app.48381.

[40] Li L, Yu Y, Su H, Zhan G, Li S, Wu P. The diffusion mechanism of water transport in amine-cured epoxy networks. Appl Spectrosc 2010;64:458–65. https://doi.org/10.1366/000370210791114220.

[41] Takeshita Y, Becker E, Sakata S, Miwa T, Sawada T. States of water absorbed in water-borne urethane/epoxy coatings. Polym (United Kingdom) 2014;55:2505–13. https://doi.org/10.1016/j.polymer.2014.03.027.

[42] International Symposium on Properties of Water (2nd : 1978 : Osaka J, Rockland LB, Stewart 1908-1982 GF, Technology IU of FS and. Water activity : influences on food quality : a treatise on the influence of bound and free water on the quality and stability of foods and other natural products. New York: New York : Academic Press, 1981.; 1981.

[43] Encyclopedia of Dairy Sciences. vol. 2nd ed. Amsterdam: Academic Press; 2011.

[44] Qiu Y, Chen Y, Zhang GGZ, Porter W, Liu L, Rao V, et al. Developing Solid Oral Dosage Forms : Pharmaceutical Theory and Practice. London, UNITED STATES: Elsevier Science & Technology; 2008.

[45] Olek W, Perré P, Weres J. Inverse analysis of the transient bound water diffusion in wood. Holzforschung 2005;59:38–45. https://doi.org/10.1515/HF.2005.007.

[46] Bonnet M, Courtier-Murias D, Faure P, Rodts S, Care S. NMR determination of sorption isotherms in earlywood and latewood of Douglas fir. Identification of bound water components related to their local environment. Holzforschung 2017;71:481–90. https://doi.org/10.1515/hf-2016-0152.

[47] Araujo CD, Avramidis S, MacKay AL. Behaviour of Solid Wood and Bound Water as a Function of Moisture Content. A Proton Magnetic Resonance Study. Holzforschung 1994;48:69–74. https://doi.org/10.1515/hfsg.1994.48.1.69.

[48] Choe C, Schleusener J, Lademann J, Darvin ME. Keratin-water-NMF interaction as a three layer model in the human stratum corneum using in vivo confocal Raman microscopy. Sci Rep 2017;7:1–14. https://doi.org/10.1038/s41598-017-16202-x.

[49] Choe C, Lademann J, Darvin ME. Depth profiles of hydrogen bound water molecule types and their relation to lipid and protein interaction in the human stratum corneum: In vivo. Analyst 2016;141:6329–37. https://doi.org/10.1039/c6an01717g.

[50] Gilard V, Martino R, Malet-Martino M, Riviere M, Gournay A, Navarro R. Measurement of total water and bound water contents in human stratum corneum by in vitro proton nuclear magnetic resonance spectroscopy. Int J Cosmet Sci 1998;20:117–25. https://doi.org/10.1046/j.1467-2494.1998.171743.x.

[51] Berkowitz K, Idolor O, Pankow M, Grace L. Combined effects of impact damage and moisture exposure on composite radome dielectric properties. Int. SAMPE Tech. Conf., vol. 2018- May, 2018.

[52] Grace LR. The effect of moisture contamination on the relative permittivity of polymeric composite radar-protecting structures at X-band. Compos Struct 2015;128:305–12. https://doi.org/10.1016/j.compstruct.2015.03.070.

[53] Heys KR, Friedrich MG, Truscott RJW. Free and bound water in normal and cataractous human lenses. Investig Ophthalmol Vis Sci 2008;49:1991–7. https://doi.org/10.1167/iovs.07-1151.

[54] Carneiro I, Carvalho S, Henrique R, Oliveira L, Tuchin V V. Simple multimodal optical technique for evaluation of free/bound water and dispersion of human liver tissue. J Biomed Opt 2017;22:1. https://doi.org/10.1117/1.jbo.22.12.125002.

[55] Wong EH. Characterizing the kinetics of free and bound water using a non-isothermal sorption technique. Dry Technol 2017;35:46–54. https://doi.org/10.1080/07373937.2016.1158722.

[56] Popineau S, Rondeau-Mouro C, Sulpice-Gaillet C, Shanahan MER. Free/bound water absorption in an epoxy adhesive. Polymer (Guildf) 2005;46:10733–40. https://doi.org/10.1016/j.polymer.2005.09.008.

[57] Sales R, Thim G, Brunelli D. Understanding the water uptake in F-161 glass-epoxy composites using the techniques of luminescence spectroscopy and FT-NIR. Polímeros 2017;27:171–82. https://doi.org/10.1590/0104-1428.05516.

[58] Mijović J, Zhang H. Local dynamics and molecular origin of polymer network-water interactions as studied by broadband dielectric relaxation spectroscopy, FTIR, and

molecular simulations. Macromolecules 2003;36:1279–88. https://doi.org/10.1021/ma021568q.

[59] Robinson W. FREE AND BOUND WATER DETERMINATIONS BY THE HEAT OF FUSION OF ICE METHOD. J Biol Chem 1931;92:699–709. https://doi.org/10.1016/S0021-9258(17)32613-3.

[60] Guha RD, Idolor O, Grace L. Molecular Dynamics (MD) Simulation of a Polymer Composite Matrix with Varying Degree of Moisture: Investigation of Secondary Bonding Interactions. Am. Soc. Compos. 2019, Lancaster, PA: DEStech Publications, Inc.; 2019. https://doi.org/10.12783/asc34/31367.

[61] Mijović J, Zhang H. Molecular Dynamics Simulation Study of Motions and Interactions of Water in a Polymer Network. J Phys Chem B 2004;108:2557–63. https://doi.org/10.1021/jp036181j.

[62] Behera A, Dupare P, Thawre MM, Ballal A. Effects of hygrothermal aging and fiber orientations on constant amplitude fatigue properties of CFRP multidirectional composite laminates. Int J Fatigue 2020;136:105590. https://doi.org/10.1016/j.ijfatigue.2020.105590.

[63] ISO. International standard {ISO} 20473 ({Optics and photonics - Spectral bands}). ISO - International Organization for Standardization; 2007.

[64] Cholake S, Mada M, Raman R, Bai Y, Zhao X, Rizkalla S, et al. Quantitative Analysis of Curing Mechanisms of Epoxy Resin by Mid- and Near- Fourier Transform Infra Red Spectroscopy. Def Sci J 2014;64:314–21. https://doi.org/10.14429/dsj.64.7326.

[65] Koenig JL. Spectroscopy of Polymers. 1999. https://doi.org/10.1016/b978-0-444-10031-3.50012-8.

[66] Colthup NB, Daly LH, Wiberley SE. Introduction to infrared and Raman spectroscopy.

Boston: Boston : Academic Press, [1990]; 1990.

[67] Hollas JM (John M. Modern spectroscopy. Chichester: Chichester ; New York : J. Wiley, [1996]; 1996.

[68] Coates J. Encyclopedia of Analytical Chemistry -Interpretation of Infrared Spectra, A Practical Approach. Encycl Anal Chem 2004:1–23.

[69] Afrin T, Karobi SN, Rahman MM, Mollah MYA, Susan MABH. Water structure modification by sugars and its consequence on micellization behavior of cetyltrimethylammonium bromide in aqueous solution. J Solution Chem 2013;42:1488–99. https://doi.org/10.1007/s10953-013-0050-6.

[70] Giannoukos G, Min M, Rang T. Relative complex permittivity and its dependence on frequency. World J Eng 2017;14:532–7. https://doi.org/10.1108/WJE-01-2017-0007.

[71] Fernández DP, Mulev Y, Goodwin ARH, Sengers JMHL. A Database for the Static Dielectric Constant of Water and Steam. J Phys Chem Ref Data 1995;24:33–70. https://doi.org/10.1063/1.555977.

[72] Komarov V, Wang S, Tang J. Permittivity and Measurements. Encycl. RF Microw. Eng., Hoboken, NJ, USA: John Wiley & Sons, Inc.; 2005. https://doi.org/10.1002/0471654507.eme308.

[73] Hallikainen MT, Ulaby FT, Dobson MC, El-Rayes MA, Wu L-K. Microwave Dielectric Behavior of Wet Soil - Part I: Emprical Models and Experimental Observations. IEEE Trans Geosci Remote Sens 1985;GE-23:25–34. https://doi.org/10.1109/TGRS.1985.289497.

[74] Krupka J. Frequency domain complex permittivity measurements at microwave frequencies. Meas Sci Technol 2006;17. https://doi.org/10.1088/0957-0233/17/6/R01.

[75] Krupka J. Precise measurements of the complex permittivity of dielectric materials at

microwave frequencies. Mater Chem Phys 2003;79:195–8. https://doi.org/10.1016/S0254-0584(02)00257-2.

[76] Duchene P, Chaki S, Ayadi A, Krawczak P. A review of non-destructive techniques used for mechanical damage assessment in polymer composites. J Mater Sci 2018;53:7915–38. https://doi.org/10.1007/s10853-018-2045-6.

[77] Nsengiyumva W, Zhong S, Lin J, Zhang Q, Zhong J, Huang Y. Advances, limitations and prospects of nondestructive testing and evaluation of thick composites and sandwich structures: A state-of-the-art review. Compos Struct 2021;256:112951. https://doi.org/10.1016/j.compstruct.2020.112951.

[78] Revel GM, Pandarese G, Cavuto A. Advanced ultrasonic non-destructive testing for damage detection on thick and curved composite elements for constructions. J Sandw Struct Mater 2013;15:5–24. https://doi.org/10.1177/1099636212456861.

[79] Strobl M, Manke I, Kardjilov N, Hilger A, Dawson M, Banhart J. Advances in neutron radiography and tomography. J Phys D Appl Phys 2009;42. https://doi.org/10.1088/0022-3727/42/24/243001.

[80] Francis D, Tatam RP, Groves RM. Shearography technology and applications: A review. Meas Sci Technol 2010;21. https://doi.org/10.1088/0957-0233/21/10/102001.

[81] Gholizadeh S. A review of non-destructive testing methods of composite materials. Procedia Struct Integr 2016;1:50–7. https://doi.org/10.1016/j.prostr.2016.02.008.

[82] Jolly M, Prabhakar A, Sturzu B, Hollstein K, Singh R, Thomas S, et al. Review of Non-destructive Testing (NDT) Techniques and their Applicability to Thick Walled Composites. Procedia CIRP 2015;38:129–36. https://doi.org/10.1016/j.procir.2015.07.043.

[83] Pagliarulo V, Rocco A, Langella A, Riccio A, Ferraro P, Antonucci V, et al. Impact damage

investigation on composite laminates: Comparison among different NDT methods and numerical simulation. Meas Sci Technol 2015;26. https://doi.org/10.1088/0957-0233/26/8/085603.

[84] Mirala A, Foudazi A, Al Qaseer MT, Donnell KM. Active Microwave Thermography to Detect and Locate Water Ingress. IEEE Trans Instrum Meas 2020;PP. https://doi.org/10.1109/TIM.2020.3003394.

[85] Krauklis AE, Gagani AI, Echtermeyer AT. Near-infrared spectroscopic method for monitoring water content in epoxy resins and fiber-reinforced composites. Materials (Basel) 2018;11. https://doi.org/10.3390/ma11040586.

[86] Neşer G. Polymer based composites in marine use: History and future trends. Procedia Eng 2017;194:19–24. https://doi.org/10.1016/j.proeng.2017.08.111.

[87] Caputo F, De Luca A, Lamanna G, Lopresto V, Riccio A. Numerical investigation of onset and evolution of LVI damages in Carbon-Epoxy plates. Compos Part B Eng 2015;68:385–91. https://doi.org/10.1016/j.compositesb.2014.09.009.

[88] Dattoma V, Panella F, Pirinu A, Saponaro A. Advanced NDT Methods and Data Processing on Industrial CFRP Components. Appl Sci 2019;9:393. https://doi.org/10.3390/app9030393.

[89] Pelivanov I, Buma T, Xia J, Wei CW, O'Donnell M. NDT of fiber-reinforced composites with a new fiber-optic pump-probe laser-ultrasound system. Photoacoustics 2014;2:63–74. https://doi.org/10.1016/j.pacs.2014.01.001.

[90] Kumar Gupta S, Hojjati M. Microcrack Detection in Composite Laminates at Early Stage of Thermal Cycling Using Moisture/Freeze/Dry Cycle. Int J Compos Mater 2019;2019:7–15. https://doi.org/10.5923/j.cmaterials.20190901.02.

[91] Herrera-Gómez A, Velázquez-Cruz G, Martín-Polo MO. Analysis of the water bound to a polymer matrix by infrared spectroscopy. J Appl Phys 2001;89:5431–7. https://doi.org/10.1063/1.1365427.

[92] Garden L, Pethrick RA. A dielectric study of water uptake in epoxy resin systems. J Appl Polym Sci 2017;134:1–12. https://doi.org/10.1002/app.44717.

[93] Zhou J, Lucas JP. Hygrothermal effects of epoxy resin. Part I: the nature of water in epoxy. Polymer (Guildf) 1999;40:5505–12. https://doi.org/10.1016/S0032-3861(98)00790-3.

[94] Hougham G, Tesoro G, Viehbeck A, Chapple-Sokol JD. Polarization Effects of Fluorine on the Relative Permittivity in Polyimides. Macromolecules 1994;27:5964–71. https://doi.org/10.1021/ma00099a006.

[95] Levy RA, Collier RJ. *Principles of Solid State Physics*. Phys Today 1969;22:75–6. https://doi.org/10.1063/1.3035636.

[96] De Luca S, Kannam SK, Todd BD, Frascoli F, Hansen JS, Daivis PJ. Effects of Confinement on the Dielectric Response of Water Extends up to Mesoscale Dimensions. Langmuir 2016;32:4765–73. https://doi.org/10.1021/acs.langmuir.6b00791.

[97] Senapati S, Chandra A. Dielectric constant of water confined in a nanocavity. J Phys Chem B 2001;105:5106–9. https://doi.org/10.1021/jp011058i.

[98] Boyarskii DA, Tikhonov V V., Komarova NY. Model of dielectric constant of bound water in soil for applications of microwave remote sensing. Prog Electromagn Res 2002;35:251–69. https://doi.org/10.2528/PIER01042403.

[99] Kumar, BG., Singh, RP., Nakamura T. Degradation of Carbon Fiber-reinforced Epoxy Composites by Ultraviolet Radiation and Condensation. J Compos Mater 2002;36:2713–33. https://doi.org/10.1106/002199802028682.

[100] Toivola R, Afkhami F, Baker S, McClure J, Flinn BD. Detection of incipient thermal damage in carbon fiber-bismaleimide composites using hand-held FTIR. Polym Test 2018;69:490–8. https://doi.org/10.1016/j.polymertesting.2018.05.036.

[101] Claus J, Santos RAM, Gorbatikh L, Swolfs Y. Effect of matrix and fibre type on the impact resistance of woven composites. Compos Part B Eng 2019;in submiss:107736. https://doi.org/10.1016/j.compositesb.2019.107736.

[102] ASTM. Standard Test Methods for Constituent Content of Composite Materials. ASTM Int 2010:1–6. https://doi.org/10.1520/D3529M-10.2.

[103] ASTM standard. ASTM D 5229– 92 – Standard Test Method for Moisture Absorption Properties and Equilibrium Conditioning of Polymer Matrix Composite Materials. Annu B ASTM Stand 2010;92:1–13. https://doi.org/10.1520/D5229_D5229M-14.

[104] Riccio A, De Luca A, Di Felice G, Caputo F. Modelling the simulation of impact induced damage onset and evolution in composites. Compos Part B Eng 2014;66:340–7. https://doi.org/10.1016/j.compositesb.2014.05.024.

[105] Burneau A. Near infrared spectroscopic study of the structures of water in proton acceptor solvents. J Mol Liq 1990;46:99–127. https://doi.org/10.1016/0167-7322(90)80048-O.

[106] Krupka J, Gregory AP, Rochard OC, Clarke RN, Riddle B, Baker-Jarvis J. Uncertainty of complex permittivity measurements by split-post dielectric resonator technique. J Eur Ceram Soc 2001;21:2673–6. https://doi.org/10.1016/S0955-2219(01)00343-0.

[107] Idolor O, Guha R, Bilich L, Grace L. 2-Dimensional Mapping of Damage in Moisture Contaminated Polymer Composites Using Dielectric Properties. Am. Soc. Compos. 2019, Lancaster, PA: DEStech Publications, Inc.; 2019. https://doi.org/10.12783/asc34/31312.

[108] Bull DJ, Helfen L, Sinclair I, Spearing SM, Baumbach T. A comparison of multi-scale 3D

X-ray tomographic inspection techniques for assessing carbon fibre composite impact damage. Compos Sci Technol 2013;75:55–61. https://doi.org/10.1016/j.compscitech.2012.12.006.

[109] Meola C, Carlomagno GM. Non-destructive evaluation (NDE) of aerospace composites: Detecting impact damage. 2013. https://doi.org/10.1533/9780857093554.3.367.

[110] Liu J, Koenig L. A New Baseline Correction Algorithm Using Objective Criteria 1987;41:447–9.

[111] Musto P, Karasz FE, MacKnight WJ. Fourier transform infra-red spectroscopy on the thermo-oxidative degradation of polybenzimidazole and of a polybenzimidazole/polyetherimide blend. Polymer (Guildf) 1993;34:2934–45. https://doi.org/10.1016/0032-3861(93)90618-K.

[112] Huo Z, Anandan S, Xu M, Chandrashekhara K. Investigation of three-dimensional moisture diffusion modeling and mechanical degradation of carbon/bismaleimide composites under seawater conditioning. J Compos Mater 2018;52:1339–51. https://doi.org/10.1177/0021998317725159.

[113] ROQUETA G. FMQ; JL. Non-destructive evaluation (NDE) of composites: microwave techniques. Non-Destructive Eval. Polym. Matrix Compos., Elsevier Science & Technology; 2013.

[114] Milosevic M, Berets SL. A review of FT-IR diffuse reflection sampling considerations. Appl Spectrosc Rev 2002;37:347–64. https://doi.org/10.1081/ASR-120016081.

[115] Cole KC, Noël D, Hechler J -J. Applications of diffuse reflectance fourier transform infrared spectroscopy to fiber-reinforced composites. Polym Compos 1988;9:395–403. https://doi.org/10.1002/pc.750090605.

[116] Lin YC, Chen X. Investigation of moisture diffusion in epoxy system: Experiments and molecular dynamics simulations. Chem Phys Lett 2005;412:322–6. https://doi.org/10.1016/j.cplett.2005.07.022.

[117] Idolor O, Guha RD, Berkowitz K, Grace L. An experimental study of the dynamic molecular state of transient moisture in damaged polymer composites. Polym Compos 2021:13. https://doi.org/10.1002/pc.26066.

[118] Pethrick RA. Non-destructive evaluation (NDE) of composites: Dielectric techniques for testing partially or non-conducting composite materials. Non-Destructive Eval Polym Matrix Compos Tech Appl 2013;2013:116–35. https://doi.org/10.1533/9780857093554.1.116.

[119] Masoumi S, Valipour H. Effects of moisture exposure on the crosslinked epoxy system: An atomistic study. Model Simul Mater Sci Eng 2016;24. https://doi.org/10.1088/0965-0393/24/3/035011.

[120] Guha RD, Idolor O, Berkowitz K, Pasquinelli MA, Grace LR. Exploring secondary interactions and the role of temperature in moisture-contaminated polymer networks through molecular simulations. Soft Matter 2021. https://doi.org/10.1039/D0SM02009E.

[121] Schaaf C, Gekle S. Spatially resolved dielectric constant of confined water and its connection to the non-local nature of bulk water. J Chem Phys 2016;145. https://doi.org/10.1063/1.4960775.

[122] Abdelmola F, Carlsson LA. State of water in void-free and void-containing epoxy specimens. J Reinf Plast Compos 2019;38:556–66. https://doi.org/10.1177/0731684419833469.

[123] Fittipaldi M, Rodriguez LA, Damley-Strnad A, Grace LR. Improving tensile strength of an

injection-molded biocompatible thermoplastic elastomer. Mater Des 2015;86:6–13. https://doi.org/10.1016/j.matdes.2015.07.070.

[124] ASTM International. Designation: D7136/D7136M - 12 “Standard test method for measuring the damage resistance of a fiber-reinforced polymer matrix composite to a drop-weight impact event.” Annu B ASTM Stand 2012;i:1–16. https://doi.org/10.1520/D7136.

[125] Troiano A, Pasero E, Mesin L. Experimental validation of a sensor monitoring ice formation over a road surface. Sensors and Transducers 2012;14:112–21.

[126] Sivaprakasam BT, Pakkathillam JK, Krishnamurthy C V, Arunachalam K. Freespace Microwave NDE of Aerospace Dielectric Composites. Electromagn Nondestruct Eval XXII 2019;44:104–9. https://doi.org/10.3233/SAEM190019.

[127] MacLeod JM, Rosei F. Directed Assembly of Nanostructures. Compr. Nanosci. Technol., Elsevier; 2011, p. 13–68. https://doi.org/10.1016/B978-0-12-374396-1.00098-2.

[128] Springer GS. Moisture content of composite under transient conditions. J Compos Mater 1977;11:107–22.

[129] Rodriguez LA, Damley-Strnad A, Grace LR. Temperature and anisotropy effects in the application of the hindered diffusion model to composite laminates. J Reinf Plast Compos 2019;38:628–39. https://doi.org/10.1177/0731684419839220.

[130] Grace LR. Projecting long-term non-Fickian diffusion behavior in polymeric composites based on short-term data: a 5-year validation study. J Mater Sci 2016;51:845–53. https://doi.org/10.1007/s10853-015-9407-0.

[131] Grace LR, Altan MC. Three-dimensional anisotropic moisture absorption in quartz-reinforced bismaleimide laminates. Polym Eng Sci 2014;54:137–46. https://doi.org/10.1002/pen.23549.

[132] L. W. Jelinski, J. J. Dumais, A. L. Cholli, T. S. Ellis and FEK. Nature of the Water-Epoxy Interaction 1985:1091–5.

[133] Moy P, Karasz FE. Epoxy-water interactions. Polym Eng Sci 1980;20:315–9. https://doi.org/10.1002/pen.760200417.

[134] Garc C, Fittipaldi M, Grace LR. Epoxy / montmorillonite nanocomposites for improving aircraft radome longevity n.d. https://doi.org/10.1002/app.42691.

[135] Guan L, Xu H, Huang D. The investigation on states of water in different hydrophilic polymers by DSC and FTIR. J Polym Res 2011;18:681–9. https://doi.org/10.1007/s10965-010-9464-7.

[136] El-Koka A, Cha KH, Kang DK. Regularization parameter tuning optimization approach in logistic regression. Int Conf Adv Commun Technol ICACT 2013:13–8.

[137] Bisong E. Google Colaboratory. Build. Mach. Learn. Deep Learn. Model. Google Cloud Platf., Berkeley, CA: Apress; 2019, p. 59–64. https://doi.org/10.1007/978-1-4842-4470-8_7.

[138] Wan X. The Influence of Polynomial Order in Logistic Regression on Decision Boundary. IOP Conf Ser Earth Environ Sci 2019;267:042077. https://doi.org/10.1088/1755-1315/267/4/042077.

[139] Pomázi Á, Toldy A. Development of fire retardant epoxy-based gelcoats for carbon fibre reinforced epoxy resin composites. Prog Org Coatings 2021;151:106015. https://doi.org/10.1016/j.porgcoat.2020.106015.

[140] DoD. MIL-DTL-64159 Detail Specification. Coating, Water Dispersible Aliphatic Polyurethane, Chemical Agent Resistant. 2002.